UNIVERSITÀ DEGLI STUDI DI PADOVA

DIPARTIMENTO DI INGEGNERIA INDUSTRIALE

CORSO DI LAUREA MAGISTRALE IN INGEGNERIA CHIMICA E DEI PROCESSI INDUSTRIALI

Tesi di Laurea Magistrale in
Ingegneria Chimica e dei Processi Industriali

PRODUCTION OF GELATIN METHACRYLATE PRINTABLE BIOINKS FOR CANCER CELLS STUDIES

Relatore: Prof.ssa Elisa Cimetta
Correlatore: Dott. Lorenzo Bova
Dott.ssa Sara Micheli

Laureanda: GAIA SANTI

ANNO ACCADEMICO 2019 – 2020

Riassunto

Il Neuroblastoma è una forma tumorale pediatrica che ha origine da alcune cellule del sistema nervoso periferico. Rappresenta circa il 10% dei tumori solidi nei neonati e nei bambini entro i 15 anni. Nel 90% dei casi il neuroblastoma viene diagnosticato prima dei 5 anni. Alcuni studi fatti su cellule di Neuroblastoma in colture bidimensionali (2D) hanno permesso di ipotizzare che nella progressione metastatica del tumore abbiano un ruolo fondamentale gli esosomi, che sono delle vescicole rilasciate da tutte le cellule per scambiarsi informazioni anche a grandi distanze. In particolare, è stato osservato come le cellule tumorali producano, rispetto a quelle sane, un'elevata quantità di esosomi arricchiti in segnali pro-tumorigenici. I meccanismi attraverso i quali tali vescicole svolgano un ruolo nello sviluppo aggressivo del Neuroblastoma sono ancora poco conosciuti. Per cercare di comprenderli al meglio, un approccio può essere quello di ricreare un microambiente di coltura tridimensionale, in quanto l'ambiente 3D è molto più simile quello "*in vivo*", all'interno del corpo umano. Tale microambiente, dopo essere stato ottimizzato nella forma e nelle dimensioni, può essere utilizzato per studiare il comportamento delle cellule di neuroblastoma in presenza di esosomi, ed in particolare per studiare effetti di migrazione e conseguente maggior aggressività del tumore stesso.

In tale ottica, questo lavoro è focalizzato sulla sintesi, caratterizzazione e validazione di *hydrogels* semisintetici che presentano una base di gelatina di origine animale funzionalizzata con gruppi metacrilici. Tali materiali saranno utilizzabili come inchiostri biocompatibili per la stampa di strutture tridimensionali al fine di studiare l'interazione tra esosomi e cellule tumorali di Neuroblastoma in ambiente 3D. Inizialmente è stato messo a punto un protocollo di sintesi e purificazione del metacrilato di gelatina che ha permesso di ottenere un prodotto finale sterile e con caratteristiche meccaniche e chimiche compatibili con le applicazioni biologiche. Il materiale ottenuto è stato successivamente sottoposto ad analisi di caratterizzazione, volte alla valutazione dell'efficienza e della riproducibilità nel tempo del protocollo di sintesi. Infine, il metacrilato di gelatina sintetizzato è stato utilizzato per produrre *hydrogels* la cui biocompatibilità è stata testata con successo tramite semplici test di vitalità cellulare.

Abstract

Neuroblastoma is a pediatric cancer that originates from cells of the peripheral nervous system. It accounts for about 10% of solid tumors in infants and children within 15 years of age. In 90% of cases, Neuroblastoma is diagnosed before the age of 5. Preliminary studies on neuroblastoma cells in two-dimensional (2D) cultures allowed to hypothesize that exosomes, which are vesicles released by all cells to exchange information even at great distances, play a fundamental role in the metastatic progression of the tumor. In particular, it has been observed how cancer cells release more exosomes than their healthy counterparts, and how these exosomes carry a high amount of pro-tumorigenic markers. The mechanisms through which these vesicles play a role in f Neuroblastoma aggressiveness is still poorly understood. In order to improve our knowledge, a possible approach would be to recreate a three-dimensional culture microenvironment, since the 3D space resembles more closely what happens *in vivo* within the human body. After having been optimized in shape and size, this 3D structure will be used to study the behavior of Neuroblastoma cells in the presence of exosomes and in particular to study migration effects, reflective of a greater aggressiveness of the tumor.

This work is focused on the synthesis, characterization and validation of semisynthetic hydrogels that present a gelatin base of animal origin, functionalized with methacrylic groups. These materials will be used as biocompatible inks for printing three-dimensional structures in order to study the interaction between exosomes and Neuroblastoma tumor cells in a 3D environment. Initially, a synthesis and purification protocol of gelatin methacrylate was developed which allowed to obtain a sterile final product with mechanical and chemical characteristics compatible with biological applications. The material obtained was subsequently subjected to characterization analysis, aimed at assessing the efficiency and reproducibility of the synthesis protocol over time. Finally, the synthesized gelatin methacrylate was used to produce hydrogels whose biocompatibility was successfully tested through simple cell viability tests.

Table of Contents

Introduction

Most research on cancer biology is based on experiments performed with two-dimensional cell cultures or experiments that involve animal testing; in particular, more than 80% of cancer biologists still rely on results obtained with 2D cell cultures before testing *in vivo*[1].

Of course 2D cell cultures provide several advantages, such as highly controlled culture conditions, high reproducibility, easy cell observation, established protocols for quantitative measurements, but are also characterized by several limitations. Two-dimensional cell cultures do not faithfully reproduce real cellular conditions in human tissues, since cells are flattened in a single layer, cell-cell and cell-environment contacts are limited, cells migration is constrained and cells' polarization is abnormal.

Animal models more closely resemble human physiology with respect to two dimensional cultures, and are used to primarily monitor drug bioavailability, therapeutic efficacy, and dose-limiting toxicity[1] animal testing is actually a prerequisite in pre-clinical drug screening. However, also animal models suffer from several limitations, especially due to the dependence on the animal species, the poor availability and feasibility, and the high costs of the experiment. Moreover, ethical issues regarding experiments on animals for tumor research, are highly controversial and the general guideline is to replace animal models with mathematical modelling or *in vitro* biological systems, whenever possible.

The solution to the low representativeness of 2D models and to the necessity of avoiding test on animals for cancer studies, tissue engineering and drug discovery, was found in the development of three-dimensional (3D) structures for cell culture. Three-dimensional cell cultures (made of natural, synthetic or semisynthetic polymers) are certainly more expensive and laborious, but allow to grow cells in 3D environments, well mimicking the *in vivo* microenvironment of the human body.

The aim of this work of thesis, proposed to be the continuation of a previous research[2], concerns the development of three dimensional polymeric cultures through micro extrusion bioprinting technologies. The work was divided in several steps, starting from the production of easily reproducible, biocompatible printable materials, to the design of structures optimized in shape and size to study the migration and the motility of cancer cells in different environment conditions. The biological field of application of this research is Neuroblastoma, a malignant childhood tumor of the sympathetic nervous system that develops from immature nerve cells. In this context, the main objective was to realize 3D cultures of Neuroblastoma cells in order to reproduce cells' movement and clustering phenomena at the presence of Neuroblastoma-derived exosomes, in a more realistic environment with respect to a two dimensional one. In this perspective, several studies have confirmed that exosomes, nanovescicles released by all

cells (both healthy and cancerous), seem to play a fundamental role in Neuroblastoma cancer progression and metastatic dissemination.

Gelatin methacrylate hydrogels were selected as suitable materials for 3D scaffolds realization according to the defined goals and on the basis of the wide use of the material for similar purposes, reported in the literature. Gelatin methacrylate hydrogels are semisynthetic materials obtained from porcine gelatin molecules, modified with the introduction of methacrylic groups, and that can swell and retain large amount of water or biological fluids without dissolving and maintaining their original network structure.

The entire work done is structured in four main sections. In Chapter 1, there is a brief introduction about 2- and 3D cell cultures, together with a discussion on some important biological phenomena such as mechanotransduction and cell migration. 3D bioprinting technologies are then introduced, and gelatin methacrylate hydrogels are described as suitable materials for 3D bioprinting applications. Key information on Neuroblastoma, and on the tumor microenvironment more in general, are provided. The goals of the proposed research are then described.

In Chapter 2, procedures and methods used for project development are described and discussed. Synthesis and purification protocols of gelatin methacrylate and gelatin methacrylate hydrogels are reported, and all the tests used to characterize these materials are explained. Printing and bioprinting protocols developed are reported, and cellular experiments performed are described.

In Chapter 3, synthesis and purification methods used to obtain gelatin methacrylate are compared in terms of efficiency. Results of all the tests performed in order to characterize both gelatin methacrylate and gelatin methacrylate hydrogels are reported and discussed. Lastly, the results of all cellular tests performed are shown and explained.

In a final section, general conclusions about the methods applied and the results obtained are drawn, and improvements on the performed procedures are suggested for the continuation of the project.

Chapter 1

State of the art

In this Chapter some fundamental arguments are introduced in order to understand the project designed and developed in this work of thesis. The subjects treated in this first Chapter include: *i.* the explanation of phenomena such as mechanotransduction and cell migration, *ii* the distinction between 2D and 3D cell cultures, and *iii.* the introduction of 3D bioprinting technologies for the printing of cellular constructs. Moreover, a brief overview about hydrogels, and gelatin methacrylate hydrogels in particular, is given thanks to their properties that elect them as suitable materials for 3D bioprinting applications.
Lastly, there are a brief description of Neuroblastoma, with a focus on the features of the tumor microenvironment, and the complete specification of the targets set for proposed research activities.

1.1 Mechanotransduction

Living tissues consists of groups of cells, characterized by similar structure, that act together to perform a specific function. Cells are embedded within the extracellular matrix (ECM), the non-cellular component present within all tissues and organs, which is mainly composed of water, proteins and polysaccharides[3]. The composition of the extracellular matrix is tissue dependent; actually, ECM composition and topology are specified and generated with tissue development, through a dynamic and reciprocal biochemical and biophysical dialogue between the various cellular components and the evolving cellular and protein microenvironment[4]. The complex resulting microenvironment, which includes the ECM, mixed cell populations and a medley of cell-secreted factors, is extremely structured and lays geometric and mechanical constraints on cells[4]. Particularly, the close relationship between the local microenvironment and cells is mainly due to the presence of cell-cell and cell-ECM adhesions. These adhesive interactions contribute to the definition of cell shape and organization, and therefore directly affect cell behavior, including growth and migration.
Within the described microenvironment, cells are subjected to mechanical forces/stresses, such as pulls, distortions, compressions and stretching, that firstly affect their shape, as the result of a balancing act of different forces. Mechanical stresses do not only contribute to the definition of cells' shape, but are also experienced and then transduced by cells into a crucial set of signals that control their own structure and functions[5].

The translation of mechanical signals and deformations, characteristic of cells and tissues, into specific intracellular biochemical cues by the activation of signaling pathways or changes in the concentration of intracellular calcium, is known as mechanotransduction[6]. This phenomenon is based on mechanically induced changes in protein conformation, or inhibition of signaling protein via endocytosis, leading to junctional or cytoskeletal rearrangements, cell division modulation or cell differentiation. Despite significant progress over the last decades, the underlying molecular mechanism of cellular mechanotransduction is still not completely clear.

For several years the influence of physical and mechanical cues on stem cells fate has been ignored. Nowadays, it is well accepted that both soluble (such as cytokines and growth factors) and insoluble factors, can affect stem cells differentiation and phenotypic expression. Particularly, while much effort has intensively been focused on soluble factors influence, little is known about the importance of insoluble factors such as the density, stiffness, and dimensionality of the ECM within which stem cells are embedded. Cell adhesion to the ECM regulates both cell proliferation and differentiation; mechanotransduction is therefore the intermediate fundamental step between mechanical cues and stem cell differentiation[7].

Recently, several cancer studies focused on mechanotransduction: cancer cells form tissues characterized by abnormal mechanical properties that activate tumorigenic biochemical pathways that seem to be essential in tumor progression. All the surrounding microenvironment is affected by this variation in mechanical properties and can be altered to promote the development of the tumor itself. Aberrant changes in tissue structure and mechanics, or in the cellular response to mechanical stresses, are general features of most human diseases, not only in cancer, but also in fibrosis and vascular diseases. Accumulating evidence indicates that altered cell and tissue distortions anticipate overt disease and play a causal role in disease etiology and progression.

1.1.1 Mechanotransduction in cancer

Living tissues are complex systems within which every single cell perceives and interacts with the surrounding ones, and, in general, with the overall microenvironment, therefore influencing the whole tissue development. The chemical interaction among cells involves signals that, in the case of cancerous tissues, are abnormal or entirely absent. This is evident in uncontrolled cancerous cell growth: in normal conditions cells are able to control the production and release of growth factors involved in cell division, while tumor cells no longer respond to many of the signals that control cell growth and death. Cancer cells, in the long term, become increasingly able to escape the control mechanisms ensuring the normal growth of tissues (homeostasis),

and become able to divide rapidly, being more and more independent on signals from other cells[8]. Actually, cancer cells can evade apoptosis, the programmed cell death.
The transfer of information cannot however be confined to the chemical transfer only. The role of mechanotransduction in tumor growth and progression is generally recognized, especially in terms of metastasis' formation. Stiffness, porosity, and in general the topography of the extracellular matrix, can influence the development of tissues, since it provides them physical support and integrity. A classic feature of cancerous tissues is the augmented stiffness of the ECM: during the progression of tumors, the expression and deposition of several proteins of the extracellular matrix is strongly altered, leading to both biochemical and biomechanical changes, also inducing stiffness changes on the tumor microenvironment[9]. The increase in ECM stiffness is mainly related to the altered deposition and crosslinking of type I collagen, that ultimately affects the metastatic progression of tumors. In the specific case of breast cancer, evidence shows that an increased matrix stiffness promotes tumor development, and the insurgence of more invasive phenotypes[10].
Cancer cells, once subjected to abnormal conditions, are further able to remodel the surrounding microenvironment in order to recreate a favorable status for their growth, both physically and chemically. Cancer cells are also able to take advantage of the modified architecture of the extracellular matrix to spread in other areas, far from the main site of the tumor, giving rise to the formation of metastases. Cancer cells are characterized by a higher adaptability to the altered ECM stiffness with respect to the healthy ones; the ability to adapt to different physical conditions is essential for metastatic colonization, because secondary sites can also present highly different conditions with respect to the ones of the original tumor site[9].

1.1.2 ECM influence on cell migration

As already mentioned, the microstructure and physical properties of the ECM can significantly affect cell migration. The migration of cells in fibrous extracellular matrix is involved in several physiological and pathological processes, such as tissue regeneration, immune response and cancer progression through metastasis formation[11]. It consists in a complex dynamic process that involves both intra- and extracellular activities, including the development of filopodia, formation of local adhesion sites, locomotion due to actin filament contraction, and detachment of the rear end. Besides chemotaxis, the microstructure and physical properties of the ECM significantly influence cell migration via durotaxis, haptotaxis and contact guidance[12]. Chemotaxis is the directed motion of biological organisms as a response to an extracellular chemical signal and depends on the presence of spatial gradients of chemical substances that are identified by cells along their membranes[13]. Haptotaxis, consists in cell motion as response to a gradient of extracellular adhesion sites or substrate-bound chemo-attractant/repellents[14]. Durotaxis is a type of directed cell migration in which cells respond to a gradient of extracellular

stiffness; this means that every single cell can sense and respond to the rigidity gradient in the local microenvironment, which in turn guides its migration[15]. Contact guidance is instead described as cells- tendency to migrate along the fiber alignment direction.
During migration, cells generate active pulling forces via actin filament contraction; these forces are then transmitted to the ECM fibers through focal adhesion complexes and they result in ECM's remodeling and can also be sensed by other cells in the system. Actually, in multi-cellular systems, the pulling forces generated by individual cells can give rise to a dynamically evolving force network: forces propagate in the ECM, and influence the migration of the individual cells, which in turn alters the ECM structure and properties, and thus the tensile force network[16].

1.1.3 Biomimetic structures, from 2D to 3D cell cultures

On the basis of previous considerations, the necessity of developing natural, synthetic or semisynthetic three-dimensional structures that perfectly mimic the extracellular microenvironment inside which cells can experience physical forces as well as chemical stimuli, becomes very important.
For several years, researchers focused their attention on the influence and mechanisms of action of soluble molecules such as growth factors, cytokines, and chemotactic molecules on biological functions of living cells, just ignoring mechanical aspects. Cells behavior has largely been investigated by studying cells cultured on two-dimensional glass or plastic surfaces. Most of the actual knowledge regarding biological mechanisms therefore comes from studies on 2D cells cultures; however, tissues and organs are three dimensional and, *in vivo*, cells live in 3D structures where cell-cell and cell-environment interactions cooperatively determine the physiological phenomena.
An optimal solution was found in the development of three-dimensional polymeric structures for cell culture, which fill the gap between two-dimensional cell cultures and whole-animal systems. 3D *in vitro* models mimic features of the *in vivo* environment while taking advantage of the same tools used to study cells in traditional 2D cell cultures.
One of the main differences encountered when comparing 2D and 3D cells cultures is the dissimilarity in cells' morphology. Cells grown in monolayer systems are flat and can adhere and spread in the horizontal plane but have no support for spreading in the vertical direction. Cell-cell and cell-environment crosstalks are in this way very limited[4]. As a consequence, cells cultured on 2D surfaces have a forced apical-basal polarity, which is unnatural for most types of cells such as mesenchymal. Changes in cell geometry and organization can directly impact fundamental cell functions such as cell proliferation, apoptosis, and differentiation.
On the other hand, living cells in our tissues grow within a 3D environment where the extracellular matrix, secreted by cells, plays a supportive role for the organization of cells in

tissues and organs. In addition, cell-cell and cell-environment interactions are not limited. Actually, it is possible to see that several cell types, when isolated from tissues and placed into standard 2D culture, become progressively flatter, divide aberrantly and lose their differentiated phenotype. When these cells are transferred back in a three-dimensional culture environment, can regain their physiological form and function.

Essentially, research performed on two-dimensional cultures can be used for the understanding of phenomena relative to the single cell, while cannot be used to fully reproduce the real behavior of *in vivo* cells.

The extracellular matrix with its mechanical properties can influence adhesion, morphogenesis, stem cell differentiation and maintenance. Particularly, matrix stiffness plays a crucial role in regulating multiple cellular functions. The stiffness of the microenvironment in which cells are embedded varies according to the type of tissue considered. Wide differences in stiffness exist between soft adipose tissue and the tightly woven basement membrane, as well as between loose matrices used by cells for migration during embryogenesis, dense connective tissue in skin, and pre-calcified osteoid versus rigid mature bone[17].

In 2D cultures, cells are placed in static mechanical environments, that are supraphysiological in terms of stiffness (glass or plastic surfaces, as mentioned above). In 3D systems instead, physiological stiffness values can be obtained. This key issue must be considered when differences are noticed in the behavior of cells cultured in 2D or 3D microenvironments.

Cells in living tissues are not only subjected to passive mechanical cues. As already mentioned, tissues experience active loads, with implications at cellular level through mechanotransduction processes. Most living tissues are fibrous, structurally heterogeneous and anisotropic. The transmission of forces to cells therefore depends on the scale organization of matrix fibers relative to that of cells, and on the physical connection established between cells and the microenvironment. Cells morphology and orientation with respect to the direction of applied forces and matrix architecture can have a profound effect on the cellular response[17].

Mechanical forces are obviously perceived differently by cells cultured in 2D and 3D structures, and differences in cells' behavior is encountered accordingly.

Basically, three-dimensional scaffolds allow for in-depth analysis of biological mechanisms, reproducing more faithfully the extracellular environment, with respect to two-dimensional ones. Indeed, the simplicity of two-dimensional platforms corresponds to aberrant behaviors of cells, that display flattened shapes, abnormal polarization, altered response to pharmaceutical reagents and loss of differentiated phenotype. Three-dimensional culture systems better mimic the cellular microenvironment, where cells receive signals not just at their ventral surface but in all three dimensions[18]. Actually, the main advantage related to the use of 3D polymeric scaffolds is the control over a large number of parameters that enable the modulation of the mechanical properties of structures, for a better reproduction of native tissues' features.

In Figure 1.1[4], the differences between 2D and 3D cell cultures discussed in this paragraph are summarized.

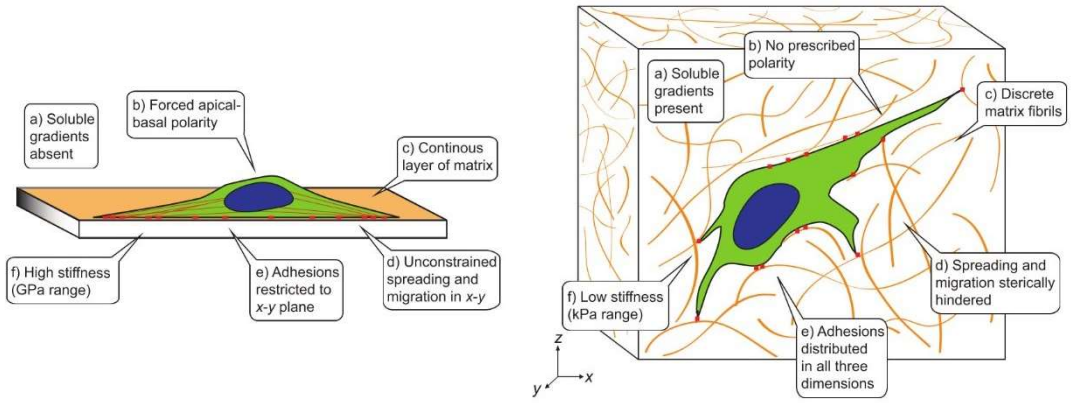

Figure 1.1. *Schematic illustration of the main differences between 2D and 3D cell cultures; adapted from Baker et al.[4].*

1.2 Three-dimensional bioprinting

Three-dimensional bioprinting technologies allow for the additive manufacturing of 3D constructs by printing multiple biomaterials, cells and biochemicals in predesigned spatial positions, with high resolution, accuracy and reproducibility[19]. Biodegradable 3D cellular constructs with intricate architectures and heterogeneous composition are printed through the layer-by-layer deposition of bioinks. High structural complexity can be achieved, making 3D bioprinting technologies relevant in the field of tissue engineering, for applications in tissue repair and regeneration, and for the development of *in vitro* models for cell biology, drug development and study of several diseases.

Certainly, the evolution of 3D bioprinting technologies has been strictly dependent on the development of biocompatible, biodegradable, easily printable polymeric materials, characterized by mechanical properties reproducing the ones of human tissues, and able to quickly undergo crosslinking in cell-compatible conditions. Photocrosslinkable polymers are actually the most suitable materials for these applications because of the exceptional spatiotemporal control over the crosslinking process given by photopolymerization, which can be performed in cell-compatible conditions, immediately after printing.

Bioprinting technologies can be classified according to several criteria. The classification can be made according to the stimuli used to assist the deposition of bioinks, the printing modality, so that it is possible to distinguish between drop-based or extrusion-based bioprinting. Another criterion is based on the mode of ejection of bioinks from the reservoir, and distinction is made between orifice-free or orifice-based bioprinting.

Independently of the mechanism used to assist the deposition of cells and biomaterials, all bioprinters include a reservoir containing the bioink to print, a system to generate the ejection of bioink from the reservoir and a receiving stage that collects the printed material. Computer-aided design and computer-aided manufacturing tools allow to generate personalized constructs, organized at different length scales[19].

The main technologies used for deposition and patterning of biological materials are inkjet, micro extrusion and laser-assisted printing. These three bioprinting technologies, that differ in the stimuli employed to assist the printing process, are described in the following paragraphs.

1.2.1 Inkjet Bioprinting

Inkjet bioprinting is a non-contact technology based on the deposition of small droplets of a bioink, with diameters on the order of tens of microns (with corresponding volumes in the range of 1-100 picolitres) onto a receiving platform with micrometer resolution[19]. Inkjet printers, also known as drop-on-demand printers, are widely used for both non-biological and biological applications.

Thermal or acoustic forces are used to eject drops of liquid onto a substrate, which can support or form part of the final construct.

In the first case, the printer head is electrically heated to produce pulses of pressure that force droplets from the nozzle. The localized heating, that can range from 200 to 300 °C, has a negligible impact on the stability of biological molecules and on the viability or post-printing cells function, because of the short heating time interval (~ 2 μs) that results in an overall temperature rise in the printer head just between 4 and 10 °C. Thermal inkjet printers allow for high print speed, are characterized by low costs and wide availability. On the other hand, cells and materials are nonetheless exposed to both thermal and mechanical stresses, low droplet directionality and non-uniform droplet size are frequently encountered, as well as frequent clogging of the nozzle and unreliable cell encapsulation[20].

In the second case, the inkjet printer is characterized by the presence of a piezoelectric crystal that, when subjected to a voltage, shows a rapid change in shape and creates an acoustic wave inside the printer head that breaks the liquid into droplets at regular intervals[20]. Alternatively, an acoustic radiation force, associated with an ultrasound field, can be used to eject liquid droplets from an air-liquid interface. Ultrasound parameters can be adjusted according to the desired size of droplets and rate of ejection. With this bioprinting technology, a high uniformity in droplets' size is obtained as well as a high ejection directionality. Furthermore, exposure of cells to heat and pressure stressors is avoided, and the potential loss of cells viability and functions is therefore reduced, and problems of nozzle clogging are not verified. Some concerns regarding the frequencies used by piezoelectric inkjet bioprinters remain because of their potential to induce damage of the cell membrane and lysis. Upper limitations on material

viscosity (10 centipoise) are anyway necessary to avoid the need of excessive forces to eject droplets when using solutions at higher concentrations[21].
In Figure 1.2[21] a simplified illustration of inkjet 3D bioprinting in its main components is shown.

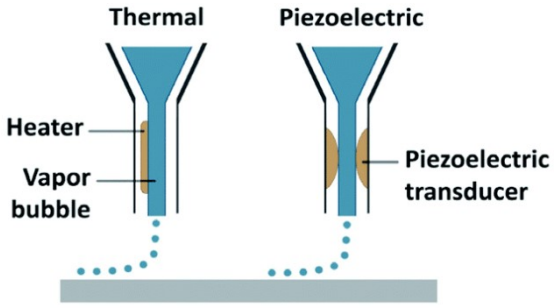

Figure 1.2. *Illustration of 3D inkjet bioprinting process, and of its main components; adapted from Selcan et al.[21].*

1.2.2 Laser-assisted bioprinting

Laser-assisted bioprinting (LAB) evolved from the conventional laser-induced transfer process, originally developed to direct writing of metals[19]. This bioprinting technology consists in the application of a high-energetic pulsed laser onto a donor ribbon, coated with the bioink to be printed, to generate the local ejection of small droplets. A near infra-red laser is generally used. Particularly, as shown in Figure 1.3[19], a typycal laser-assisted bioprinting device includes a pulsed laser beam, a focusing system, a ribbon with a donor transport support usually made of glass and covered with a laser-energy-absorbing layer and a layer of biological material prepared in a liquid solution, and lastly, a receiving substrate facing the ribbon. The absence of nozzles avoids nozzle clogging issues.

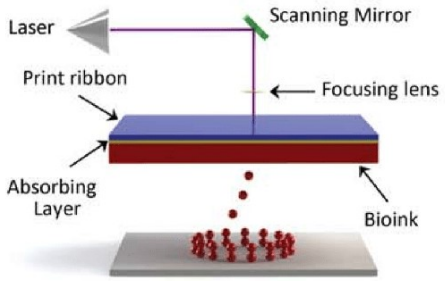

Figure 1.3. *Illustration of 3D laser-assisted bioprinting and of its main components; adapted from Pereira et al.[19].*

Several factors can affect the resolution of laser-assisted bioprinted structures, among them are the laser fluence (the energy delivered per unit area), the surface tension, the wettability of the

substrate, the air gap between the ribbon and the substrate, the thickness and viscosity of the biological layer.

LAB is increasingly being used for tissue and organ-engineering applications. Biomaterials characterized with a range of viscosity comprised between 1 and 300 mPa/s can be easily laser-assisted bioprinted. Cells are laser-assisted bioprinted without significant effect on their viability and functions, and can be deposited at a density of up to 10^8 cells/ml, with microscale resolution of even a single cell per drop. However, the high resolution is achieved through rapid gelation kinetics, that actually allow for a high shape fidelity, while resulting in a relatively low overall flow rate. Other problems have then to be considered: the preparation of individual ribbons is time-consuming and becomes onerous if multible cell types and/or materials have to be co-deposited. Moreover,because of the nature of the ribbon cell coating, it can be difficult to accurately target and position cells. Finally, metallic residues are present in the final bioprinted structure, owing to the vaporization of the metallic laser-absorbing layer during printing[19].

1.2.3 Microextrusion bioprinting

The most common and affordable biological 3D printers use microextrusion. Actually, this is the most used method to fabricate 3D cell-laden constructs for tissue regeneration. The great success of this technology is related to the possibility of printing viscous biomaterials, containing relatively high cell densities, into 3D structures with clinically relevant dimensions within a realistic time frame, that is not obtainable using inkjet or laser-assisted bioprinting. The ability to deposit very high cell densities achieving physiological values in tissue-engineered organs is a major goal for the bioprinting field.

As schematically illlustrated in Figure 1.4[21], by using this technology, a polymeric solution is loaded within disposable medical grade syringes or reservoirs, and subsequently dispensed via either pneumatic, piston driven, or rotating screw-driven force on a building platform.

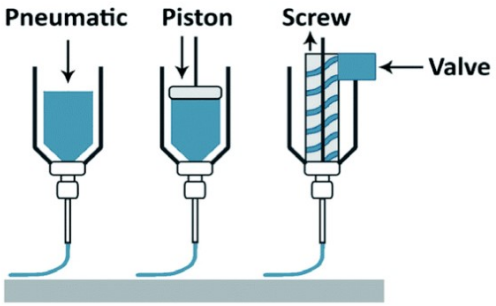

Figure 1.4. *Illustration of 3D micro extrusion bioprinting and of its main components; adapted from Selcan et al.[21].*

Pneumatic systems are more effective when working with highly viscous molten polymer, however they are associated with a delay in dispensing due to the compressed gas. The piston driven deposition often allows for more direct control over the flow of the biomaterial from the nozzle. Screw based estrusion systems ensure more spatial control and are suitable for the dispensing of polymers with higher viscosities.
Bioink viscosity and the induction of *in situ* gelation of temperature-sensitive polymers can be controlled with the inclusion of temperature-controlled modules that continuosuly allow to adjust the temperature of both the bioink and the construction platform.
Cells can be incorporated as suspended in prepolimer solutions, and then printed with high viability using pneumatic and piston-driven systems. Screw driven exstrusion systems can also be used, however it is necessary to consider that larger pressure drops at the nozzle can be generated, with detrimental consequences for the encapsulated cells; this problem can be solved by specifically designing the screw for bioprinting applications.
Cell viability after microexstrusion bioprinting is anyway lower than the one obtained with inkjet-based bioprinting. Cell survival rates stand between 40-86%, with the rate decreasing while increasing exstrusion pressure and increasing nozzle gauge[22]. The decreased viability of deposited cells results from the shear stresses inflicted on cells in viscous fluids. Dispensing pressure may have a more substantial effect on cell vability than the nozzle diameter, and therefore higher cell viability could be obtained with lower pressures and larger nozzle sizes, however obtaining lower resolution and print speed. Actually, the resolution that can be achieved with exstrusion based printers is in the order of 200 μm, that is considerably lower than the one achievable by using laser-based or inkjet-based systems. Poor resolution and low mainteinance of the predesigned shape for 3D constructs, still remain unsolved problems.

1.3 Hydrogels: a brief description

Hydrogels are highly swellable three-dimensional networks made of hydrophilic polymer chains crosslinked via covalent bonds or physical attraction, either intra- or intermolecular. In chemical hydrogels, the covalent bonds connect polymeric chains, while physical hydrogels are characterized by the presence of molecular entanglements or secondary forces (hydrogen bonds or ionic interactions). Physical hydrogels are reversible, and can be dissolved with simple variation of solvent's properties: i.e. by changing temperature and pH, or with the application of an appropriate stress[23]. Chemical hydrogels are instead irreversible, and the presence of covalent bonds ensures a higher mechanical stability of materials.
The main property of these materials is the possibility to absorb and retain water or aqueous fluids (such as biological fluids) without dissolving and maintaining their original structure, due to chemical or physical cross-linking of individual polymer chains. The water content inside

hydrogels ranges from at least 10% of the total weight (or volume), up to and even beyond 90%[23].
Hydrogels are viscoelastic materials characterized by poor mechanical features. The properties such as hardness, resistance to stress and elasticity are directly connected to the original stiffness of polymeric chains, to the presence of a higher or lower number of bonds between macromolecules and also to fluids' retention. Mechanical properties and others features such as degradation velocity and retention of fluids, can anyway be modulated with the modification of the original macromolecules.

The interest in the use of hydrogels for biological applications arises from the possibility of using them for the realization of bi-dimensional or three-dimensional scaffolds that mimic the extracellular environment and that can be used to study the behavior of different cells. As already mentioned in §1.1, several studies have shown that the cellular microenvironment contributes to the spatially and temporally complex signaling domain that directs cell phenotype, and therefore a faithful reproduction of the original extracellular microenvironment is fundamental. Actually, these materials are characterized by chemical and physical properties that can be modulated in a range that is compatible with the properties of human tissues: hydrogels scaffolds are soft and rubbery in the swollen state and can be designed in order to optimally mimic the mechanical properties of the natural extracellular matrix (ECM). Reticulated structures of cross-linked polymer chains can retain and absorb biological fluids and allow for easy transportation of oxygen, nutrients and waste (all soluble factors). In hydrogels scaffolds, cells can therefore be supported (both mechanically and in terms of nutrition) and can follow their normal life cycle, so they can maintain a high viability and their natural behavior with the possibility to grow, migrate, proliferate, differentiate, and eventually die[24].
Anyway, not all hydrogel materials are suitable for biological applications; cells can follow their normal life cycle only when encapsulated in inherently biocompatible and bioactive environments. The biocompatibility and bioactivity of hydrogel materials directly depends on the nature of polymeric chains, and, according to the origin of their polymeric chains, hydrogels can be classified as natural based, partially synthetic or completely synthetic[25].
Synthetic hydrogels are obtained through flexible and replicable processes. The main advantage in the synthesis of synthetic hydrogels is the high degree of control over the properties of the material, especially over mechanical properties and the degradation velocity; this is possible through molecular scale control of the polymeric structure. Synthetic hydrogels are however characterized by the absence of bioactive molecules that can promote cell behavior in terms of adhesion, growth, proliferation, differentiation, and secretion of molecules in the surrounding environment. Moreover, synthetic hydrogels lack the cell-binding and protease-cleavage motifs that are naturally found in ECM. This limitation can be overcome by adding cell-responsive

sites, such as integrin cell-binding motifs, to synthetic polymers, therefore engineering biomimetic materials.

Natural based hydrogels are composed of natural proteins, in particular of ECM components such as collagen, hyaluronic acid, or Matrigel, or can be obtained from other biological sources such as chitosan, alginate, or silk fibrils[24]. Natural based materials are inherently biocompatible and bioactive and are able to promote several cellular functions because of the presence of endogenous factors, which are useful for the viability, proliferation and the development of different types of cells. These materials are however affected by low batch to batch consistency, that result in the inevitable variability in terms of cell proliferation, differentiation and migration inside the same types of hydrogel. The control over mechanical and biochemical properties in natural hydrogels is not high and time of degradation could be inconsistent with experimental time[25]. In natural materials, the risk of contamination is very high due to the presence of impurities.

The development of bioactive hydrogels for three-dimensional cell culture is therefore a complex problem. The goal would be to engineer semi-synthetic materials, combining the strengths of both synthetic and natural hydrogels, obtaining highly reproducible, biocompatible and bioactive hydrogels, with easily modulable properties. One of the major challenges facing the use of hydrogels for tissue engineering is the ability to replicate tissues' mechanical and viscoelastic characteristics.

1.3.1 Suitable materials for 3D bioprinting

Hydrogels are suitable materials for 3D bioprinting applications, mainly because of the possibility to rapidly form them *in situ* and in the presence of cells, through a variety of physical and chemical crosslinking methods, including photopolymerization. Particularly, photopolymerization, through the incidence of light energy selected at appropriate wavelengths, provides an exceptional control over the spatiotemporal formation of the hydrogel and over its network properties, including crosslinking density and matrix stiffness.

Free radical photopolymerization includes three steps. Firstly, a photosensitive system made of unsaturated prepolymers, cells and photoinitiators is irradiated with UV light or visible light, at specific wavelengths, to excite the photoinitiator and initiate the formation of free radicals. Secondly, radicals created from light exposure give rise to the formation of new free radicals and crosslinks between polymeric chains. Reaction proceeds as long as light exposure is ensured, and termination reactions take place (third step).

Photopolymerization offers several advantages with respect to other crosslinking methods, but also has a few drawbacks, including oxygen inhibition, lack of control over the crosslinking kinetics, and the generation of heterogeneities within the hydrogel network. Elements of inhomogeneity in the network, that result from the random chain polymerization, affect

mechanical integrity and swelling behavior of the constructs[19]. For cell encapsulation applications, it is also necessary to consider the potential deleterious effects of UV light irradiation, the cytotoxicity of radicals generated by the disassociation of photoinitiators, and the local inflammation due to unreacted double bonds[26]. Particularly, radicals generated by the action of photoinitiators can react with cellular components in the propagation step both via direct contact or the formation of reactive oxygen species, therefore affecting cell viability and ultimately inducing DNA damage. The reduction of deleterious effects on biological systems can be firstly obtained by using light sources in the UV-A range or visible lights, by the selection of appropriate light wavelengths, intensity and irradiation time. To ensure high cell viability, the selected wavelength must overlap the absorption spectra of photoinitiator. Then, the concentration of photoinitiator must be optimized considering a trade-off between crosslinking time and cell viability. Efficient and biocompatible photoinitiators must be selected; among them, the most used are Irgacure 2959 (1-[4-(2-Hydroxyethoxy)phenyl]-2-hydroxy-2-methyl-1-propane-1-one), LAP (lithium phenyl-2,4,6-trimethylbenzoylphosphinate) and VA-086 (2,20Azobis[2-methyl-N-(2-hydroxyethyl)propionamide])[26].

1.3.2 Gelatin based hydrogels: GelMA

A significant number of natural, synthetic and semisynthetic hydrogels have been successfully used to reproduce the ECM microenvironment for biological and medical studies. Among them, gelatin methacrylate (GelMA) hydrogels are often selected because they are semisynthetic materials, in which the biocompatibility of natural matrices and the reproducibility, stability and modularity of synthetic biomaterials are combined.

Gelatin is a natural protein extract, obtained through heat denaturation and partial hydrolysis of collagen extracted from skin, bones and connective tissue of animals[27]. Collagen is the primary organic constituent of native tissues, and about 90% of the 29 identified types of collagen in the human body are fibrillary. Type I collagen is the most common type and as such is the major structural component of many tissues[18]. Gelatin can be obtained by performing acid or basic treatment of collagen. Type A gelatin results from acid treatment (pH 1-2) and its isoelectric point is around pH 7-9, while type B gelatin is produced from alkali treatment (pH 12-13) and it has an isoelectric point around pH 5-6. The Bloom strength ranges from 90 to 300 g for porcine skin derived gelatin.

The overall process used to obtain gelatin is relatively inexpensive if compared to processes applied for other protein-based biomaterials, even because collagen is obtained as a by-product of the meat-processing industry[28]. Furthermore, gelatin is biodegradable and highly biocompatible. Actually, in contrast to collagen, gelatin exhibits lower antigenicity due to heat denaturation, and it retains cell-binding motifs such as arginylglycylaspartic acid (RGD) and

matrix metalloproteinase (MMP)-sensitive degradation sites, fundamental for cell encapsulation.
Gelatin can only form physical (reversible) hydrogels, stable under a limited set of gelatin concentrations and temperatures, and that are characterized by weak mechanical strength. However, gelatin can be chemically modified to enable chemical crosslinking between macromolecules, and therefore to obtain chemical hydrogels, irreversible and stable under a wider range of temperature. Several chemical strategies can be applied. One possibility is the addition of small molecule chemical reagent to cross-link gelatin macromolecules. Another possibility is the methacrylation, with different degrees of functionalization, of the amino groups of gelatin macromolecules, to obtain a photoreactive product known as gelatin methacrylate[29]. Actually, the addition of functional groups to gelatin backbone is a crosslinking strategy characterized by higher control over hydrogel design and properties if compared to direct crosslinking techniques. Moreover, photopolymerizable gelatin derivatives undergo quicker and more homogeneous crosslink compared to other derivatives obtained through the addition of small molecules[30]. What is crucial is that chemical, physical and mechanical properties of GelMA can be easily tuned by manipulating the ratio of its components.

GelMA hydrogels are widely used for biomedical applications, because of their suitable biological properties, the tunable physical characteristics, the ease of manipulation, the biodegradability and the low cost. GelMA hydrogels closely resemble some essential properties of native extracellular matrix (ECM), because of the presence of cell-attaching matrix metalloproteinase responsive peptide motifs, which allow cells to proliferate and spread in GelMA based scaffolds. Mechanical properties can simply be modulated to mimic the extracellular environment. GelMA polymers can therefore be used to prepare hydrogel-based three-dimensional cell culture models for cancer and stem cell research, as well as for tissue engineering applications. Using photolithography and 3D bioprinting, it is feasible to fabricate micropatterned 3D cell-laden GelMA hydrogel containing single or multiple cell lines for engineering different tissues. Gelatin is also an interesting base material for engineering hydrogels for drug delivery[28].

1.4 Neuroblastoma

Neuroblastoma is a malignant tumor of the sympathetic nervous system, which is part of the autonomic nervous system and that is responsible of the activation of the so-called fight or flight response. It is an extracranial tumor that originates from neuroblasts, primitive neuroephitelial cells of the embryonic neural crest, and it is the most common form of embryonal tumor. It can develop anywhere along the sympathetic nervous system and is mainly seen in very young children. Actually, according to the research of AIRTUM (Associazione Italiana Registri

Tumori), Neuroblastoma and other tumors of the sympathetic nervous system represent the 7% of all the tumors identified for children between 0 and 14 years old, while the 5% in the range from 0 to 19. In most cases, children are affected by Neuroblastoma in their first year of life, and the presence of the tumor can be identified within five years of life.
Generally, neuroblastoma tumors originate in the adrenal glands (Figure 1.4), that are endocrine glands placed above kidneys, but then can spread in other areas including the chest, the spine or spinal cord regions and the abdomen, because of the formation of metastases.

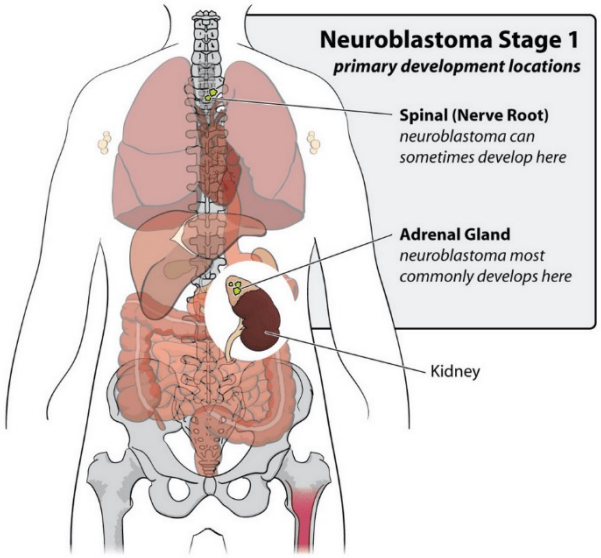

Figure 1.5. *Representation of the primary development locations of Neuroblastoma tumors.*

Bone marrow is the main site where Neuroblastoma metastasizes. Indeed, cancer cells are not only able to proliferate against the normal rules of growth but, in malignant cases, can also invade and colonize other areas of the body, since they can move by entering blood or lymphatic vessels. The abnormal reproductive capacity and the possibility to migrate toward other regions ensure tumor development.
One of the main problems is that, almost in the 50% of the analyzed cases, Neuroblastoma tumors are detected in a metastatic phase: the more cancer metastasizes, the more complicated becomes its complete removal and therefore the probability to save patients' life. Neuroblastoma is characterized by one of the lowest survival rates of all childhood cancers, with only 67% of patients surviving to five years.
Different therapies are selected according to the stage of the cancer. When possible, surgical removal of the tumor is always the first choice. In the case of advanced tumor stages, chemotherapy and radiotherapy are the most common choices. Certainly, the best situation would be an early detection of cancerous cells, anticipating the formation of metastasis.

1.4.1 Tumor microenvironment

Cancers are complex systems, closely associated with a dynamic biological landscape, which is mainly composed of fibroblast, myofibroblasts, neuroendocrine cells, adipose cells, immune and inflammatory cells, blood and lymphatic vascular networks, and extracellular matrix. The presence of other tissue-specific cells depends on the location of the tumor. Cancer cells constantly interact with their surrounding microenvironment: they alter their behavior in response to changes in the microenvironment, but also modify their environment to create a more physically, chemically, and metabolically hospitable niche conducive to continued disease progression[31].

Cancer development and progression require extensive reorganization of the extracellular matrix[32]. Cancer cells interact with their extracellular matrix through a combination of mechanical interactions, enzymatic manipulation of the matrix structure, or signaling interactions, leading to changes in the degree of inflammation and hypoxia of the tumor microenvironment as well as its levels of intracellular signalling[31].

During tumor growth, cancer cells induce changes in the stroma by secreting signaling proteins that alter the behavior of stromal cells, while stromal cells in turn affect tumor cells in different ways, secreting signaling proteins that stimulate their growth and division, and also proteases that reshape the extracellular matrix.

Cancer cells interact with the immune system, causing both pro-tumorigenic and anti-tumorigenic behaviors. The immune system helps maintaining a continuous state of inflammation in the tumor microenvironment, promoting cancer cell growth and metastasis as well as angiogenesis in the tumor microenvironment.

Cancer-associated fibroblasts (CAFs) have a significant impact on cancer progression through remodeling ECM, inducing angiogenesis, recruiting inflammatory cells, and directly stimulating cancer cell proliferation via the secretion of growth factors, immune suppressive cytokines, and mesenchymal cell interactions[33].

The tumor microenvironment is therefore the first promoter of tumor growth and supports the formation of metastasis. It also ensures the protection of the tumor from the immune system of the host organism, and it reinforces the resistance to chemotherapy.

1.4.2 Exosomes

Exosomes are nanoscale membrane vesicles with a diameter ranging from 20 to 300 nm. They are released both by healthy and cancerous cells (Figure 1.6[34]), and can be found in biological fluids, such as blood, urine, amniotic fluid, breastmilk, bronchoalveolar lavage and synovial fluids, under both physiological and pathological condition. Exosomes contain different

molecules and carry signals through the RNA content, in particular, microRNAs, proteins, lipids and DNA.

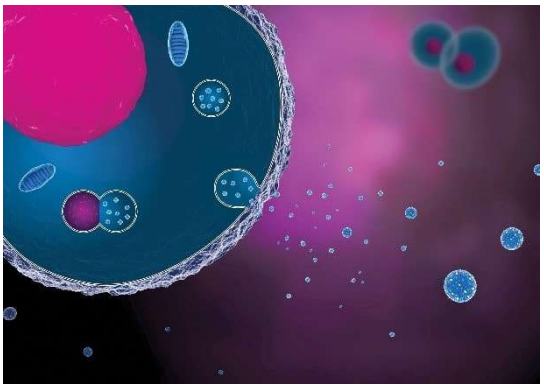

Figure 1.6. *Release of exosomes from the cellular membrane; adapted from Deaaboul G.*[34].

Exosomes seem to be involved in the communication between tumor cells and the surrounding microenvironment and have been identified as key elements in Neuroblastoma's growth and dissemination[35]. Actually, Neuroblastoma-derived exosomes express a discrete set of molecules involved in defense response, cell differentiation, cell proliferation, and regulation of other important biological processes, and can therefore play a fundamental role in modulating the tumor microenvironment to ensure tumor progression.
The knowledge of the different communication methods adopted by Neuroblastoma cells in order to organize an environment conducive to their growth is studied for early detection of cancer and also for the development of targeted treatment.
Neuroblastoma is generally discovered in the metastatic phase, when the possibility of patient survival is already very low; the idea is therefore to use molecules and substances that are present inside exosomes, as biomarkers for early diagnosis.
Precise knowledge of the molecules and signals involved in the communication between cancerous and healthy cells should then be the basis for the development of therapy strategies, intended to reduce the risk of metastasis formation and relapse. Actually, the majority of patients affected by Neuroblastoma and then healed of cancer, have recurrences in the bone marrow.

1.4.3 Mesenchymal stem cells (MSCs)

As already mentioned, Neuroblastoma frequently metastasizes in the bone marrow, the soft gelatinous tissue that fills the medullary cavities of bones. The bone marrow contains two types of stem cells, mesenchymal and hematopoietic. The red bone marrow, known as myeloid tissue, consists of a delicate, highly vascular fibrous tissue containing hematopoietic stem cells, which

are blood-forming stem cells. The yellow bone marrow, known as fatty tissue, contains mesenchymal stem cells.
Mesenchymal stem cells are multipotent stem cells, primarily present in the yellow bone marrow and, in a smaller amount, in other tissues, such as the adipose one, the Wharton's jelly, the peripheral blood and others. MSCs are characterized by a high differentiation potential, can undergo differentiation generating fibroblasts, chondroblasts, lipoblasts, osteoblasts, neurons, and others, being involved in tissues' regeneration. The differentiation of MSCs is characterized by complex mechanisms and is influenced by several factors; not all of them are already well known. MSCs are also characterized by anti-inflammatory and immunomodulatory properties and therefore have a direct control on the immune system, being able to deactivate the immune response. MSCs exercise neuroprotective function and are involved in the management of the hematopoietic niche in the bone marrow, ensuring the survival of hematopoietic stem cells (HSCs) promoting their differentiation or quiescence.
Mesenchymal stem cells are involved in the progression of neuroblastoma in the bone marrow, favoring the formation of metastasis[36]. This is verified when tumor derived exosomes, produced in large amount, are internalized by MSCs, that, according to the set of information received, differentiate and organize the tumor microenvironment. These cells are able to prepare an optimal environment for the proliferation of cancerous cells, protecting them from external factors, allowing their growth and proliferation, basically playing an essential role in metastasis formation[11].

1.5 Aim of the thesis

The work described in this thesis was started as the continuation of an earlier project[2]. On the basis of the results already achieved, the research target referred to the production of gelatin methacrylate hydrogels for the realization of three dimensional scaffolds, through microextrusion bioprinting, for cancer cells studies. Within this goal, the following sub-targets were set and pursued:

- The definition of a synthesis and purification protocol to obtain gelatin methacrylate in a defined range of degree of functionalization, compatible with subsequent biological applications of the material, followed by the study of the material, designed in order to verify the efficiency of the methods applied and for its physiochemical characterization.
- The evaluation of the biological consistency of gelatin methacrylate hydrogels prepared with the synthetized material, studying how the polymer concentration affects properties such as swelling, porosity and viscoelasticity, and performing simple cellular viability tests before working on the material printability.

Chapter 2

Materials and methods

This Chapter presents a description of all the procedures and methods used for project development. Firstly, the methods of synthesis and purification of gelatin methacrylate are described, together with the analyses performed to characterize the obtained material; secondly, gelatin methacrylate hydrogel preparation and characterization are discussed. Three-dimensional printing and bioprinting applications using gelatin methacrylate hydrogels bioinks are then introduced, with the complete description of cellular tests performed.

2.1 Gelatin methacrylate (GelMA) synthesis and characterization

GelMA synthesis, firstly proposed in 2000 [38], is based on the reaction of free amino groups of lysine/hydoxylisine residues in gelatin molecules with methacrylic anhydride (MAA), with the formation of methacrylic acid as a by-product (Figure 2.1[39]).

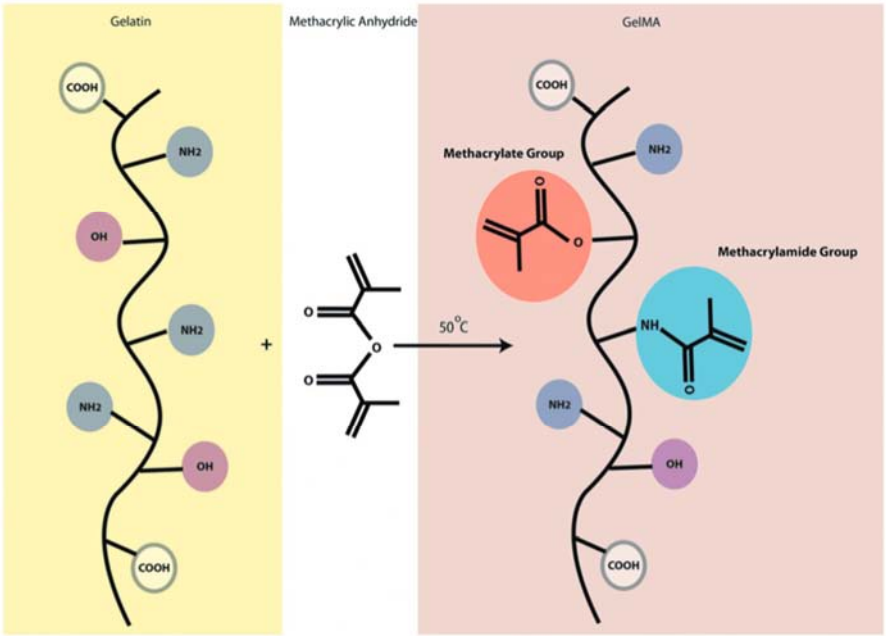

Figure 2.1. *Methacrylation of gelatin using methacrylic anhydride. The chemically modified gelatin contains methacrylate and methacrylamide groups which enable it to be photocrosslinked by the assistance of a photoinitiator; adapted from Modaresifar et al.*[39].

According to the original protocol, the reaction is carried out under physiological conditions (pH ≃ 7.4[1]) by dissolving gelatin in a phosphate-buffer saline (PBS) solution at 50°C, at an initial concentration of reagents selected depending on the desired degree of functionalization (DoF) of gelatin molecules. The control over the pH of reaction is maintained with acid or basic adjustments during the reaction time, and therefore during the two hours starting from MAA addition, particularly in the first half hour.

The original method of synthesis was studied in detail and modified in order to optimize all reaction's parameters. However, several subsequent studies proved that the original method is suboptimal, leaving considerable room for improvement, especially in terms of controllability and efficiency. In particular, performing the methacrylation according to the original protocol always requires a high excess of anhydride, regardless of the desired DoF; this can be reduced through the increase and careful control of the pH of the reaction solution, while keeping it below the upper limit to avoid the hydrolysis of the reagent.

Free amino groups of lysine in gelatin macromolecules can react with MAA only if they are neutral; the maximum efficiency of methacrylation reaction is therefore achieved when the pH of the reaction solution is maintained above the isoelectric point (IEP) of gelatin. For type A gelatin, the IEP value stands between pH 7 and 9. The methacrylation reaction can be performed with the minimum MAA molar excess to achieve degrees of functionalization up to 100%, by dissolving gelatin in a buffer solution such as a 0.25 M sodium carbonate-bicarbonate (pH ≃ 9.6), with acid pH adjustments before the introduction of MAA. Several studies showed that the optimal pH value of the reaction solution for type A gelatin is 9[29,40]. At pH values between 10 and 11, methacrylation is penalized by the hydrolysis of MAA.

Basically, if at a theoretical level the reaction of each free amino group occurs with a single anhydride molecule, using PBS a molar MAA concentration of 13 to 44 times higher than the concentration of free amino groups is required, while using a carbonate-bicarbonate (CB) buffer a molar MAA concentration of 1 to 2.2 times higher than the concentration of free amino groups is necessary[29].

In Figure 2.2[29], a schematic illustration of how solution pH affects the ionization of free amino groups on type A gelatin is shown.

[1] All the reported pH values, unless specified, are evaluated at ambient temperature.

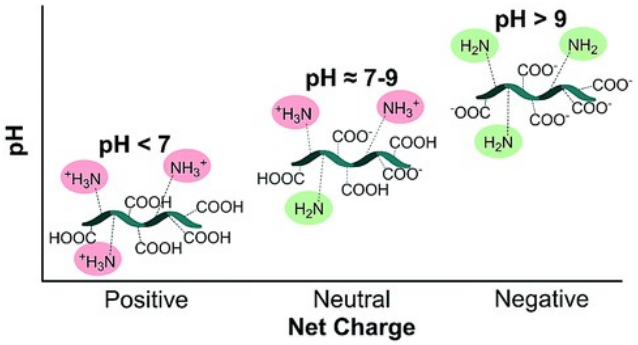

Figure 2.2. *Schematic illustration of how solution pH affects protonation stage of free amino groups on type A gelatin; adapted from Lee et al.*[29].

The concentration of MAA is directly dependent on the desired degree of functionalization and on the pH of the buffer. Actually, it has to be considered that the pH of the reaction solution lowers gradually as the reaction takes place because of the formation of methacrylic acid, and this penalizes the reaction and always implies the need for molar excess of MAA, independently of the buffer solution selected.

Gelatin concentration is a parameter that cannot be modified significantly in order to promote the reaction. Particularly, for gelatin concentration lower than 10% (w/v), phase separation arises with the formation of an aqueous and an organic phase; as a consequence, MAA cannot disperse homogeneously and functionalization is not possible because of the formation of drops of anhydride inside the reaction solution. If gelatin concentration is at least equal to 10% (w/v), the reaction takes place effectively; the greatest efficacy of the reaction occurs at a gelatin concentration equal to 20% (w/v)[40].

In order to carry out the methacrylation reaction effectively, it is obviously necessary to work at a higher temperature than the gelation point of gelatin (which in any case depends on its concentration in the solution). When gelatin is homogeneously dissolved, it is possible to ensure the dispersion of the anhydride molecules through the optimal mixing of the solution.

Experimentally it has been verified that the influence of temperature on the effectiveness of the reaction is not so crucial. An upper limit on temperature variation is imposed by the possibility of the denaturation of gelatin. The reaction is usually performed at 50°C.

Reaction time is generally varied between 1 and 2 hours. Several studies confirmed that the reaction between MAA and amino groups goes to completion within an hour, and this can be verified just by studying the variation of the pH of the reaction solution: relatively high pH variation is measured in the first half hour, corresponding to high reaction progress, while moderate pH reductions are verified in the second half hour, indicating minor reaction progress. No substantial pH changes are usually seen in the next hour. This explains the careful pH control performed in the first half hour of reaction; reaction time is anyway usually extended to up to two hours to guarantee the desired result in terms of DoF.

Different efficient protocols are available for the synthesis of GelMA, and they all give minor variations to the original method explained before.

In this project, two methods were selected and used to obtain gelatin molecules with a degree of functionalization between 50 and 70%. The first one[2,41], referred to as Method A, basically corresponds to the original synthesis method. Briefly, type A porcine skin gelatin (300 bloom), from Sigma-Aldrich, is dissolved in 1M PBS solution (pH ≃7.8) at a 10% (w/v) concentration. After complete gelatin dissolution under vigorous magnetic stirring (~ 400 rpm) at 50°C, 140 µl of MAA (Sigma-Aldrich) per gram of native gelatin are added dropwise. During the addition of MAA and for the first half hour of reaction, the pH of the reacting solution is regularly controlled, and, if necessary, adjusted to 8 with 3M NaOH. The reaction is considered as completed in around two hours and the final DoF of gelatin molecules should be around 70%.

The second method performed[37], referred to as Method B, is the optimized version of the synthesis, and was used in this context in order to obtain gelatin molecules with a DoF between 50 and 70%. Basically, type A porcine skin gelatin (300 bloom), from Sigma-Aldrich, is dissolved in 0.25 M CB buffer solution (pH ≃ 9.6), at a 10% (w/v) concentration. The solution is maintained under vigorous magnetic stirring (~ 700 rpm) at constant temperature in a water bath at 44°C. After complete gelatin dissolution, the pH of the solution is measured and adjusted to a value between 9.1 and 9.3; this value is selected in order to have a trade-off between the highest reaction efficiency, and the highest buffering effect. Always under vigorous stirring, 50 µl of MAA per gram of native gelatin are added dropwise to the solution. Reaction is considered completed after two hours since MAA addition. After two hours, the pH of the reacting solution is measured and lowered to a value equal to 7.5, with the addition of HCl (37%), in order stop the reaction.

Table 2.1 shows a schematic comparison between Method A and Method B; the main parameters for the synthesis of GelMA are considered.

Table 2.1. *Schematic comparison between Method A and Method B.*

	Method A	**Method B**
Buffer type	Phosphate Buffered Saline solution	Carbonate - Bicarbonate solution
Buffer's molarity [M]	0.15	0.25
Buffer pH (at 25°C)	8.00	9.56
Reaction Temperature [°C]	50	45
MAA/gelatin [µl/g]	140	50
pH adjustments	Basic (NaOH 3M)	Acid (HCl 12M)
Time of reaction [h]	2	2
Expected DoF [%]	70	50-70

2.1.1 Purification methods

Once the reaction is completed, GelMA has to be recovered, with the separation of unreacted MAA, methacrylic acid, and salts resulting from the original buffer solution. In this project, because of the desired biological applications, GelMA purification must be done in order to obtain a sterile product.

Two purification methods were tested. The first one[41] involves the refrigeration of the final solution to 4°C, and a GelMA separation from the solution through precipitation in large excess of ethanol (~1:8 v/v), used at - 20°C. At this point, the resulting heterogeneous mixture is rapidly centrifuged at 3000 rpm for 10 minutes, the ethanol is replaced and the solution is centrifuged a second time. Through this method it is possible to obtain solid GelMA pellets. These pellets are then vacuum dried until complete ethanol removal. GelMA pellets can be stored at - 20°C for several weeks. The use of ethanol as a means of separation allows to have a sterile final product, without any other extra step. This purification method was used only in association with the first GelMA synthesis protocol[2,41].

The second purification method[37] is based on dialysis and is more complicated than the first one, since it involves several steps:

- At the end of the reaction the solution is divided into volumes of maximum 10 ml, and centrifuged at 3500 rpm for 3 minutes at room temperature, in order to have a first separation of unreacted MAA and GelMA. The unreacted anhydride settles down, and the supernatant liquid phase, mainly composed of GelMA, can be directly withdrawn by a serological pipette, and transferred to a new tube.
- The solution is then transferred into flexible cellulose acetate tubing dialysis membrane, with a molecular weight cut-off between 12 and 14 kDa (Sigma-Aldrich), previously sterilized in boiling water (100°C) for 5 minutes. The dialysis, performed to remove the residual anhydride, the methacrylic acid and to desalt the solution, is carried out for at least 72 hours, against demineralized water (changed at least twice daily), at 40°C. The process of dialysis is considered as completed when the GelMA solution appears clear (not opaque). Due to the photosensitivity of GelMA, the solution is protected from light during dialysis.
- The solution is then filter-sterilized using 0.2-µm syringe filter units in order to remove potential biological contaminants.
- The solution is frozen in two steps, first at -80°C and then with liquid N_2 at -196°C, and eventually freeze-dried. In order to maintain a sterile barrier during lyophilisation, GelMA solution is placed in test tubes sealed with vented screw-top caps (CELLTREAT Bio-Reaction Centrifuge Vented Tube Cap, Cole-Parmer). Freeze-drying is performed until the complete drying of GelMA (almost three days).
- The purified and dried product can be stored at -20°C, protected from light and moisture.

This purification method was used in association with both the first and the second GelMA synthesis protocols tested.

2.1.2 Nuclear Magnetic Resonance, DoF determination

The degree of functionalization of gelatin macromolecules can be easily determined with proton Nuclear Magnetic Resonance (H NMR). This test is done in order to verify the reproducibility of the methods used for GelMA synthesis.
Nuclear Magnetic Resonance Spectroscopy is an analytical technique that allows to obtain detailed information on the structure of a molecule, observing the behaviour of its atomic nuclei when placed in an external magnetic field. NMR can only detect nuclei with a non-zero spin since, once subjected to an external electromagnetic field, they are forced to rotate and align with the magnetic field itself (basically, they undergo orientation). Particularly, it is necessary to consider that:

- when the number of protons and neutrons are even and are equal, the nucleus has no spin and there are no phenomena of magnetic resonance;
- if summing the number of neutrons and the number of protons of a nucleus, an odd number is obtained, then the nucleus has a half-integer spin, equal to or a multiple of ½;
- if both the number of protons and of neutrons are odd, then the atomic nucleus has an integer spin (i.e. 1, 2, 3).

Accordingly, the nucleus of ^{12}C has no magnetic spin, as well as the number of protons and neutrons are even and equal. Considering instead ^{1}H and ^{13}C, the resulting spin is different from zero, and is a half-integer spin. When ^{1}H is subjected to an external electromagnetic field, two are the possible orientations, one corresponding to m (magnetic quantum number) equal to – ½ and the other corresponding to m equal to + ½. The nuclear magnetic moment is not perfectly aligned with the external magnetic field, it oscillates, simply performing a precession motion. The two possible states of the nucleus are not characterized by the same energy, since the state with the positive magnetic quantum number corresponds to a slightly lower energy with respect to the one with negative magnetic quantum number. The precession motion of nuclear magnetic moments occurs with a frequency that is proportional to this energy difference, that increases as the external applied field increases; this is known as Larmor frequency. The equilibrium between the two possible states is quickly reached and, on average, only 50% of the nuclei immersed in the magnetic field are oriented; the remaining half assumes the opposite orientation. It is possible to excite these nuclei into the highest energy level with electromagnetic radiation, characterized by a specific frequency. The frequency of radiation depends on the external magnetic field, on the characteristic of the nucleus examined and on the chemical environment of single protons. According to their chemical environment, the

protons of a molecule are shielded in different ways, and thus the NMR signal of a certain nucleus is displaced in the spectrum at higher or lower frequencies. This happens because the electrons that belong to the neighbouring atoms, when immersed in the external magnetic field, generate a small magnetic field with their movement, opposite to the applied one. This secondary magnetic field shields the examined nucleus from the full strength of the applied field; the greater the electron density, the greater the corresponding shielding from the external field, and the neighbouring nuclei undergo the transition at a lower frequency than the ones placed in other areas (characterized by limited presence of electrons). The resulting displacement in NMR signal for a given nucleus is known as chemical displacement. In general, protons (^{1}H) or carbons (^{13}C), that are adjacent to electronegative atoms, are de-shielded so they feel as more intense the applied magnetic field and undergo transition at higher frequencies, and in the spectrum are found at a higher chemical displacement.

The reproducibility of GelMA synthesis, performed with the two synthesis methods, was therefore studied with the analysis of NMR spectra of samples made of 20 mg of dried GelMA dissolved in 0.7 ml of deuterium oxide; at least three GelMA samples for each synthesis batch were analysed.

Particularly, regarding the interpretation of the H NMR signals, it has to be considered that:

- the number of signals corresponds to the types of protons that are present;
- the position of signals is related to the shielding;
- the strength of signals is directly related to the number of specific types of protons;
- signal splitting shows the number of protons that are present on adjacent atoms.

In Figure 2.3[29], a schematic representation of a molecule of GelMA is reported, in which the protons that can be identified in NMR spectrum with signals (peaks) are marked with letters, from a to f:

- acrylic protons of methacrylamide grafts of lysine groups (a);
- acrylic protons of methacrylamide grafts of hydroxyl lysine groups (b);
- methylene protons of unreacted lysine groups (c);
- methyl protons of methacrylamide grafts (d);
- acrylic protons of methacylated grafts of hydroxyl groups (e);
- methyl protons of methacylated grafts of hydroxyl groups (f).

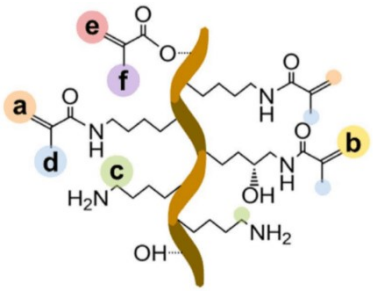

Figure 2.3. *Schematic illustration of GelMA corresponding to 1H NMR peaks; adapted from Lee et al.*[29].

2.1.3 Fourier Transform Infrared Spectroscopy, FTIR

Fourier Transform Infrared Spectroscopy (FTIR) is an analytical technique based on the interaction between electromagnetic infrared radiation and matter, that can be used to identify the presence of functional groups within both organic and inorganic molecules. It is a non-destructive molecular analysis, that measures transitions between vibrational energy levels that occur when molecules, exposed to IR radiation ($2.5\ \mu m \leq \lambda \leq 50\ \mu m$), absorb infrared photons and move from a fundamental energy state to an excited vibrational one. Frequencies of absorbed and transmitted radiations are recorded by the instrument.

FTIR analysis equipment includes Michelson interferometer, that allows to obtain the interferogram for every analyzed substance. The interferogram is then converted into a traditional infrared spectrum through Fourier transform function implementation, so that it is possible to obtain a graph that represents signal intensity (% of Transmittance or % of Absorbance) as a function of radiation wave number or wavelength; this conversion is simply performed by the computer connected to the instrument.

Distinctive chemical groups of GelMA can be identified with FTIR spectroscopy, since their presence is directly associated with absorption peaks at specific frequencies. In order to have a first proof of the successful methacrylation of gelatin molecules, FTIR analyses were performed on GelMA samples and spectra were compared to the FTIR spectrum of gelatin. Only GelMA samples obtained with Method B and purified through dialysis were analyzed.

2.1.4 Thermogravimetric analysis, TGA

Thermogravimetry is an analytical technique used to study the thermal stability of a material and of the components of its volatile fraction, by measuring the mass variation that occurs under a specific temperature program, in a controlled atmosphere.

Commercial instruments for thermogravimetric analysis include a sensitive analytical balance, a furnace, a purge gas system, and a microprocessor for instrument control, data acquisition and

display. Figure 2.4[42] schematically shows the main components included into a TGA instrument.

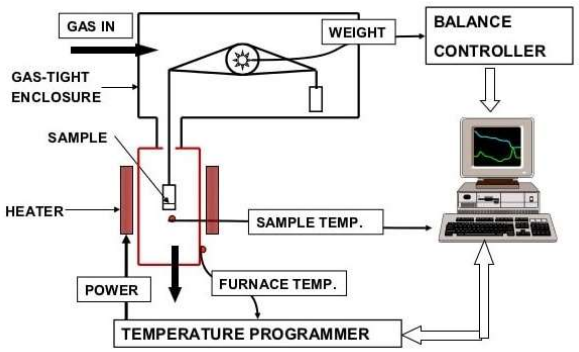

Figure 2.4. *Schematic illustration of the main components included in a TGA instrument; adapted from Raju P.M. S.*[42].

Commercially available thermobalances have a range of 1 to 100 mg, however the most common thermogravimetric instruments are provided with balances with a range of 5 to 20 mg. The sample holder is housed in the furnace, while the rest of the balance must be thermally isolated from it. Inside the furnace, temperature can be varied from 25 to 1500 °C, with heating rates selected by the operator, even up to 200 °C/min. Thermal insulation of the furnace is necessary in order to avoid heat transfer to the balance. Nitrogen or argon fluxes can be used to study thermal stability of materials in an inert atmosphere, but analyses are usually concluded in oxygen atmosphere. The temperature of the sample is generally measured with a thermocouple located in close proximity with the sample container; direct contact is actually avoided to prevent catalytic decomposition of samples, or their contamination, resulting in weighing errors. The microprocessor connected to the instrument, on the basis of the voltage output of the thermocouple, automatically adjusts the voltage to the heater to comply with the correct temperature plan set by the operator. TGA instruments are conceptually simple, but at the same time extremely sensitive and precise, requiring periodic control and calibration.
The analysis result is a thermogram, or a thermal decomposition curve, that is a plot of mass or mass percent as a function of time. TGA enables detection of physical processes such as vaporization, sublimation, and desorption, as well as decomposition and oxidation reactions. The main application of TGA is on polymers studies, because it allows to obtain information about decomposition mechanisms and thus giving operating conditions for the desired materials.

In this project, TGA analysis were performed on GelMA samples obtained with Method B, to assess the efficiency of freeze-drying process, and to evaluate the thermo-oxidative stability of the material, in order to establish an appropriate temperature program for DSC analysis. GelMA

samples from two synthesis batches were analysed, respectively characterized by a DoF of 55% and 71%, respectively. Analyses were performed both in inert and oxygen atmosphere: GelMA samples were heated at 10 °C/min from ambient temperature (25 °C) up to 40 °C; samples were then maintained at 40 °C for 20 minutes, in order to ensure water evaporation before the material degradation, and, finally, heated up to 300 °C.

2.1.5 Differential Scanning Calorimetry

Differential scanning calorimetry (DSC) is a thermal technique used to measure how the heat capacity of a material varies with temperature. Basically, with the controlled thermal scan of a sample, performing appropriately selected heating or cooling programs, changes in its heat capacity are tracked as changes in the heat flow. With DSC analysis it is possible to identify glass transitions, crystallization, and phase changes of several materials, such as polymers, metals, and ceramics. DSC is the most commonly used thermal technique for the evaluation of material purity, and, since it allows to evaluate the efficiency of purification processes, it is used for quality controls.

Commercially available instruments for differential scanning calorimetry analyses are power compensation calorimeters or heat flux calorimeters. Regardless of the instrument type, the operating principle is the same: the aim is to measure differences in heat flow into a sample and a reference, as a function of the sample temperature, while these are subjected to a controlled temperature program in a controlled inert atmosphere.

In power compensated DSC, the sample and the reference are introduced and heated in two separate identical cells, and their temperatures are kept equal. In both cells, temperature is varied linearly over time, with heating and cooling rates selected by the operator. Through a secondary control circuit, the power supply of the two furnaces is regulated so as to eliminate temperature differences that arise due to exothermic or endothermic processes occurring in the sample. The power change signal is recorded as a function of the sample temperature. Figure 2.5[43] shows a schematic illustration of the operating principle of power compensation DSC.

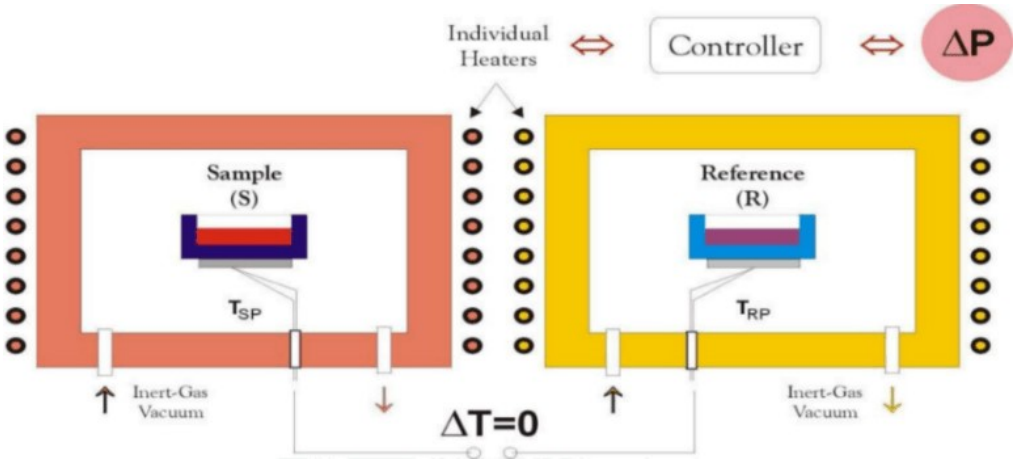

Figure 2.5. *Schematic illustration of the operating principle of power compensation Differential Scanning Calorimetry; adapted from Sabere A. S. B. M.*[34].

In this project, heat flux differential scanning calorimetry was performed with a Q200 model instrument (Figure 2.6.a). In a heat flux differential scanning calorimeter, both the sample and the reference are placed in the same thermally insulated cell (Figure 2.6.b), in a controlled atmosphere of N_2.

(a) (b)

Figure 2.6. *Heat flux Differential Scanning Calorimeter, Q200 model (a), and the thermally insulated cell opened with inside both the sample and the reference aluminium pans.*

The reference is an empty aluminum pan, while the sample aluminum pan is filled with 5 to 10 mg of the material to be analyzed (solid or liquid). A specific temperature program is selected and applied: heat flows into the sample and reference pan through an electrically heated

thermoelectric constantan platform. Temperature differences between the sample and the reference pans are due to endothermic or exothermic phenomena that take place in the analyzed material. The difference between the heat flow sent to the sample and the reference to keep them at the same temperature, is measured by thermocouples placed below each pan. The differential heat flow is directly proportional to the difference between the signals output from the thermocouples.

DSC analyses were performed on GelMA samples obtained with Method B and purified through dialysis. The temperature program applied on samples was defined on the basis of the results of thermogravimetric analysis: GelMA samples were first cooled at - 10 °C/min from ambient temperature (25 °C) down to -40 °C; samples were then heated at 10 °C/min up to 220 °C and finally cooled down to -40°C again.

2.2 GelMA hydrogels preparation and characterization

With the variation of GelMA synthesis parameters, it is possible to obtain gelatin macromolecules characterized by different degrees of methacrylation. Depending on the degree of functionalization of amino groups, macromolecules can bind together differently and consequently form three-dimensional networks characterized by different properties. Not only functionalization, but also the concentration of GelMA affects the final properties of hydrogels. Particularly, in this project, hydrogels were prepared at 5, 8, 10 and 13% (w/v) of dried GelMA in 1x PBS solution (pH ≃ 7.4). The choice of these concentration values was determined by the planned cellular tests, and is clearly explained in §2.4.

Crosslinking of functional groups can be initiated using various systems, however, only a few are suitable for simultaneous crosslinking and cells encapsulation; photo-polymerization is one of them. GelMA is a photopolymerizable (and therefore photosensitive) material, which under the presence of suitable photoinitiators, and exposed to UV radiation, undergoes crosslinking through a radical polymerization mechanism. Photo-polymerization allows for high spatial control of crosslinking, that takes place relatively quickly, and even at ambient temperature.

Hydrogel preparation consists of GelMA dissolution in 1x PBS at 50°C, under vigorous magnetic stirring, immediately after the complete dissolution of Irgacure 2959, the photoinitiator, added at a 1:100 w/v ratio. Light-curing was performed with UV LED at 365 nm, with an exposure time varied between 60 and 120 seconds, depending on the concentration of GelMA in the hydrogel. Figure 2.7[28] shows a schematic representation of GelMA crosslinking process: upon generation of a free radical (by light exposure in the presence of a photoinitiator), GelMA chains polymerize via radical addition-type polymerization, to yield a network of gelatin chains connected through short poly-methacryloyl chains.

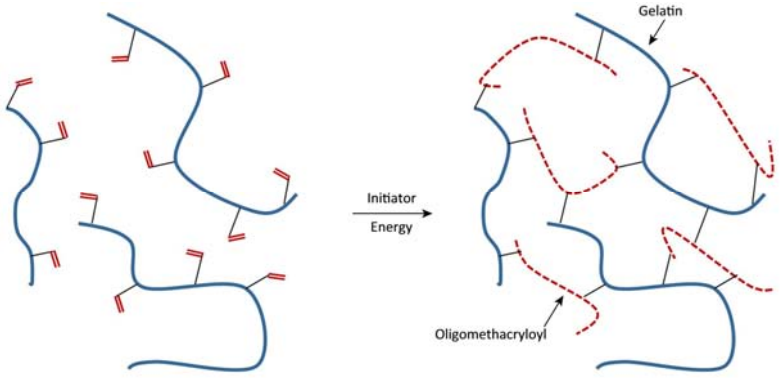

Figure 2.7. *GelMA crosslinking process; adapted from Klotz et al.*[29].

Together with the DoF of original GelMA macromolecules, and with the concentration of the material, the parameters of photo-crosslinking critically influence the properties of the resulting hydrogel. In particular, the optimization of light exposure time, light intensity, and initiator concentration are therefore fundamental in order to obtain hydrogels with specific properties.
The photoinitiator can be selected depending on the desired application of the hydrogel. In the case of biological applications, biocompatible initiators are necessary. For GelMA crosslinking, Irgacure 2959 from BASF is generally used for its relatively low cytotoxicity if compared with other photoinitiators, and because it can be activated under UV-A radiation exposure. Particularly, this water-soluble initiator, disassociates into a benzoyl and ketyl-free radical upon UV light irradiation, through an α-cleavage reaction (Figure 2.8).

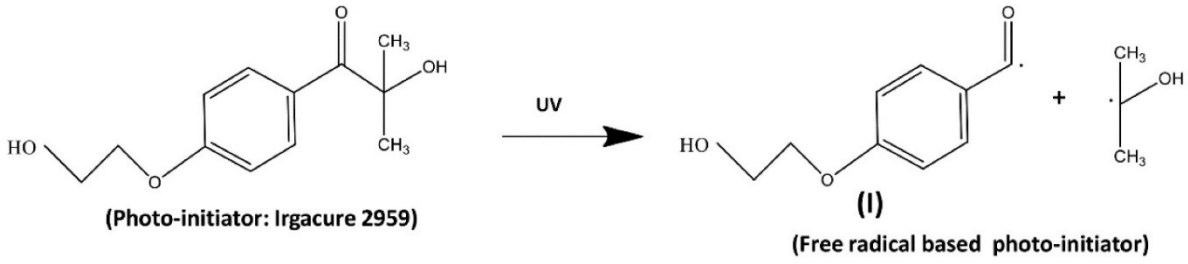

Figure 2.8. *Disassociation of Irgacure 2959 into a benzoyl and ketyl-free radical determined by UV light irradiation.*

Given the final biological application envisioned for the hydrogels, the exposure time to UV radiation has to be optimized; in this sight, exposure time was limited up to a maximum of 120 s, in order to reduce cellular apoptosis.
Furthermore, because of their application in a biological field, hydrogel solutions were prepared with different arrangements for maintaining sterility, depending on the purification method applied to obtain GelMA. Specifically, for GelMA samples purified with ethanol, no further precautionary measures were applied to ensure the final sterility of the hydrogel, already

guaranteed by the use of ethanol itself. For GelMA samples obtained through dialysis method, all necessary measures to preserve sterility were taken, and therefore hydrogel preparation was always performed under a biological hood, dissolving the sterile lyophilized GelMA in a filter-sterilized solution made of photoinitiator and PBS.

2.2.1 Swelling properties

In chemically crosslinked hydrogels, hydrophilic polymer chains are linked by covalent bonds forming three-dimensional networks. The main property of hydrogels is the capability to swell in aqueous environment (i.e. in the presence of biological fluids), absorbing large amounts of water without dissolving, and thus maintaining their original network structure. Hydrogels permeability and swelling strongly depend on the chemical nature of the polymer macromolecules, on the crosslinking structure and on its morphology, and therefore on the pore size, on the molecular weight of the chain sections between successive crosslinks, and on the concentration of the polymer in the hydrogel. The hydrogel swelling is the result of the slow absorption of water through the polymeric network; particularly, the swelling force is counterbalanced by the spring force of the crosslinked structure, and when these opposite forces are equal, the swelling equilibrium condition is reached.
The swelling degree of a hydrogel, and the possibility to retain and exchange aqueous fluids are fundamental factors in biological applications. The swelling degree evaluation, together with the determination of the hydrogel porosity, can be used to ensure that the encapsulated cells have the necessary nutrients available for their survival, growth, proliferation, and, at the same time, that they can expel waste substances. Moreover, the porosity of the hydrogels has an influence on the ability of cells to migrate and also to their possibility to exchange information with the surrounding cell or microenvironment.

The pore size of the polymeric network, and, in general, the overall morphology of the GelMA hydrogel, depend on the degree of functionalization of gelatin molecules, on GelMA concentration, on the concentration of photo-initiator, on the UV-exposure time interval, and on the interaction between polymer and solvent. In this project, the main aim was to understand how the concentration of GelMA, characterized by the same DoF, could affect hydrogel swelling. For this purpose, GelMA-based hydrogels samples were prepared at different polymer concentrations, 5%, 8%, 10%, and 13% (w/v), selected according to the desired biological applications. Ten cylindrical hydrogel samples for each GelMA concentration were realized, using PDMS annulus molds, with 8 mm diameter, 2 mm height and an overall volume of 100 µl. Light curing was performed with a UV LED, at 365 nm wavelength: the exposure time to UV radiation was of 60 s for all the samples besides the ones at 5% GelMA concentration, exposed for 120 s. The shape, volume and exposure time to UV radiation of samples were the

same used for biological tests (§2.4.5). After photo-polymerization, samples were placed in petri dishes with 3 ml of 1X PBS, and then placed in incubator at 37 °C, in a controlled atmosphere of CO_2 (5.2%) and O_2 (20.1%), for 24 hours, required to reach the swelling balance[21]. After 24 hours of incubation, samples were removed from PBS, softly dried at their surfaces with absorbent paper, and weighted (W_s), and then let air-dry for three days. After three days, when completely dried, samples were weighted again (W_d).
In order to characterize the swelling degree of hydrogel samples, it was then possible to evaluate the percentage swelling ratio, %SR, as:

$$\%SR = \frac{W_s - W_d}{W_d} \cdot 100 \quad . \tag{2.1}$$

The percent water content, %WC, was then evaluated as:

$$\%WC = \frac{W_s - W_d}{W_s} \cdot 100 \quad . \tag{2.2}$$

These tests were performed separately on hydrogels obtained with GelMA synthetized using the Method A and then purified with ethanol and with GelMA obtained with Method B and then purified through dialysis.

2.2.2 Porosity characterization

The study of the morphology and structure of GelMA hydrogels was completed by Scanning Electron Microscopy (SEM) analysis, in order to determine how polymer concentration affects porosity. GelMA-based hydrogels samples were prepared at the same polymer concentrations specified for the swelling tests, 5%, 8%, 10%, and 13% (w/v), using GelMA obtained with Method B and purified through dialysis, with a degree of functionalization equal to 71%. Two cylindrical hydrogel samples for each GelMA concentration were realized, using PDMS annulus molds, with 16 mm diameter, 2 mm height and an overall volume of 500 µl. Light curing was performed with a UV LED, at 365 nm wavelength: the exposure time to UV radiation was of 60 s for all the samples, besides the ones at 5% (w/v) GelMA concentration, exposed to UV light for 120 s to ensure the stability of the material after photopolymerization. Samples were then placed in petri dishes with 3 ml of 1X PBS, and then incubated at 37 °C, in a controlled atmosphere of CO_2 (5.2%) and O_2 (20.1%), for 24 hours. After 24 hours of incubation, samples were removed from PBS, cooled down to -80 °C and freeze-dried (Figure 2.9); freeze-drying allows to maintain the hydrogel structure that would instead collapse with simple air drying. Freeze-drying can alter the porosity of the material, however since the effect of the drying process was the same on all samples, regardless of GelMA concentration, it was evaluated as negligible according to the main aim of the analysis.

(a) (b)

Figure 2.9. *GelMA-based hydrogel sample before (a) and after (b) freeze-drying. Samples used for porosity analysis.*

Freeze-dried samples were then analyzed with a Scanning Electron Microscope (SEM). To perform this analysis the hydrogel sample must be prepared following these steps: the samples were attached to the sample stage using a conductive copper tape (Figure 2.10) and gold spray deposition under high vacuum was performed (Figure 2.11). Finally, the samples were placed in the microscope support, as shown in Figure 2.12.

Figure 2.10. *Freeze-dried hydrogel samples at 5%, 8%, 10% and 13% (w/v) GelMA concentration, attached to the sample stage with conductive tape, before vacuum spray of gold film.*

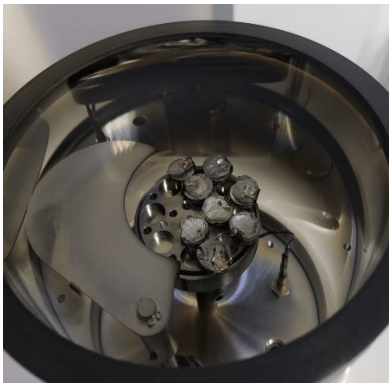

Figure 2.11. *Freeze-dried hydrogel samples at 5%, 8%, 10% and 13% (w/v) GelMA concentration, covered with a thin gold film.*

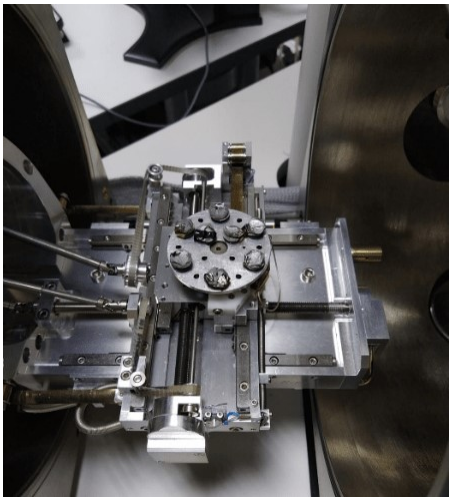

Figure 2.12. *Freeze-dried hydrogel samples at 5%, 8%, 10% and 13% (w/v) GelMA concentration, covered with a thin gold film and introduced in the electron scanning microscopy support.*

All samples were examined only on their upper surface. Images of hydrogels at 5, 8, 10 and 13% (w/v) GelMA concentration were then analyzed with ImageJ to evaluate the frequency distribution of pores diameters, grouped in classes of the same amplitude, and an overall analysis of data distribution was performed using a box plot diagram. Data were analyzed using MATLAB.

2.2.3 Dynamic oscillatory shear tests

Dynamic oscillatory shear tests were performed on GelMA-based hydrogels samples in order to study potential changes in their viscoelastic behavior at varying GelMA concentration.
Dynamic mechanical testing consists on the measurement of the strain or stress response of a material when subjected to a sinusoidal stress or strain, at determined frequencies and temperatures of interest. A motor is used to apply a sinusoidal stress or a strain to a sample, and the resulting response is measured with a force transducer (stress) or with a position sensor (strain). In order to remain within the linear viscoelastic region, maintaining a linear relation between the applied stress or strain and the measured quantities, small stress or strain amplitudes are applied in all the oscillatory experiments. This allows to measure properties as function of time or frequency, at constant temperature. With dynamic oscillatory shear tests it is possible to decouple and measure the elastic and viscous components of the response of a polymeric material: the elastic component is immediate, while the viscous one is delayed and responsible for an overall delay in the material response to stress or strain. The resulting phase shift between stress and strain, δ, stands between 0° and 90° ($\delta \in]0°; 90°[$) for viscoelastic materials and represents an index of the elasticity of the sample. δ is equal to 0° for elastic materials and to 90° for viscous ones. Consequently, if $\delta = 45°$ or, equivalently, if $tan(\delta) = 1$,

the material is equally elastic and viscous. The phase shift can be used to determine the elastic or storage modulus *G'* and the loss modulus *G''* of the material. The storage modulus is a measure of the elastic response, while the loss modulus is a measure of the viscous response and represents the energy that is dissipated as heat. The square root of the sum of squared *G'* and *G''* is the complex modulus, *G**, used to evaluate the complex viscosity η^*.

In this context, dynamic oscillatory shear tests were performed using a rotational parallel plate rheometer, ARES-RFS model, shown in Figure 2.13.

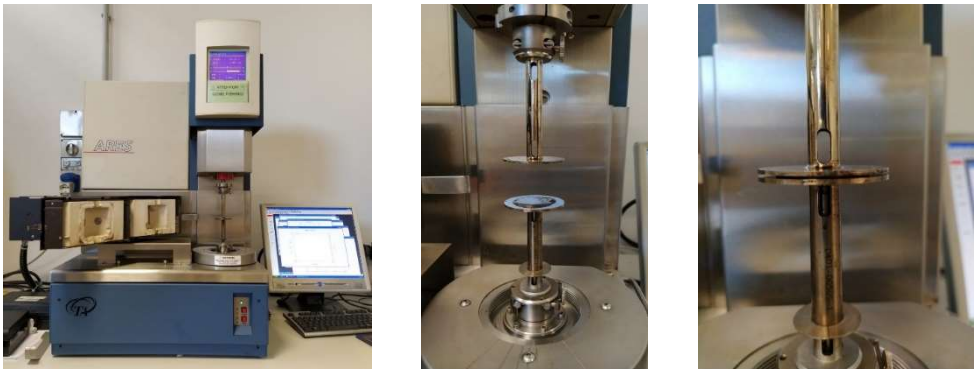

(a) (b) (c)

Figure 2.13. *Rotational parallel plate rheometer, ARES-RFS model (a); circular plates of the rheometer (b,c).*

Tests were carried out on cylindrical hydrogels samples, with 16 mm diameter, ~2 mm high and overall volume of 450 µl, obtained with PDMS molds. Samples were prepared using GelMA obtained with Method B, purified through dialysis, and characterized by a DoF of 55%. Tests were performed at 37°C, in strain-controlled mode. The rotation frequency of the lower circular plate of the rheometer was set to vary from 0.1 to 100 rad/s, with a displacement ramp of 0.5%, selected in order to keep the oscillation amplitude within the linear viscoelasticity range/edge.
The following equations were used to evaluate G', and G'', at the imposed experimental frequency ω:

$$G^I(\omega) = \frac{\tau}{\varepsilon}\cos(\delta) \quad , \tag{2.3}$$

$$G^{II}(\omega) = \frac{\tau}{\varepsilon}\sin(\delta) \quad , \tag{2.4}$$

$$\frac{G^{II}}{G^I} = \tan(\delta) \quad , \tag{2.5}$$

τ is the tangential shear stress and ε the deformation response of the material.

Data were processed using MATLAB.

2.3 Cellink bioprinter, applications

Three-dimensional printing and bioprinting tests were performed with the INKREDIBLE™ bioprinter model, developed and sold by Cellink®, the Swedish biotechnology start-up, officially found in 2016 by Erik Gatenholm. The INKREDIBLE bioprinter, shown in Figure 2.14, is a pneumatic-based extrusion bioprinter, with dual printerheads and a UV LED curing system. A compressor is used to convey air to the extruders.

Figure 2.14. Cellink® INKREDIBLE bioprinter.

The dual-printerheads system allows to print different hydrogels at the same time. This is fundamental for biological applications since it gives the opportunity to use different cells types in the same structure, without changing the extruder and pausing the bioprinting process. The presence of this system therefore ensures shorter printing time.
The UV light curing system is integrated within the bioprinter; this model is equipped of a 365 nm LED that can be activated immediately after the print is done and therefore, by using suitable photo-initiators (according to the available wavelength), it is possible to crosslink a structure without removing it from the printing support.
The bioprinter also has an integrated memory where G-Code files are stored, and it can be used even without any computer connected. In this context, structures to be printed were designed with AUTOCAD® 2020, exported as STL files (Stereo Lithography interface format) and then converted into machine language with Slic3r, and saved as G-Codes. Every G-code contains sequences of commands, parameters and instructions, in the form of coordinates, that the printer follows to print objects. Particularly, Slic3r is an open source slicing software that allows to define printing parameters, such as the number of layers for a single structure, their height, the

structure's percent infill and the corresponding fill pattern, the printing speed, the filament dimension, and the number of available extruders. Structures' design and printing parameters' selection were directly correlated to the type of bioink and to the end-use of structures.
This bioprinter model is not provided with the Cellink's patented Clean Chamber Technology, that allows to operate under sterile conditions; it can however be easily placed under a biological hood. One problem concerning this bioprinter model is the lack of a temperature control system, thus making the use of temperature-sensitive bioinks more difficult.
Extruders are sold separately, as well as tips. The nozzle diameters of tips are available in the range from 0.25 mm to 0.41 mm. Both the extruders and tips can be sterilized for biological applications.

2.3.1 GelMA hydrogels for 3D printing

GelMA hydrogels, obtained as described in §2.2, were used as bioinks for three-dimensional printing and bioprinting applications. In three-dimensional printing, there are constraints on the concentration of GelMA in hydrogels and on the operating temperature conditions that are related to thermal reversibility and to the viscosity of the material. In three-dimensional bioprinting applications, in addition to the aforementioned limitations, there are also constraints, on the same parameters, related to the viability of encapsulated cells.
Three-dimensional printing tests were performed as trial tests, carried out in order to evaluate the optimal operating conditions for subsequent three-dimensional bioprinting tests: the main aim was the development of a printable material useful for cells encapsulation, and the identification of optimal printing conditions.
In order to achieve these goals, GelMA with fixed DoF (that according to the performed synthesis methods was never higher than 60%), was used at different concentrations to obtain hydrogels, as described in §2.2, for the purposes of:

- ensuring the three-dimensional printability of structures with different degrees of complexity, with high resolution, avoiding their collapse before light curing, and preventing grainy filament condition;
- avoiding clogging of the printer-heads;
- having a UV-exposure time equal or lower than 120 s;
- having printing pressures below 200 kPa;
- having high printing speed ($\leq$ 4 mm/s), to limit the influence of temperature on the viscosity of the hydrogel.

The viscosity of hydrogels was at first optimized modifying GelMA concentration, and varying the refrigeration time prior to printing. The viscosity of GelMA hydrogels is highly sensible to

temperature, because these are thermo-reversible materials and therefore, above and below determined temperature values, dependent on GelMA concentration, gel-sol and sol-gel transitions occur. In the first case, viscosity is too low and the material is not printable, in the second case, viscosity is too high and determines grainy filaments and frequent printer-heads clogging. In both cases, the bioink is not homogeneous.

The optimization of the bioink for three-dimensional printing does not exactly correspond to the one of bioinks for three-dimensional bioprinting applications. Bioinks for 3D bioprinting is partially composed of cells homogeneously suspended in their growth medium, and, even though this can be introduced at maximum in the ratio 1: 25 (v/v) with respect to the hydrogel, it changes the overall material viscosity. The firs optimization, performed with GelMA hydrogels without encapsulated cells, is anyway fundamental in order to determine printing parameters such as the percent and the fill pattern of the infill, the printing speed, and the UV exposure time for light curing. The refrigeration time prior to printing, and printing pressure cannot be pre-determined for bioprinting and need to be reoptimized.

According to previous results[2], the concentration of GelMA in hydrogels was fixed at 13% (w/v) for both printing and bioprinting applications; below this concentration it is actually not possible to print structures with high resolution, and under 10% (w/v) of GelMA in hydrogel, printability is almost completely lost. This upper limit in GelMA concentration to obtain optimal hydrogels for 3D printing of structures with high resolution, was evaluated using GelMA obtained with Method A and purified with ethanol.

For the biological applications developed in this project, it would be ideal to use hydrogels at 5% (w/v) GelMA concentration. In hydrogels characterized by lower concentration of GelMA, cells should experience a normal life cycle, come into contact with surrounding cells, not being restricted to a rounded shape because of the high density of the surrounding environment, and migrate[45].

A first solution to approach this problem was to realize 3D cylindrical scaffolds with encapsulated cells using PDMS annulus molds, as described in §2.4.5. The main idea was to verify biological results with these simple cylindrical scaffolds, and then, eventually, to use natural-based additives to increase the viscosity of the hydrogel, keeping GelMA concentration at the desired value, to obtain a printable bioink.

2.3.2 3D printing protocol

The optimization of GelMA-hydrogel bioinks for 3D bioprinting applications, was carried out performing 3D printing tests. The protocol used for 3D printing of structures with one extruder follows.

The GelMA hydrogel at the desired concentration is prepared as described in §2.2. The hydrogel is then stored into a test tube, and kept in the liquid state at 37°C. The hydrogel is introduced

into a disposable extruder with a syringe (avoiding the formation of air bubbles), and placed at 4°C for 8÷15 minutes, depending on GelMA concentration. After refrigeration, when the hydrogel is viscous enough but not grainy, the extruder is loaded on the printer. A tip with an appropriate nozzle diameter has to be selected according to the structure to be printed. The desired printing support (a petri dish, a multiwall plate, or a glass slide) is placed on the mobile plate of the printer. At this point the instrument is calibrated and the compressor is activated. The G-Code of the desired structure, loaded on the bioprinter integrated memory, is selected. Printing pressure is manually set up to 250 kPa by the operator, by means of two knobs located on the printer side, one for each extruder. Once the structure is printed, light curing can be performed with the UV LED of the bioprinter.

2.4 Biological validation

GelMA-based hydrogels were used as scaffolds to perform cellular tests with human embryonic kidney 293 cells (HEK 293), neuroblastoma cells (SK-N-AS) and mesenchymal stem cells (MSC). HEK cells were firstly used to perform preliminary viability tests. The tests were performed in order to evaluate cell viability when encapsulated in 3D hydrogel scaffolds. Potential cell migration and clusters formation was assessed using neuroblastoma cells, with or without neuroblastoma-derived exosomes conditioning. This behavior has already been observed in the laboratory using traditional two-dimensional cell cultures. Mesenchymal stem cells were finally used in sight of the planned co-culture experiments. Three dimensional scaffolds with encapsulated cells were realized both with 3D bioprinting, and with PDMS molds, as explained in the following paragraphs.

2.4.1 2D cellular cultures

The cell lines used to carry out the experiments, were grown in conventional 2D cell culture, using T-flask with vented caps; particularly, T-25, T-75, or T-150 were used according to the necessary area for the cell culture, of 25 cm^2, 75 cm^2, 150 cm^2, respectively. Cell cultures were maintained in a controlled atmosphere (20% of O_2, 5% CO_2) at the physiological temperature of 37°C. Different cells types require different growth media, with the necessary nutrients for their survival and growth, in controlled pH conditions. SK-N-AS requires a growth medium made of 87% Dulbecco's Modified Eagle Medium (DMEM), 10% Fetal Bovine Serum (FBS), 1% Penicillin-Streptomycin, 1% Glutamine and 1% of Mineral Essential Medium (MEM).
The growth medium for bone marrow derived MSC cell culture, is made of 90% MesenCult™ MSC Basal Medium (Human) and 10% MesenCult™ MSC Stimulatory Supplement (Human). HEK 293 require a growth medium made of 88% DMEM, 10% FBS, 2.5% Glutamine, and 2.5% Penicillin-Streptomycin.

Culture media also include phenol red, $(C_6H_4OH)_2C_7H_4SO_3$, whose color is sensible to pH: in alkaline solutions red phenol takes on a red color, it turns orange in neutral ones, and yellow in acid ones. The color shift of the growth medium from red to yellow is due to the attack of carbohydrates by microorganisms and makes it possible for the operator to understand when it is necessary to substitute it.

2.4.2 3D Bioprinting protocol

In order to bioprint 3D structures with encapsulated cells, it is necessary to work in sterile conditions, to avoid any type of contamination and therefore to prevent testing failure. The bioprinter was therefore always used under the biological hood, and the necessary extruders, syringes, nozzles, were sterilized before using by autoclaving at 121°C for 40 minutes.
All the 3D structures with encapsulated cells were printed using 13% (w/v) GelMA hydrogels, prepared as described in §2.2, and therefore considered and treated as sterile.
The complete bioprinting protocol followed for these experiments, regardless of the cell line used, assuming the use of T-75 flasks, is reported below; all these steps are performed in sterile conditions:

- Once 80-90% cells confluence is reached inside a T-75 flask, the growth medium is removed, and a light washing with 7 ml of HBSS is performed in order to remove dead cells, cellular debris and waste.
- HBSS is removed and 3 ml of 0.04% trypsin are used to detach the cells from the culture flask, that is placed in the incubator for 5 minutes; actually, 0.04% trypsin is a dilute solution of the enzyme trypsin, a pancreatic serine protease, used in order to loosen cells from cell cultivation plates. The time limit of 5 minutes is set to avoid damage to nuclear membranes.
- After 5 minutes, cells' detachment is verified, and the trypsin solution is deactivated by adding at least 6 ml of cellular medium; at least a double volume of medium with respect to the trypsin one is actually necessary for its deactivation.
- The resulting solution, made of cells suspended in growth medium and trypsin, with an overall volume V, is removed from the T-flask and placed inside a falcon tube; 1 ml of the solution is set aside for cell count, while the remaining volume is centrifuged at 1000 rpm for 5 minutes (soft deceleration activated) in order to obtain a pellet of cells.
- Cell count is performed in the spin time. The 1 ml solution, set apart for cell count, can also be diluted with growth medium to simplify this step. Anyway, 10 µl of the original solution (or of the diluted one) are mixed with 10 µl of Trypan Blue solution (0.4%), a stain used to quantify live cells by labelling dead cells exclusively. Especially, Trypan Blue cannot penetrate the cell membrane of live cells, while it can pass through the porous cell membrane of dead cells, entering and staining in blue their cytoplasm.

Bürker chamber can be used to determine the average number of live cells per volume unit of the resulting solution of Trypan Blue and medium, N_c. The number of cells in the original volume V, can be evaluated as:

$$N_{cells} = N_c \cdot 2 \cdot \mathrm{V} \cdot 10^4 \quad , \tag{2.6}$$

where 2 is a dilution factor that derives from the dilution with Trypan Blue solution, and 10^4 is a correction factor for the Bürker chamber.

- Once the centrifuge is completed, the solution of trypsin and growth medium is separated from the cellular pellet, settled at the bottom of the falcon tube. The pellet is subsequently re-suspended in fresh growth medium. This step is performed gently and slowly in order to limit cell death and air-bubbles formation, but, at the same time, ensuring the break of clusters of cells. The re-suspension is carried out with a volume of medium that depends on the number of cells previously evaluated, on the number of cells desired per ml of hydrogel, and on the maximum amount of medium that can be added to the hydrogel to avoid excessive variation in its viscosity, such as not to compromise bioprinting performances. Specifically, the number of cells encapsulated per ml of hydrogel was varied between $40*10^3$ and $6*10^6$, always maintaining a medium-hydrogel volumetric ratio below 1: 25.
- The solution of growth medium and cells is slowly added to liquid hydrogel, at 37°C, and appropriately mixed obtaining a homogenous solution.
- At least 2.5-3 ml of the hydrogel solution with encapsulated cells is loaded with a syringe into a sterile extruder, that is then sealed with parafilm and placed at 4°C for 8-10 minutes. The refrigeration time is varied in order to obtain a printable, not grainy material.
- The extruder is loaded into the printer, placed under the biological hood, with sterile tip, with an appropriate nozzle, selected depending on the structure to be printed. The printing support (a petri dish, multiwell plate, or glass slide) is placed on the printing plate.
- The G-Code of the desired structure, already loaded on the bioprinter integrated memory, is selected. Printing pressure is modulated by the operator, and always maintained below 200 kPa, in order to limit cells' death. Once the structure is printed, photopolymerization can be easily performed with the UV LED of the bioprinter. UV light exposure time is limited to 60 s. The polymerized printed structure is covered with growth medium and placed in incubator at 37°C, in a controlled atmosphere.

  If it is necessary to repeat the bioprinting procedure to have more technical replicates for the same experiment, the hydrogel solution with encapsulated cells can be refrigerated again, simply placing the charged extruder (appropriately sealed) at 4°C.

Hydrogel refrigeration can be performed no more than three times in order to avoid cell death.

2.4.3 Bioprinting with SK-N-AS cells

3D bioprinting of GelMA-hydrogels with encapsulated neuroblastoma cells was performed to evaluate cellular viability inside 3D hydrogel structures, and to verify the potential migration of cells at the presence of neuroblastoma-derived exosomes, added to the growth medium used to cover the printed structures.

For these purposes, the structure represented in Figure 2.15 was designed: 2.15.a shows the structure designed with AutoCAD (dimensions in mm), while Figure 2.15.b shows how the printing of the overall structure was performed according to the pattern fill and percentage of the infill selected. The structure is composed of two layers, each 0.3 mm high, and is characterized by four separate areas for the evaluation of cell viability and migration.

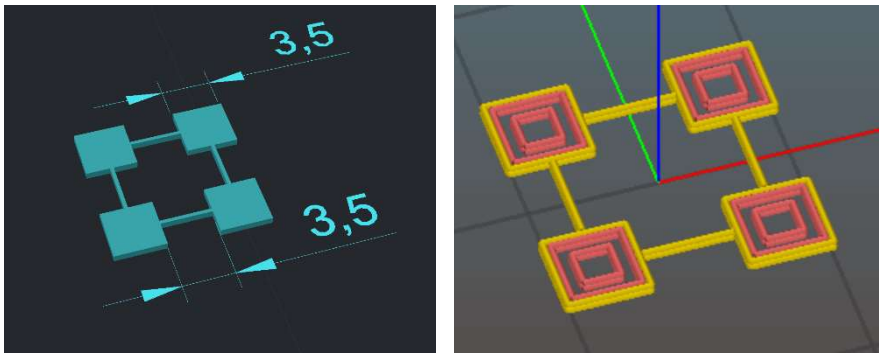

(a) (b)

Figure 2.15. *First structure designed for SK-N-AS encapsulation, with AutoCAD (a) and G-Code generation with Slic3r (b).*

Bioprinting parameters were previuosly optimized by printing the same structure with hydrogels at 13% GelMA concentration, without encapsulated cells. The gelatin metacrylate used for both printing and bioprinting tests was obtained with Method A and purified with ethanol. The structure was printed with one extruder, with a tip characterized by nozzle diameter of 0.25 mm, with a circular infill of the 40%, at 2 mm/s speed; the maximum applied printing pressure was kept below 200 kPa, while the light curing time interval was 60 s. A multiwell plate was selected as printing support; one structure per multiwell plate was printed, with the goal of printing three structures at a time to have at least three technical replicates of the same test. Intermediate refrigeration of the hydrogel with encapsulated cells was necessary between each printing cycle.

Two cellular tests were performed using this structure, and in both cases 1 million cells per ml of 13% GelMA hydrogel was used; the relatively low number of encapsulated cells was selected

in order to ease following the formation of clusters. With the first test print, three structures were obtained and two of them were covered with 1 ml of growth media containing neuroblastoma-derived exosomes. In the second printing test, two structures were printed and both of them were covered with 1 ml of pure growth medium.
The analysis of these structures was carried out using fluorescence markers at different time points, as explained in §2.4.6.

A second optimized structure was then designed for solving the problems encountered by printing the first structure (high printing times, low printing resolution). The second structure is merely the first structure halved, with a slight variation in the size of the square base area, and made of two layers, both of them 0.3 mm high. This second structure is shown in Figure 2.16: in Figure 2.16.a, the structure designed with AutoCAD is shown (dimensions in mm), while Figure 2.16.b shows how the printing of the first layer of the structure was performed, according to the percentage and fill pattern of the infill selected.

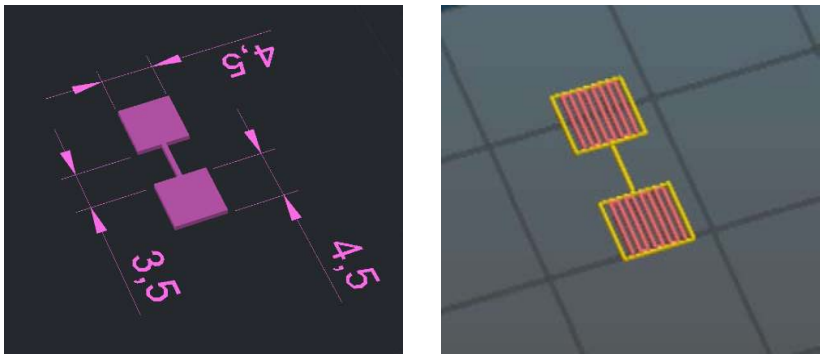

(a) (b)

Figure 2.16. *Second structure designed for SK-N-AS encapsulation, with AutoCAD (a) and G-Code generation with Slic3r (b).*

Printing parameters were those previuosly optimized by printing the same structure with hydrogels at 13% (w/v) GelMA concentration, without encapsulated cells, and both for printing and bioprinting tests the GelMA used was obtained with Method A and purified with ethanol. The structure was printed with one extruder, with a tip characterized by nozzle diameter of 0.25 mm, with a rectilinear infill of the 55%, at the speed of 4 mm/s; the maximum applied printing pressure was kept below 200 kPa, and the light curing time interval was maintained at 60 s. A multiwell plate was selected as printing support, and three structures per multiwell plate were printed without intermediate refrigeration of the hydrogel, obtaining three technical replicates of the same test at once.This was possible thanks to the reduction of the dimensions of the structure, the increase in the printing speed, and because of the optimization of the percent and fill pattern of the infill.

The test involving this structure was performed once, with three different concentration of cells in hydrogels: $40*10^3$, $400*10^3$ and $4*10^6$ cellsper 1 ml of 13% GelMA hydrogel. After bioprinting, structures were covered with growth medium without exosomes and used to study the viability of encapsulated cells at different concentrations immediately after printing, and after 3 and 7 days of incubation.
The analysis of these structures was carried out by fluorescence markers as explained in §2.4.6.

2.4.4 Bioprinting with MSCs

Three dimensional bioprinting of GelMA-hydrogels with encapsulated MSCs was performed to evaluate cellular viability using the same conditions already tested for neuroblastoma cells[2]. With this purpose, two printing tests were performed: the structure to be printed was selected according to the results of previous tests of viability and migration performed with SK-N-AS cells[2]. The chosen structure is shown in Figure 2.17: in Figure 2.17.a the structure designed with AutoCAD is represented, and Figure 2.17.b shows how the printing of the structure was performed, according to the fill pattern and percentage of the infill selected. The structure is composed of two layers, each 0.3 mm high, so that the overall structure is 0.6 mm high. It has a ladder-like shape, with two parallelepiped of equal length (23 mm) and height, characterized by different width (in order to easily distinguish them), connected by eight 10 mm long, 0.5 mm wide, channels. This structure was designed with this shape and dimensions to verify cellular migration of neuroblastoma cells in the presence of exosomes.

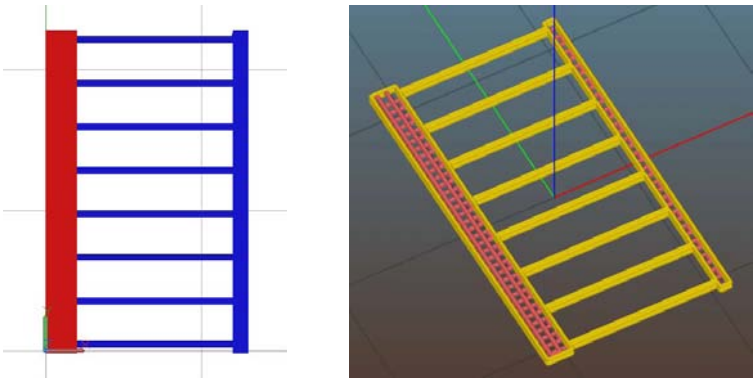

(a) (b)

Figure 2.17. *Ladder-like structure used for MSC encapsulation designed with AutoCAD (a); G-Code generation of the structure with Slic3r.*

The structure was disegned to be printed with two extruders, using tips characterized by nozzle diameter of 0.28 mm, with a rectilinear infill of the 40%, at the speed of 2 mm/s; the maximum applied printing pressure was kept below 100 kPa, and the light curing time interval was set at 60 s. The first extruder was loaded with 13% GelMA hydrogel with encapsulated cells

(500*10^3cells per 1 ml of hydrogel), and this bioink was used to print the thickest parallelpid, represented as red in Figure 2.16.a, while the second extruder was loaded with 13% GelMA hydrogel and used to print the thinnest parallelepid and the connecting channels, represented as blue in Figure 2.16.a.
The printed structures were used to study the viability of encapsulated cells after 3, 7 and 14 days of incubation. The analysis of these structures was carried out by fluorescence markers as explained in §2.4.6.

2.4.5 3D cylindrical scaffolds

Based on the results obtained with three-dimensional bioprinting of hydrogels structures with encapsulated cells, it was necessary to use hydrogels at lower GelMA concentration in order to observe a better cell migration. The solution was to realize 3D cylindrical scaffolds just using PDMS annulus molds of two types: the first characterized by 8 mm diameter, 2 mm height and an overall internal volume of 100 µl, and the second with 4 mm diameter, 2 mm height and an internal volume of 25 µl. The preparation of hydrogels with encapsulated cells to reproduce cylindrical scaffolds was the same used for bioprinting applications described in §2.4.2. Briefly, the hydrogel with encapsulated cells was introduced into PDMS molds with a micropipette and photopolymerization was performed with the UV LED of the bioprinter at 365 nm for 60 seconds. This protocol based on the use of annulus molds made it possible to obtain scaffolds even at the lowest 5% GelMA concentration. At this GelMA concentration, cells should experience a normal life cycle when encapsulated, should communicate with the surrounding ones, migrate, and not be restricted to a rounded shape because of the high density and low porosity of the surrounding environment[45].
In §2.4.5.1 and §2.4.5.2 all the tests carried out with 3D cylindycal scaffolds and cells are schemtically reported.

2.4.5.1 HEK cells in 3D cylindrical scaffolds

In order to perform simple viability tests, in the view of future tests with neuroblastoma cells, HEK cells were encapsulated in GelMA hydrogels under different conditions of interest.
A first test was performed using hydrogels made of GelMA obtained with Method A and purified with ethanol. Hydrogels at three different GelMA concentrations were used, 10%, 8% and 5% (w/v), to realize cylindrical samples of 100 µl, at two cellular concentrations, 1.5*106 and 3*10^6 of cells per ml of hydrogel. All the other key parameters varied in samples' preparation are reported in Table 2.2.

Table 2.2. *List of parameters and their values used in the preparation of hydrogel samples in the first viability test with HEK cells.*

GelMA [%]	Concentration of cells [million/ml of hydrogel]	Medium with cells/hydrogel [v/v %]	N. of samples	Volume [µl]	UV exposure time [s]
5	1.5	3	2	100	120
5	3	3	2	100	120
8	1.5	3	2	100	60
8	3	3	2	100	60
10	1.5	3	2	100	60
10	3	3	2	100	60

These samples, after photopolymerization, were simply covered with HEK's growth medium and then placed in incubator. For every tested condition, analysys were performed after 1 and 3 days from incubation and every sample was anlysed once with fluorescence marker to test the viability of cells.

According to the results obtained with the first test, a second one was arranged: the preparation of cylindrical samples of 5% (w/v) GelMA hydrogel was repeated, keeping the cellular concentrations selected constant, simply increasing the number of samples to 3, in order to extend the incubation time to 7 days. Also for this second test, hydrogels were prepared using GelMA obtained with Method A and purified with ethanol. All the parameters varied in samples' preparation, for the second test, are reported in Table 2.3.

Table 2.3. *List of parameters and their values used in the preparation of hydrogel samples in the second viability test with HEK cells.*

GelMA [%]	Concentration of cells [million/ml of hydrogel]	Medium with cells/hydrogel [v/v %]	N. of samples	Volume [µl]	UV exposure time [s]
5	1.5	3	3	100	120
5	3	3	3	100	120

These samples, after light curing, were covered with HEK's growth medium and then placed in incubator. Analysis were performed after 1, 3 and 7 days from incubation with fluorescence markers in order to check the viability of cells.

A third test was then perfomed with 5% and 10% (w/v) GelMA hydrogels, used to prepeare samples of 100 µl, at the lowest cellular concentration. Hydrogels were prepared with GelMA obtained with Method A and purified with ethanol. The modified parameters with respect to previous tests were the medium/hydrogel volumetric ratio and the number of samples realized. In Table 2.4 the parameteres varied in the this third test, for samples preparation, are reported.

Table 2.4. *List of parameters and their values used in the preparation of hydrogel samples in the third viability test with HEK cells.*

GelMA [%]	Concentration of cells [million/ml of hydrogel]	Medium with cells/hydrogel [v/v %]	N. of samples	Volume [µl]	UV exposure time [s]
5	1.5	15	3	100	120
10	1.5	15	3	100	60

After photopolymerization, samples were covered with HEK's growth medium and the placed in incubator. Test with fluorescence markers were performed after 1, 3 and 7 days from incubation.

A fourth test for cellular viability analisys was carried out using GelMA obtained with Method A, purified through dialysis, with a DoF equal to 80% and using GelMA obtained with Method B, purified through dyalisis, with a DoF equal to 71%. Hydrogels cylyndrical samples of 100 µl were prepared at 8% and 10% (w/v) GelMA concentration, in order to keep the UV exposure time of samples equal to one minute, therefore limiting cells' death, but still ensuring a favourable environment for their adhesion, and normal growth. Cells were encapsulated at two cellular concentration in hydrogels, 1.5 and 3 million of cells per ml of hydrogel. The parameters selected for samples preparation are reported in Table 2.5.

Table 2.5. *List of parameters and their values used in the preparation of hydrogel samples in the fourth viability test with HEK cells.*

GelMA [%]	Concentration of cells [million/ml of hydrogel]	Medium with cells/hydrogel [v/v %]	N. of samples	GelMA DoF [%]	Volume [µl]
8	1.5	5	2	80 ± 10	100
8	3	5	2	80 ± 10	100
8	1.5	5	2	71 ± 10	100
8	3	5	2	71 ± 10	100
10	1.5	5	2	80 ± 10	100
10	3	5	2	80 ± 10	100
10	1.5	5	2	71 ± 10	100
10	3	5	2	71 ± 10	100

All samples were covered with HEK's growth medium and then placed in incubator. Test with fluorescence markers were performed after 1 and 3 days from incubation.

2.4.5.2 MSC in 3D cylindrical scaffolds

Three dimensional cylindrical scaffolds of 5% GelMA hydrogel were prepared in order to reproduce viability tests with mesenchymal stem cells[22]. Hydrogels were prepared with GelMA obtained with Method A and purified with ethanol.

One single test was performed with a cellular concentration of $1*10^6$ cells per ml of hydrogel, with a medium/hydrogel ratio equal to 3%. Sample volume was lowered to 25 µl and three samples were prepared in order to perform test with fluorescence markers after 1, 3 and 7 days from incubation.

2.4.6 Experimental analysis: fluorescent markers

In order to verify cell viability and migration whitin the 3D bioprinted structures, or whitin the cylindrical scaffolds realized with PDMS annulus molds, fluorescent dyes were used and fluorescence microscopy analysys were performed. Hoechst 33258, Calcein AM, Propidium Iodide and Vybrant™ Dil were used. ,

Hoechst 33258 is a fluorescent stain for detecting DNA in fluorescence microscopy, flow cytometry and immunohistochemistry applications. Hoechst 33258 emits blue fluorescence (λ = 461 nm) when bound to DNA of both live and dead cells nuclei, therefore allowing to determine all the cells encapsulated in the hydrogels. Figure 2.18[2] shows the chemical structure of Hoechst dye.

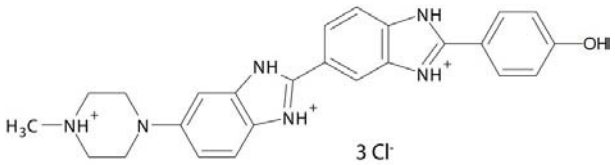

Figure 2.18. *Chemical structure of Hoechst dyes; adapted from Mantovani M.[2].*

Calcein AM is a fluorogenic, cell-permeant dye, used to determine cell viability in most eukaryotic cells, as it only stains the cytoplasm of live cells. When the acetoxymethyl ester is intact, this probe is non-fluorescent; in live cells instead the non-fluorescent calcein AM is converted to green-fluorescent calcein, thanks to the acetoxymethyl ester hydrolysis by intracellular esterases. The probe, whose chemical structure is shown in Figure 2.19[2], emits at 520 nm with a signal that is proportional to cell viability.

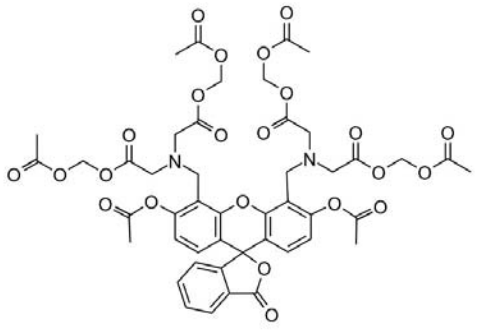

Figure 2.19. *Chemical structure of Calcein AM; adapted from Mantovani M.[2].*

Propidium Iodide (PI), whose chemical structure is shown in Figure 2.20[2], is a red-fluorescent nuclear and chromosome counterstain; it is not permeant to live cells and it is therefore used to detect nuclei of dead cells.

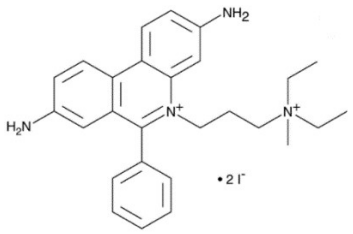

Figure 2.20. *Chemical structure of Propidium Iodide stain; adapted from Mantovani M.[2].*

PI has exitacion/emission maxima of 493/636 nm: when the dye is bound, its fluorescence is enhanced 20 to 30 fold, the fluorescence excitation maximum is shifted ~30–40 nm to the red and the fluorescence emission maximum is shifted ~15 nm to the blue, resulting in an excitation maximum at 535 nm and luorescence emission maximum at 617 nm.
Dil is a lipophilic membrane stain that diffuses laterally to stain the entire cell; it is weakly fluorescent until incorporated into cellular membranes. This red fluorescent dye, whose chemical structure is shown in Figure 2.21, is spectrally similar to tetramethylrhodamine, and it is often used as a long-term tracer for neuronal and other cells. Dil was here used in a volume ratio of 1:1000 in order to stain exosomes membranes before adding them to the growth medium used to cover bioprinted structures.

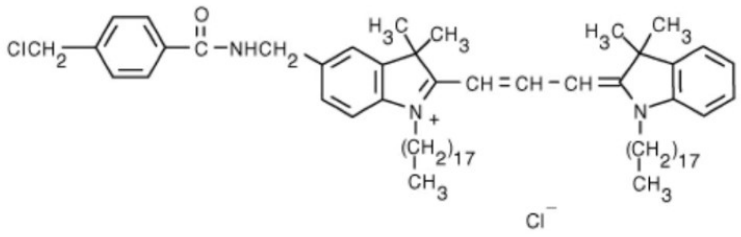

Figure 2.21. *Chemical structure of Dil stain.*

Hoechst 33258, Calcein AM, Propidium Iodide and Dil are soluble in water and organic solvents. Especially, staining solutions for the analysis of bioprinted structures were prepared with the following composition: in a total volume of HBSS or DMEM without FBS Hoechst 33258 is added in a volume ratio of 1:250, Calcein AM with a volume ratio of 1000 as the Propidium Iodide.

After the established incubation time, every single structure to be analyzed, was washed at least two times with HBSS for at least 30 s. Then, after HBSS was discarded, it was covered with the staining solution and placed in the incubator for at least 45 minutes before being analyzed with a fluorescent microscope (EVOS); this time interval was necessary to allow the solution to permeate inside the structure. Every structure was analyzed in different areas, in order to have at least three images representing all the encapsulated cells, the three corresponding images with live cells only, and, possibly, also the three images with dead cells only.

2.4.6.1 Viability evaluation

Cellular viability within structures was numerically evaluated using ImageJ, the Java-based image processing program developed at the National Institutes of Health (NIH). With this program, the captured images for every structure were analyzed performing cell counting and determining: *i.* an average value of all cells encapsulated in a determined area (n_{tot}), *ii.* an average value of live cells encapsulated in the same area (n_{live}), and *iii.* an estimate of dead cells in the same area (n_{dead}). The percentage of cellular viability was therefore determined as:

$$\%\ viability = \frac{n_{live}}{n_{tot}} \cdot 100 \quad . \tag{2.7}$$

2.5 Instruments

The main instruments used in this project for the characterization of GelMA, of GelMA hydrogels and to perform biological tests are:

- Nuclear Magnetic Resonance Spectrometer (DISC, Padova, Prof. Sgarbossa P.),
- Fourier Transformed InfraRed Spectrometer (DII, Padova, Prof. Modesti M.),
- Thermogravimetric Analyzer (DII, Padova, Prof. Modesti M.),
- Heat flux Differential Scanning Calorimeter, Q200 model (DII, Padova, Prof. Modesti M.),
- Scanning Electron Microscope (DII, TeSi lab, Rovigo, Prof. Lucchetta G.),
- Rheological measurements, ARES-RFS model (DII, TeSi lab, Rovigo, Prof. Lucchetta G.),
- Cellink INKREDIBLE bioprinter (DII, BiaMET lab, Prof.ssa Cimetta E.),
- EVOS microscope (DII, BiaMET lab, Prof.ssa Cimetta E.).

Chapter 3

Experimental results

In this Chapter, the efficiency of the synthesis and purification methods applied to obtain GelMA in the desired functionalization range, is discussed; results of all the characterization analysis carried out on GelMA and on GelMA-based hydrogels used for biological applications are reported and commented. Ultimately, results of all cellular tests performed, are reported and discussed.

3.1 GelMA characterization

Two methods of synthesis were used in this context in order to obtain GelMA with a DoF between 50 and 70%, compatible with planned biological applications, as already explained in §2.1.

The main point of comparison between Method A and Method B concerns the reproducibility and the efficiency of GelMA synthesis in the desired range of degree of functionalization, and it is therefore based on the results of H NMR analysis. Due to the inefficiency of the ethanol based GelMA purification method, discussed in §3.1.1, the comparison on the reproducibility of the two methods of synthesis was only performed on the basis of the analysis of GelMA samples purified through dialysis. The DoF of only one batch of GelMA prepared with Method A and then purified through dialysis was determined and it was equal to 80 ± 10 %. Functionalization results related to the application of Method B are instead schematically reported in Table 3.1. H NMR analysis graphs are shown in Appendix 1.

Table 3.1. *Degree of functionalization of GelMA samples obtained with Method B.*

Batch number	***DoF [%]***
1	60 ± 10
2	60 ± 10
3	58 ± 10
4	57 ± 10
5	55 ± 10
6	71 ± 10

The uncertainty on DoF values was reasonably fixed to the 10% because measurements are obtained from the analysis of a weak signal, that decreases as the degree of methacrylation increases.
According to functionalization results, the high reproducibility of Method B is verified, since it allows to easily obtain GelMA at degrees of functionalization that are in the precise range of interest, appropriate for biological applications. The comparison in terms of reproducibility between the Method A and Method B is instead not possible because of the lack of data related to Method A.
Method B is anyway certainly more efficient than the first one: the use of a CB buffer solution as the reaction medium, allows to perform the methacrylation at pH ~9.2, and therefore above the IEP of gelatin, and below the critical value for MAA hydrolysis, with the consequent minimization of the required molar excess of anhydride. In terms of pH control, Method B is less operator-dependent, since acid adjustments are required only before the addition of the anhydride. Moreover, based on a simple economic analysis, performed considering the difference of reagents' cost, it was verified that Method B is significantly cheaper than Method A, that costs about 5.3 times more, to be performed with the same results.

3.1.1 Efficiency of GelMA purification methods

As explained in §2.1.1, two different purification methods have been tested in order to have the desalinization of the solution obtained after methacrylation, together with the complete removal of the un-reacted anhydride, and of the methacrylic acid, the reaction's byproduct.
The first method of purification, performed with ethanol, was used in combination with Method A; while the second purification method was used with both Method A and Method B.
The first purification method, albeit rapid and ensuring the sterility of the final product (which was fundamental in view of biological applications), was ineffective due to the incomplete removal of ethanol. The presence of residual ethanol inside GelMA after vacuum-drying, was at first detected simply by observing that the core of the material was not perfectly dry and was not homogenous in terms of colour and consistency (Figure 3.1).

Figure 3.1. *GelMA obtained with Method A, purified with ethanol, and vacuum-dried; clearly not dried in the inner part.*

The inefficiency of this purification method was also confirmed by the results of H NMR analysis performed on GelMA samples, since signals related to an ethyl group were identified in the vacuum-dried material. In addition, the presence of residual ethanol in GelMA prevented the accurate determination of the degree of methacrylation of gelatin molecules, that was therefore assumed to be equal to ~ 70%, according to the literature[41]. As a consequence, the first purification method was evaluated as inefficient and therefore discarded.

The second purification method, based on dialysis of the solution obtained after methacrylation against deionized water, was successful. The complete removal of salts, of un-reacted anhydride and of methacrylic acid, was at first evident in the variation of the trasparency of the solution after 72 hours of dyalisis, and was then confirmed by H NMR analysis, since the presence of foreign substances in the freeze-dried material was not detected. The second purification method, followed by the filter-sterilization of the solution and freeze-drying, despite being much more complex compared to the first one, was therefore preferred, since it allowed to obtain a pure, dried and sterile material (as reported in Figure 3.2).

Figure 3.2. *GelMA after dialysis, filter-sterilization and freeze-drying.*

3.1.2 FTIR spectra interpretation

The FTIR spectra of pure gelatin powder, and of two GelMA samples, obtained with Method B, purified through dialysis and characterized by DoF of 55 and 71%, are shown in Figure 3.3, where the characteristic peaks are highlighted and labelled.

From the graphical comparison of FTIR spectra, it is clear how the methacrylation of gelatin molecules cannot be verified with this analysis due to the limited presence of methacrylamide groups, whose signals are too low to be detected. The FTIR spectra of pure gelatin (referred to as Gelatina semplice in Figure 3.3) and GelMA samples functionalized at 55 and 71% (referred to as CB1.1 and CB2.1 in Figure 3.1, respectively) are quite similar and the difference in signals intensity cannot be related to the chemical difference of these molecules but it is probably due to the fact that pure gelatin was analyzed as a powder, while GelMA as a highly porous solid material.

In the functional groups region, peaks associated with the stretching vibrations of primary amine (3500–3300 cm^{-1}) and of CH groups (3300-2700 cm^{-1}) are identified. Peaks in the fingerprint region are instead associated with the stretching vibrations of secondary amide (1640 cm^{-1}) and carbonyl groups (1500 cm^{-1}), while other minor peaks are due to the stretching vibrations of CH groups.

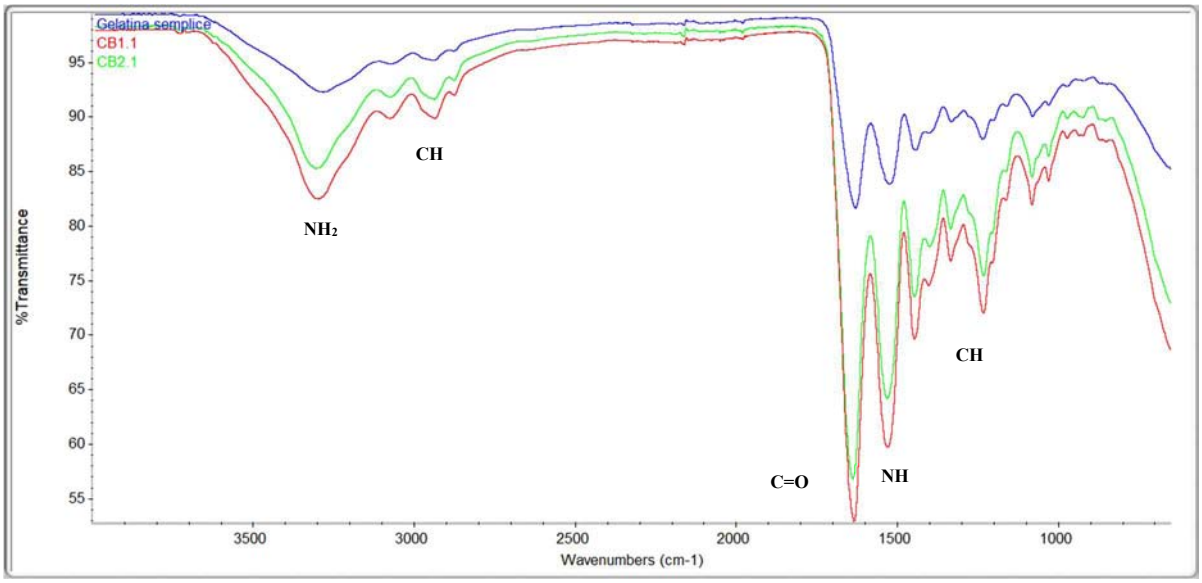

Figure 3.3. *FTIR spectra of gelatin (Gelatina semplice), GelMA functionalized at 55% (CB1.1) and GelMA functionalized at 71% (CB2.1).*

3.1.3 Thermogravimetric analisys results

Thermogravimetric analyses were performed on GelMA samples obtained with Method B, purified through dialysis and freeze-dried; only samples from two different synthesis batch were analyzed. The thermal decomposition curves and the corresponding heat flow curves, as function of temperature and time, result of the analysis of GelMA samples from the first synthesis batch (DoF 55%), in inert and oxygen atmosphere, are shown respectively in Figure 3.4 and 3.5 and in Figure 3.6 and 3.7. The thermal decomposition curves and heat flow curves, as function of temperature and time, result of the analysis in inert atmosphere of GelMA samples from the second synthesis batch (DoF 71%), are instead reported in Figure 3.8 and 3.9.

As clear from Figure 3.4 and Figure 3.8, no significant differences were verified between thermal decomposition curves of GelMA samples from the two different synthesis batches, when analyzed in inert conditions from ambient temperature up to 220°C. The first weight loss of samples is identified in the range from ambient temperature to 110°C, and is related to water evaporation. In both cases the percentage weight loss is close to 7%, suggesting the efficiency of the freeze-drying process. In the temperature range up to approximately 220°C samples show

thermal stability; thermal degradation is verified above this temperature, and, up to 300°C, the weight loss of samples is ~17% and ~22% for GelMA at 55 and 71% of functionalization, respectively. This relevant difference may be due to the semi-crystalline nature of GelMA and therefore to the different degree of crystallization and size of the crystals that are formed during freeze-drying process. The percent weight loss of GelMA samples functionalized at 55% in the temperature range 220-330°C in oxygen atmosphere is instead higher because of thermal-oxidative degradation of the material, and it is overall equal to 22%.

Thermogravimetric analysis results were also used to determine an upper temperature limit for DSC analysis on GelMA samples in inert atmosphere. In particular, the temperature value corresponding to the beginning of the thermal degradation of the material when heated in inert atmosphere, 220°C, was selected as the highest attainable temperature in the heating program of differential scanning calorimetry analysis. This limit was fixed to see if it was possible to have the recrystallization of GelMA with and adequate subsequent cooling program.

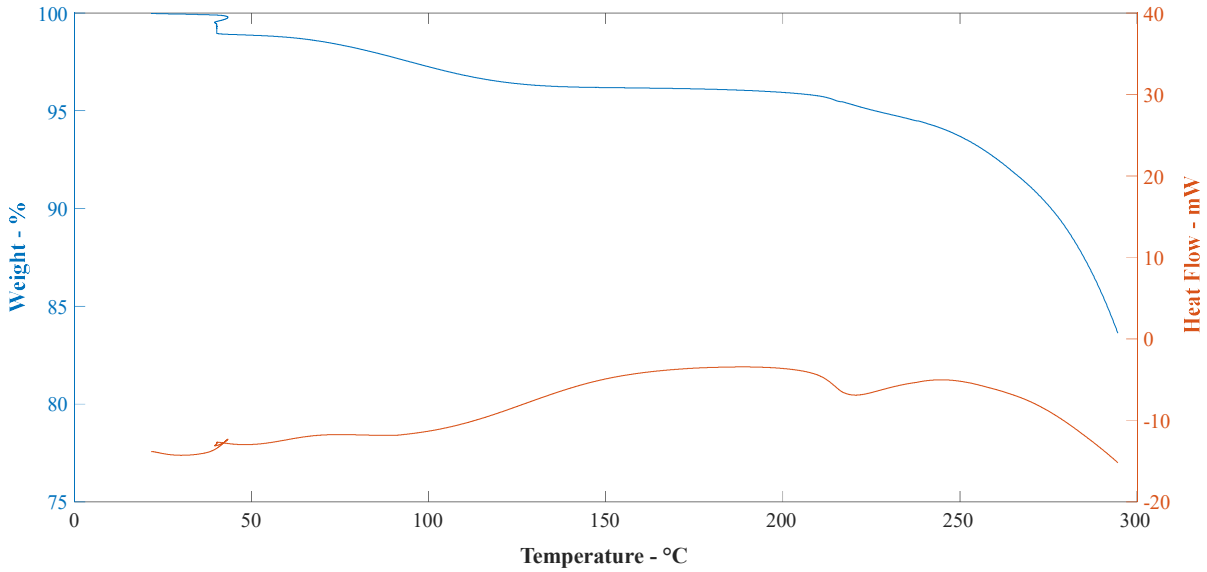

Figure 3.4. *Thermal decomposition curve (blue) and heat flow curve (red) of GelMA functionalized at 55%. Analysis performed in inert atmosphere.*

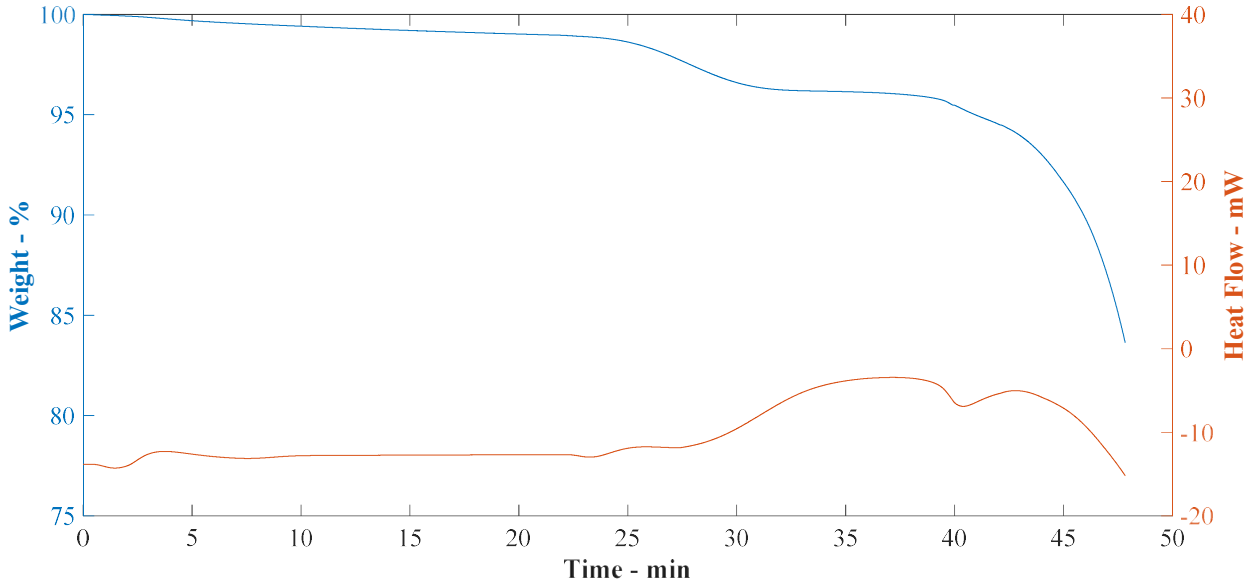

Figure 3.5. *Thermal decomposition curve (blue) and heat flow curve (red) of GelMA functionalized at 55%. Analysis performed in inert atmosphere.*

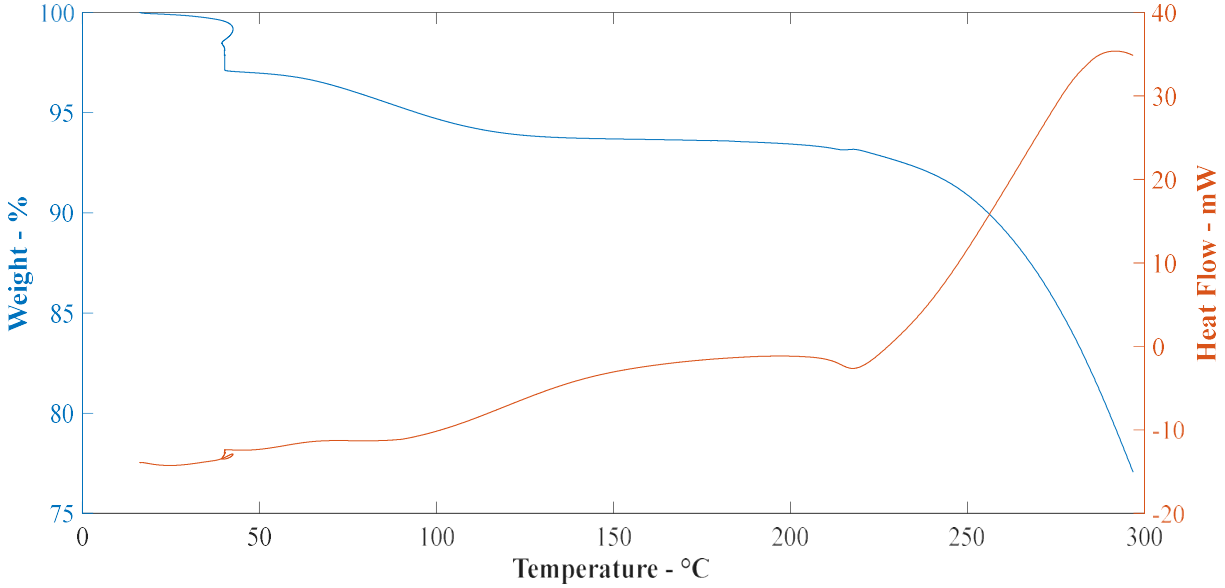

Figure 3.6. *Thermal decomposition curve (blue) and heat flow curve (red) of GelMA functionalized at 55%. Analysis performed in oxygen atmosphere.*

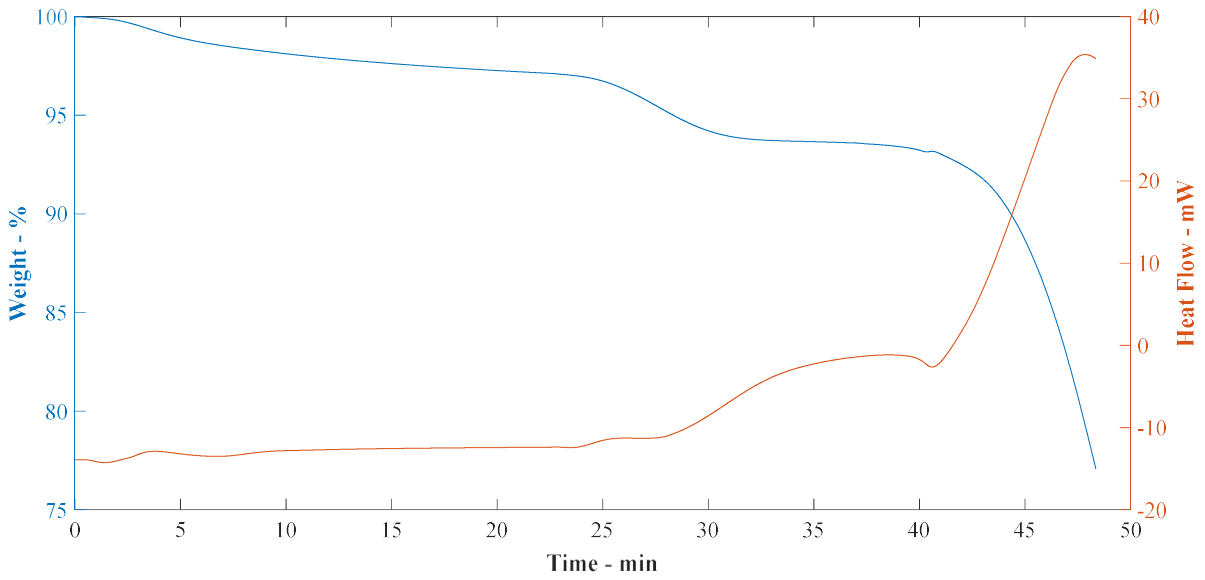

Figure 3.7. *Thermal decomposition curve (blue) and heat flow curve (red) of GelMA functionalized at 55%. Analysis performed in oxygen atmosphere.*

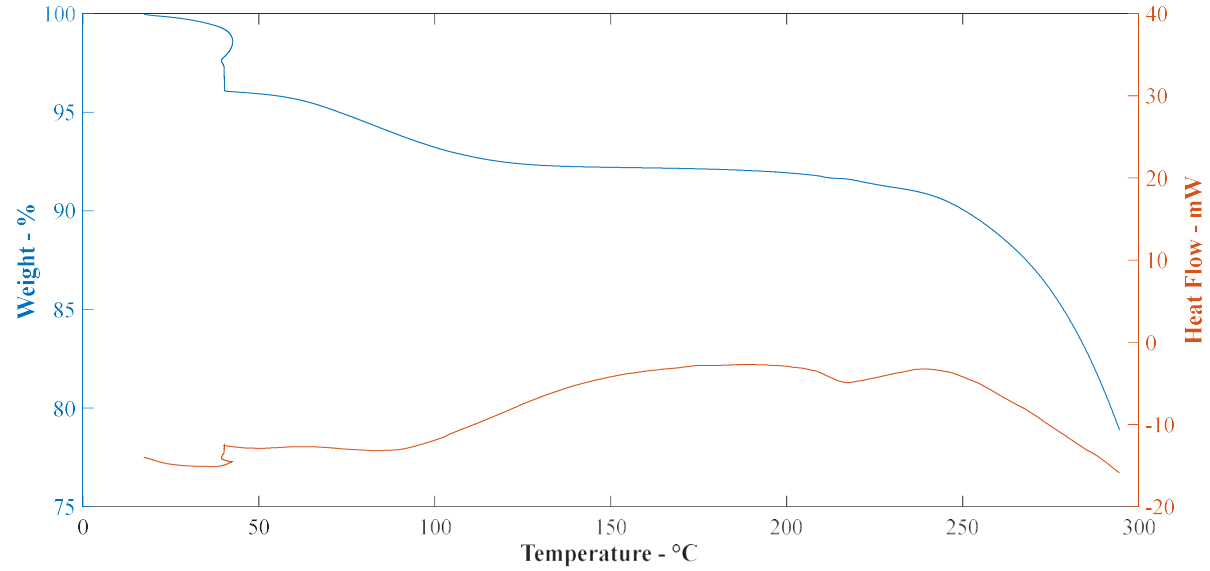

Figure 3.8. *Thermal decomposition curve (blue) and heat flow curve (red) of GelMA functionalized at 71%. Analysis performed in inert atmosphere.*

.

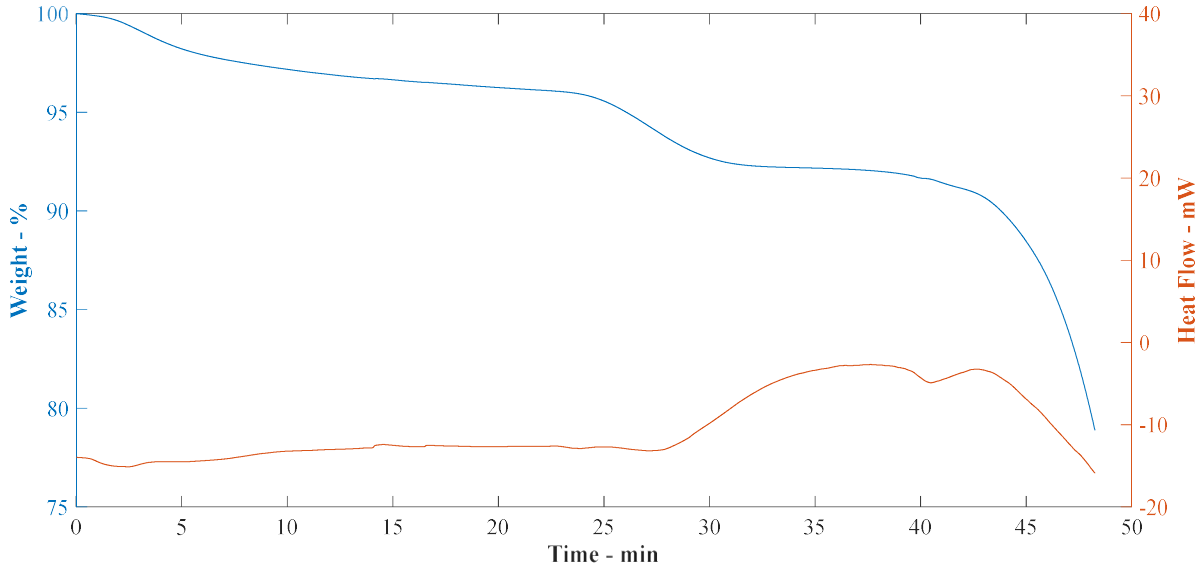

Figure 3.9. *Thermal decomposition curve (blue) and heat flow curve (red) of GelMA functionalized at 71%. Analysis performed in inert atmosphere.*

3.1.4 Differential Scanning Calorimetry

Differential scanning calorimetry analysis was performed on one single sample of GelMA, with a DoF equal to 55%, obtained with Method B and purified through dialysis. The resulting thermogram is shown in Figure 3.10 and confirms the semi-crystalline nature of GelMA.

The DSC heating scan revealed a second order glass transition at approximatively 47.5°C, probably related to glass transition of amino acid blocks in the peptide chains of GelMA amorphous region[46], followed by a first order endothermic transition at 84.6°C and another more relevant one at 154.5°C, result of the melting of the crystalline zones of the material. The first melting peak is less significant compared to the second one and is related to the presence of smaller crystals; the second melting peak is instead the main one and, unlike the former, it is not supposed to shift repeating the analysis on different samples. To get further confirmation, analysis should be repeated on more GelMA samples, from different synthesis batches.
In the cooling cycle, no crystallization peaks were identified, suggesting that protein chains, denatured at temperature higher than 70°C, are not able to rearrange themselves in an orderly way to reform crystals. Nothing significant was detected below ambient temperature in the temperature range of GelMA storage.

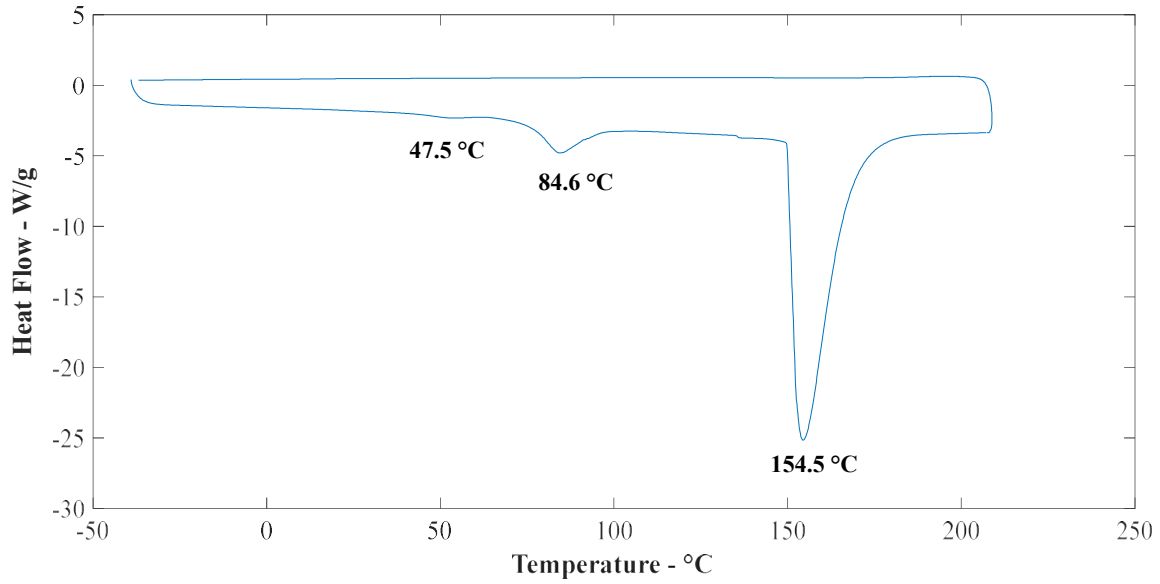

Figure 3.10. *DSC thermogram of GelMA functionalized at 55%, in inert atmosphere.*

3.2 GelMA-based hydrogels properties

Hydrogels prepared at different GelMA concentrations, used for biological applications, were analyzed in terms of swelling, porosity, and viscoelastic properties; analysis results are reported and discussed in the following paragraphs. The main aim was not only to characterize these materials, but also to verify their suitability as scaffolds for cells encapsulation and, if necessary, to study how optimize them for biological applications.

3.2.1 Swelling properties

Swelling tests were performed on GelMA-based hydrogel samples in order to evaluate the influence of GelMA concentration on the ability of the material to absorb and retain aqueous solutions.

Swelling tests were performed separately both on hydrogel samples prepared with GelMA obtained with Method A and purified with ethanol, and with GelMA obtained with Method B and then purified through dialysis. Because of the verified inefficiency of the first purification method, results of tests performed on hydrogels prepared with GelMA purified with ethanol were considered as inaccurate and therefore discarded; results are anyway available in Appendix 2.

In Table 3.2, the percentage swelling ratio and water retention evaluated for hydrogels at the four analyzed GelMA concentrations, based on tests performed on hydrogels prepared with GelMA purified through dialysis, are reported.

Table 3.2. *Results of swelling tests performed on hydrogels samples prepared at different GelMA concentrations.*

GelMA [%]	*UV exposure time [s]*	*Swelling Ratio [%]*	*Water content [%]*
5	120	975 ± 42	90.7 ± 0.4
8	60	734 ± 28	88.0 ± 0.4
10	60	644 ± 14	86.5 ± 0.3
13	60	544 ± 15	84.5 ± 0.3

The influence of GelMA concentration on the overall morphology of the polymeric network of hydrogels can be inferred on the variation of hydrogels swelling ratio, and accordingly on hydrogels water retention. The fractional increase of hydrogels weight due to water absorption, as well as the water retention, increases linearly with the decrease of GelMA concentration, and is maximum for samples at 5% (w/v) GelMA concentration. The difference in UV time exposure for hydrogels at 5% (w/v) GelMA concentration doesn't significantly affect this linear trend.

Considering the biological applications of these materials, evidence shows that hydrogels at lower GelMA concentration are best suited to ensure the exchange of fluids, providing the appropriate microenvironment for cells growth in 3D; the exchange rates and modes are anyway dependent on the material porosity.

3.2.2 Porosity evaluation

The porous structure of freeze-dried hydrogels was analyzed with scanning electron microscopy (SEM) in order to determine the effect of GelMA concentration on their morphology, therefore studying the possibility to control micro-architectural features of these materials.

SEM images of hydrogels at 5, 8, 10 and 13% (w/v) GelMA concentration and the corresponding frequency distribution graphs of pores diameters are shown in Figure 3.11. The boxplot of pores diameters distribution for each GelMA concentration is reported in Figure 3.12.

Images analysis revealed that, in the concentration range examined, freeze-dried hydrogels are characterized by a honeycomb-like super-porous structure, with interconnected pores with diameters between 6 and 80 μm. According to frequency distribution graphs, most of pores diameters fall between 10 and 20 μm for each GelMA concentration. These data confirm that GelMA-based hydrogels are suitable for cells encapsulation, since cells can enter the porous framework of hydrogels, maintaining their natural 3D shapes and experiencing a normal life cycle, interacting with adjacent cells to create tissue-like structures.

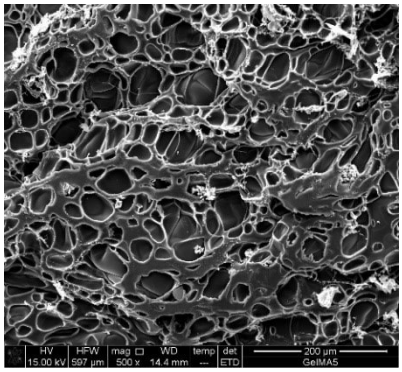

(a)

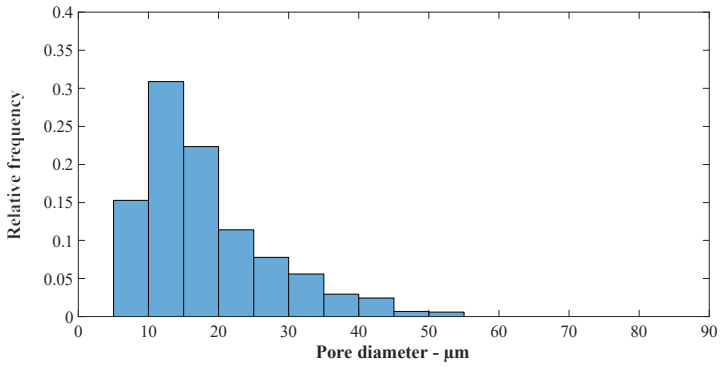

(e)

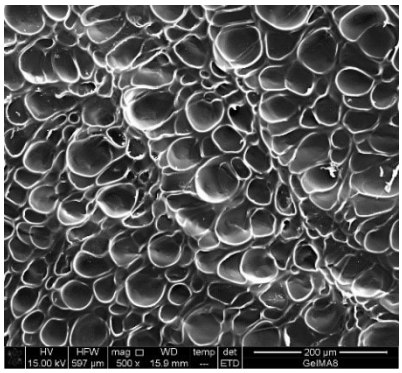

(b)

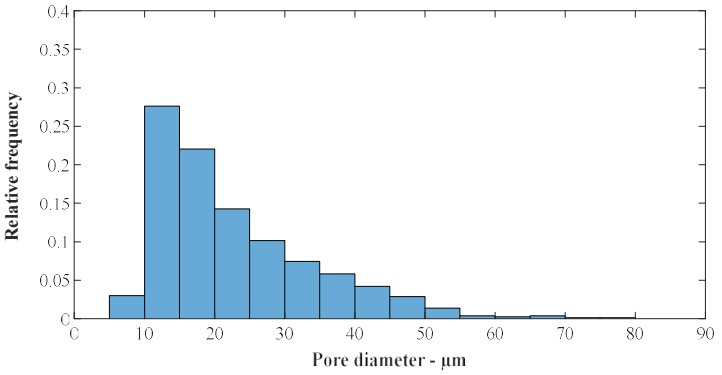

(f)

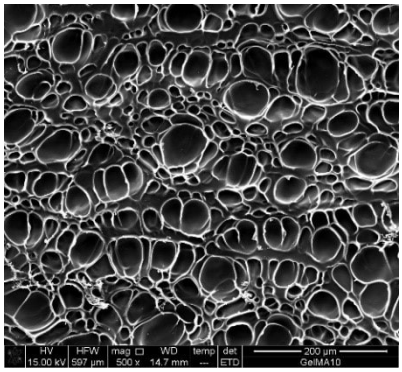

(c)

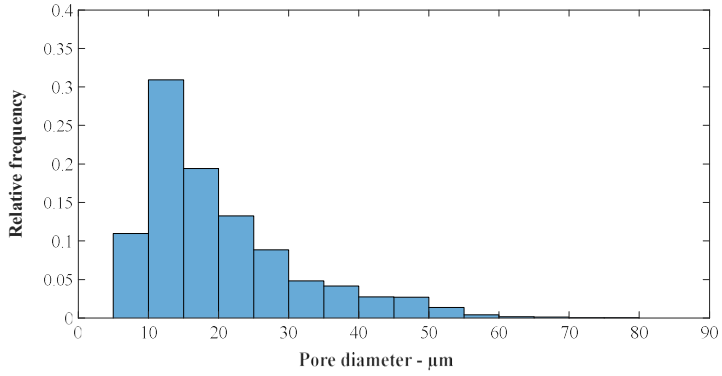

(g)

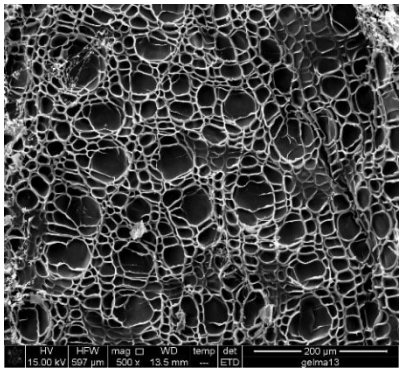

(d)

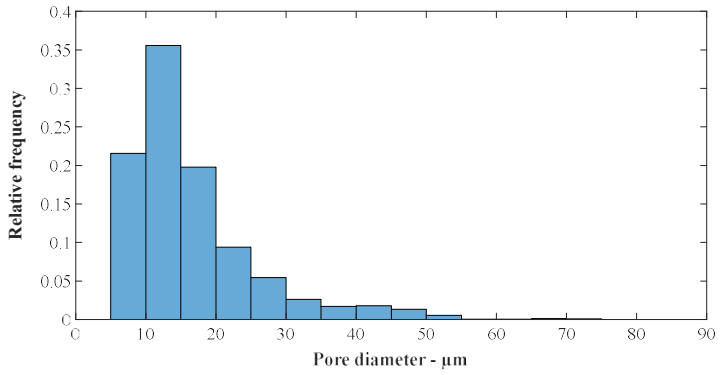

(h)

Figure 3.11. *SEM images of freeze-dried hydrogel samples at 5, 8, 10 and 13% (w/v) GelMA concentration (a-d) and corresponding pores diameter relative distributions (e-h).*

Pores diameter distributions, as confirmed by the analysis of the boxplot diagram, are asymmetrical independently of GelMA concentration, being all positive skewed; the boxplot related to 13% (w/v) GelMA concentration is comparatively shorter, suggesting the lower variability of pores size.

The boxplot diagram revealed the presence of an inversely proportional correlation between GelMA concentration in the hydrogel and pores diameter distribution: the minimum, the lower quartile, the median, the upper quartile and the maximum values of pores diameter increase at lower concentration of the polymer in hydrogels. This relationship was verified excluding data related to 5% (w/v) GelMA concentration, since even UV exposure time seems to affect pores size distribution; to prove this second influence on pores size distribution, samples at constant GelMA concentration should be prepared varying photo-polymerization time interval.

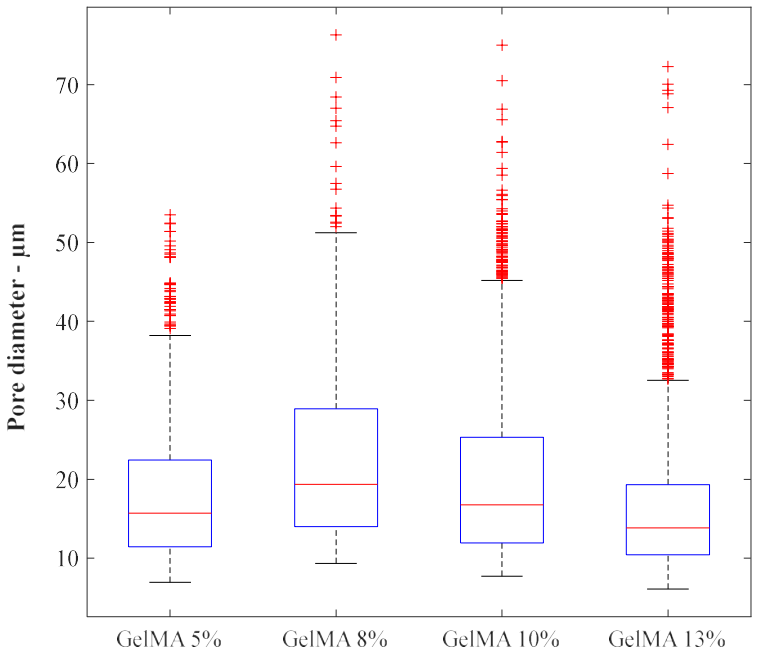

Figure 3.12. *Boxplot of pore diameters distribution of freeze-dried hydrogel samples at 5, 8, 10 and 13% (w/v) GelMA concentration.*

It might be useful to repeat the same analysis studying the combined action of different parameters variation, such as the photo-initiator concentration, GelMA concentration, UV exposure time interval, on the final hydrogel structure, always aiming at the preparation of scaffolds suitable for cell encapsulation.

3.2.3 Dynamic oscillatory shear tests, results

The viscoelastic behavior of hydrogel samples, prepared at different GelMA concentrations (to parity of molecules functionalization), was studied by performing dynamic oscillatory shear tests in strain mode.

The frequency dependence of the storage and loss modulus in the selected frequency range of hydrogels prepared at the four analyzed GelMA concentrations, is shown in Figure 3.13-16: G' and G'' average values with corresponding standard deviation error bars are plotted.

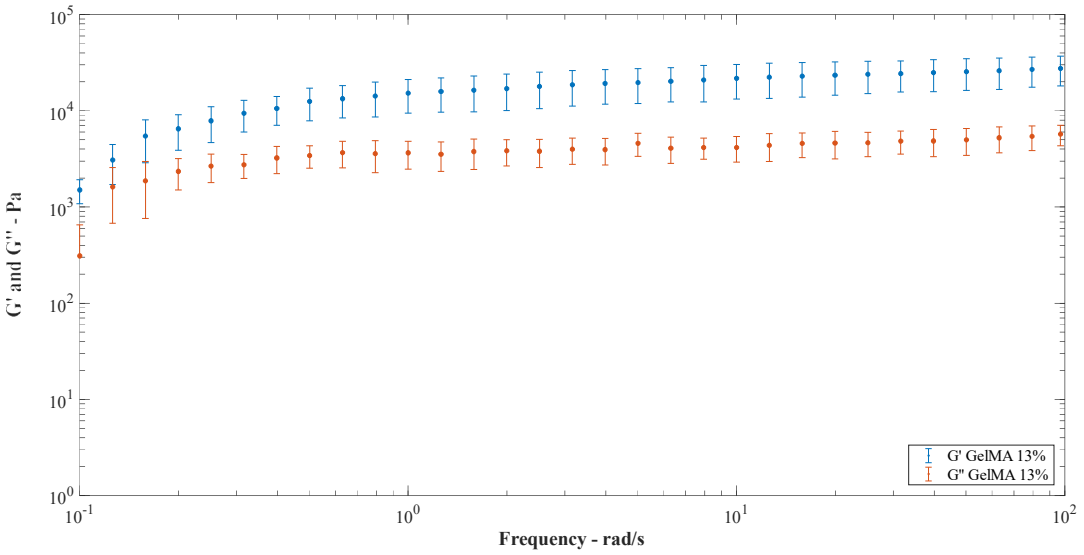

Figure 3.13. *Frequency sweep test of hydrogel samples at 13% (w/v) GelMA concentration: storage (G') and loss modulus (G'') average values; logarithmic scales.*

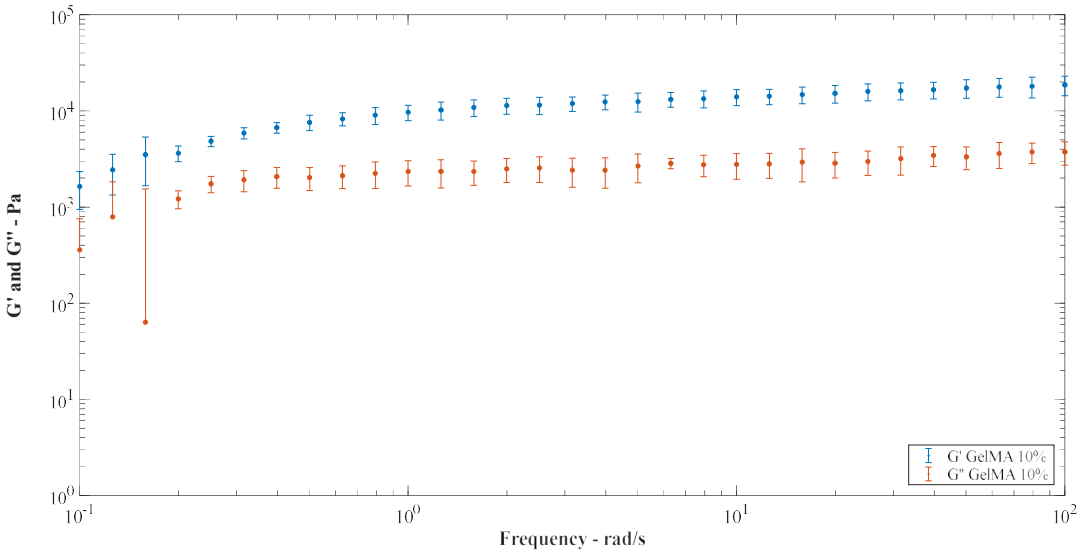

Figure 3.14. *Frequency sweep test of hydrogel samples at 10% (w/v) GelMA concentration: storage (G') and loss modulus (G'') average values; logarithmic scales.*

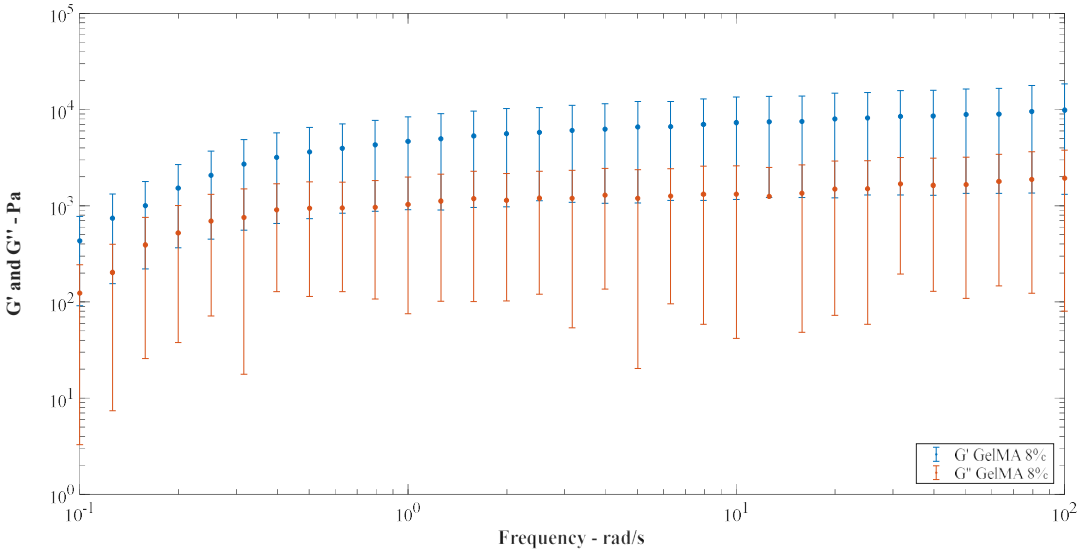

Figure 3.15. *Frequency sweep test of hydrogel samples at 8% (w/v) GelMA concentration: storage (G') and loss modulus (G'') average values; logarithmic scales.*

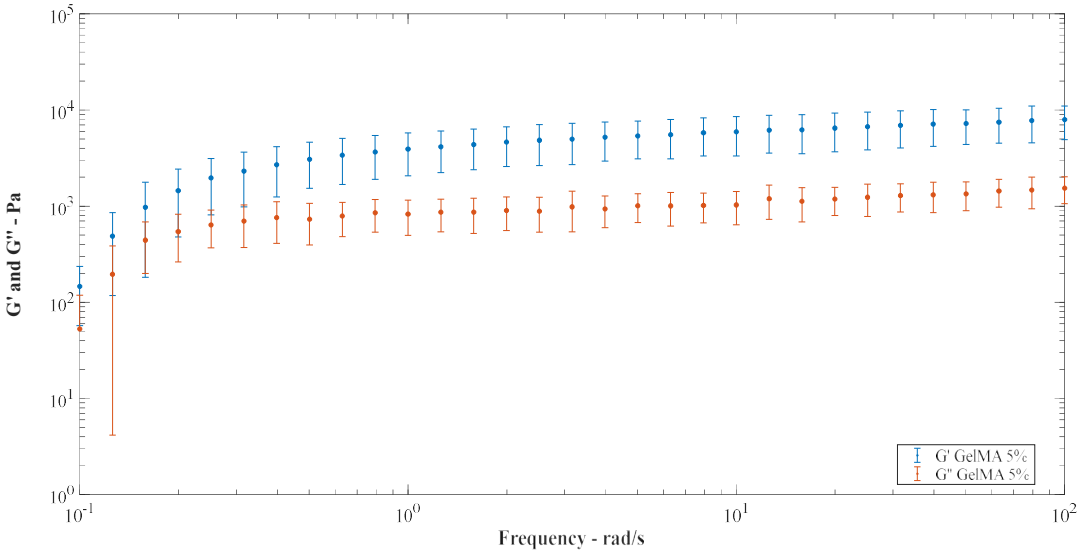

Figure 3.16. *Frequency sweep test of hydrogel samples at 5% (w/v) GelMA concentration: storage (G') and loss modulus (G'') average values; logarithmic scales.*

As clear from the analysis of graph in Figure 3.15, hydrogels samples at 8% GelMA concentration showed high results variability, and these were therefore excluded in the determination of general considerations about viscoelasticity's dependence on GelMA concentration. The high results variability was probably due to problems in samples preparation; especially, not all samples were characterized by flat surfaces and by the same width, necessary features for the success of rheological tests.

The analysis of individual graphs relative to samples at 5, 10 and 13% GelMA concentrations, shows the viscoelastic behavior of hydrogels: within the entire examined frequency range, G' values are greater than G'' values, both showing slight frequency dependence and exhibiting a plateau at higher frequencies The average tan(δ) values are consequently stable, almost independent of frequency variation, and indicative of the predominantly elastic response of these materials (Table 3.2).

Table 3.2. *Evaluation of average tan(δ) values for hydrogels at different GelMA concentrations, at specific frequency values.*

GelMA [%]	*UV exposure time [s]*	$tan(\delta)_{1\ rad/s}$ *[-]*	$tan(\delta)_{100\ rad/s}$ *[-]*
13	60	0.24 ± 0.03	0.21 ± 0.02
10	60	0.24 ± 0.02	0.20 ± 0.02
5	120	0.22 ± 0.05	0.20 ± 0.03

From graphs comparison, it is clear that the increase of GelMA concentration in hydrogels determines the increase of both the storage and loss modulus of the material, within the analyzed frequency range; however, according to results reported in Table 3.2, the variation of G' and G'' is such that their ratio, tan(δ), does not change.
In chemically crosslinked hydrogels, elastic behavior of three-dimensional polymeric networks varies considerably varying crosslinking density. In this context, GelMA concentration in hydrogels preparation was varied, however the difference in concentration was probably not high enough to see significant differences in hydrogels elastic response; moreover, the stability of hydrogels at lower GelMA concentration was ensured only by increasing the UV exposure time, therefore further affecting the polymeric network, and consequently the elastic response of the material.

3.3 Biological tests: results

Most of cellular tests were performed using hydrogels prepared with GelMA obtained with Method A and purified with ethanol. As already discussed in §3.1.1, because of the inefficiency of the first purification method, the complete removal of ethanol from GelMA was not possible, and ethanol presence therefore compromised the majority of cellular experiments, firstly in hydrogels preparation at different GelMA concentrations, and then in the phase of cells encapsulation, because of the introduction of cells in an unsuitable environment for their survival. Only in a few cases, bacteriological contamination problems were detected and therefore encapsulated cells death was jointly attributed to the presence of ethanol and of bacteria in the material.

The failure of experiments was verified both through test with fluorescence markers, and through direct observation of cells using a microscope: after only a few days of encapsulation in GelMA-based hydrogels, most of the cells were in pre-apoptotic or apoptotic stages. Especially, in fluorescence studies performed on hydrogels prepared with GelMA purified with ethanol, several problems of dyes introduction were encountered and also a high material autofluorescence was observed; in most cases this prevented the evaluation of cells viability. These issues were instead not found in the analysis of hydrogels prepared with GelMA purified through dialysis. Results of all the cellular tests performed described in §2.4 are reported and discussed in the following paragraphs.

3.3.1 Bioprinting with SK-N-AS cells: results

Considering the first designed structure for bioprinting tests with neuroblastoma cells, it was verified that the selected circular infill pattern was not ideal to ensure the homogenous filling of the four square-base parallelepipeds as reported in Figure 3.17. The homogenous filling of parallelepipeds was possible only by changing the infill pattern from circular to rectilinear; however, this change resulted in an increase in bioprinting time, prompting the design, at a later stage, of a second simplified structure.

Figure 3.17. *First structure designed for cellular tests with SK-N-AS cells, bioprinted with circular pattern infill in a multiwell plate.*

Bioprinting tests with the first structure were performed twice and in both cases the death of all cells was verified after 24 hours from encapsulation. The failure of both tests was mainly attributed to the residual presence of ethanol in the GelMA. Moreover, in all the three bioprinted structures of the first cellular test, a bacteriological contamination was detected.

About the first bioprinting test, once verified the contamination of all the structures with encapsulated cells, only one of them was analyzed with immunofluorescence after one day of incubation; one of the structures placed in medium with neuroblastoma-derived exosomes was

selected and analyzed using Hoechst 33258, and PI. In Figure 3.18, images of different areas of the square-based parallelepipeds of this structure are shown. Figure 3.18.a and 3.18.c show all cells present in the examined areas marked in blue (Hoechst 33258), while Figure 3.18.b and 3.18.d show dead cells, present in same examined areas, marked in red (PI).
As evident, there were staining problems with Hoechst 33258, and the high autofluorescence made the interpretation of these images complicated; the death of all encapsulated cells was anyway clear.

About the second bioprinting test with this structure, the failure of the experiment was not only attributed to the presence of ethanol in the hydrogel, it was actually also due to the abnormal behavior of SK-N-AS cells, probably related to high cell culture passage numbers. Both the bioprinted structures were analyzed with immunofluorescence after one day from incubation, using Hoechst 33258, Calcein AM and PI. In both cases staining problems were encountered, mainly using Hoechst 33258 and Calcein AM, and high material autofluorescence was verified. The death of almost all encapsulated cells was evident.

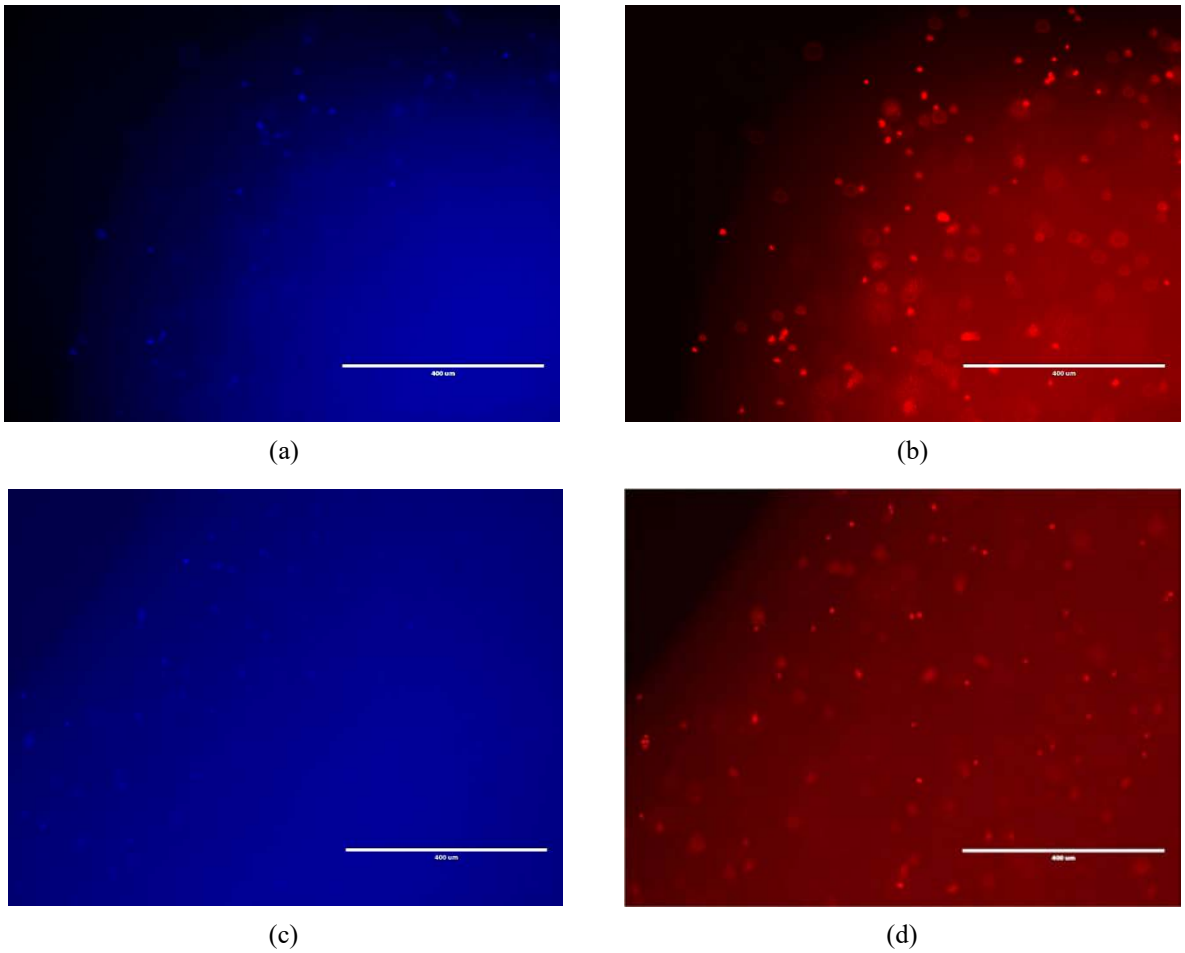

Figure 3.18. *Results of test with fluorescent markers on one structure of the first printing test after 24 hours from incubation: cells nuclei marked in blue by Hoecst 33258 (a), dead cells marked in red by Propidium Iodide(b); 10X magnification.*

Printing problems were solved using the second structure designed for tests with neuroblastoma cells: since the second structure was the first one halved and slightly modified in dimensions and size, printing time was reduced and by selecting the rectilinear infill of the square-based parallelepipeds, high printing resolution was achieved (Figure 3.19).

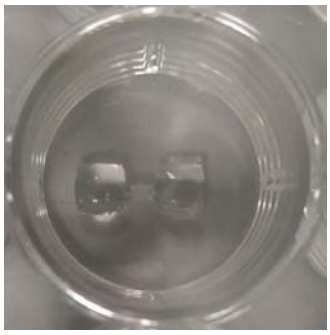

Figure 3.19. *Second structure designed for cellular tests with SK-N-AS cells, bioprinted with rectilinear pattern infill in a multiwell plate.*

The second structure was used to perform one single test using three cellular concentrations: for every cells concentration three structures were printed and, for every condition, one structure was analyzed using Hoechst 33258 and Calcein AM immediately after the printing (day 0), and then after 3 and 7 days from incubation.

Independently of the cellular concentration tested, cell viability was verified only in the fluorescence analysis performed immediately after printing; images of the structures analyzed on day 0 are shown in Figure 3.20, 3.21 and 3.22, for the three cellular concentrations. Even after only three days from incubation, high autofluorescence of GelMA hydrogels was verified and this made it not possible to evaluate cellular viability.
The failure of this test was mainly traced to the use of GelMA purified with ethanol for the preparation of hydrogels.

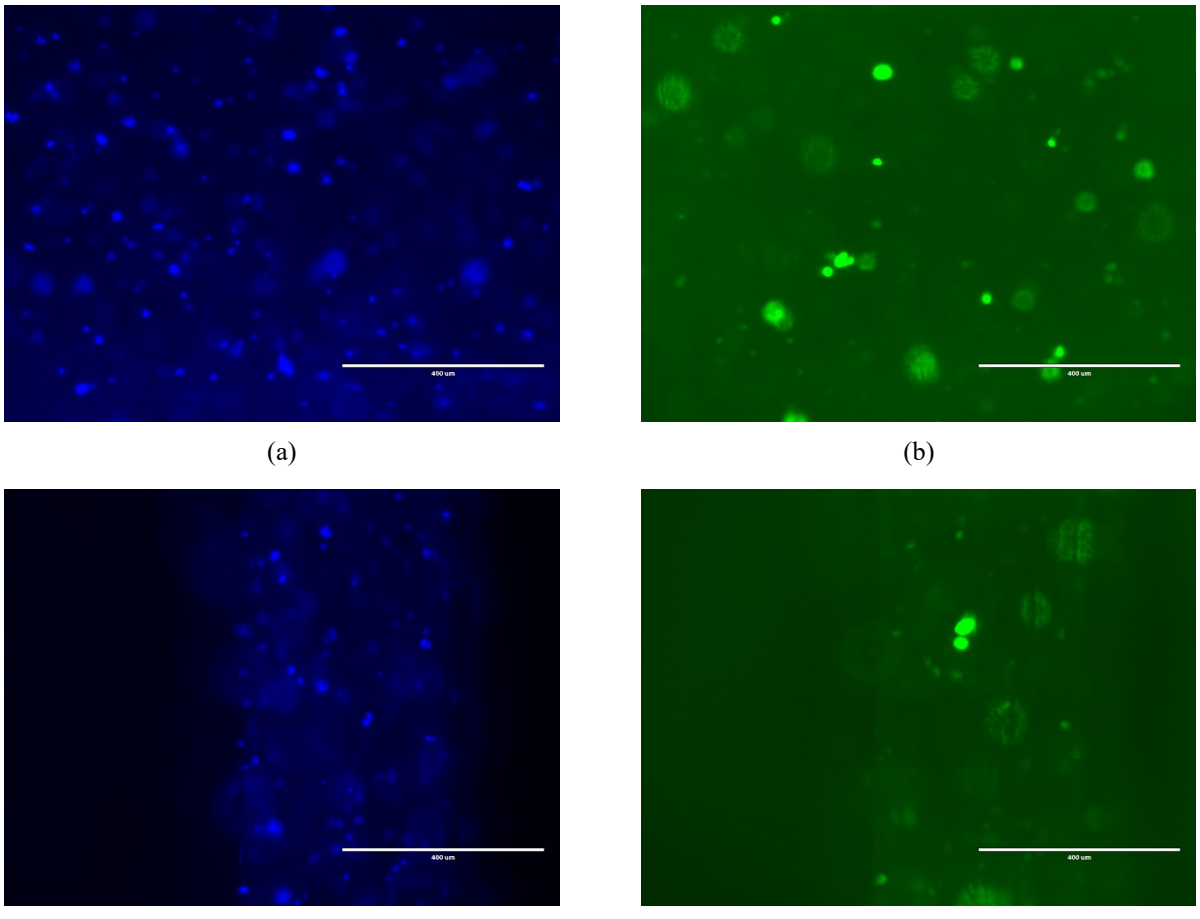

(a) (b)

(c) (d)

Figure 3.20. *Results of fluorescence analysis of one structure of the second cellular test with SK-N-AS cells, immediately after printing: 4*10^6 cells per ml of hydrogel. Cells nuclei marked in blue by Hoechst 33258 (a,c) and live cells marked in green by Calcein AM (b,d), in two different areas of the structure; 10X magnification.*

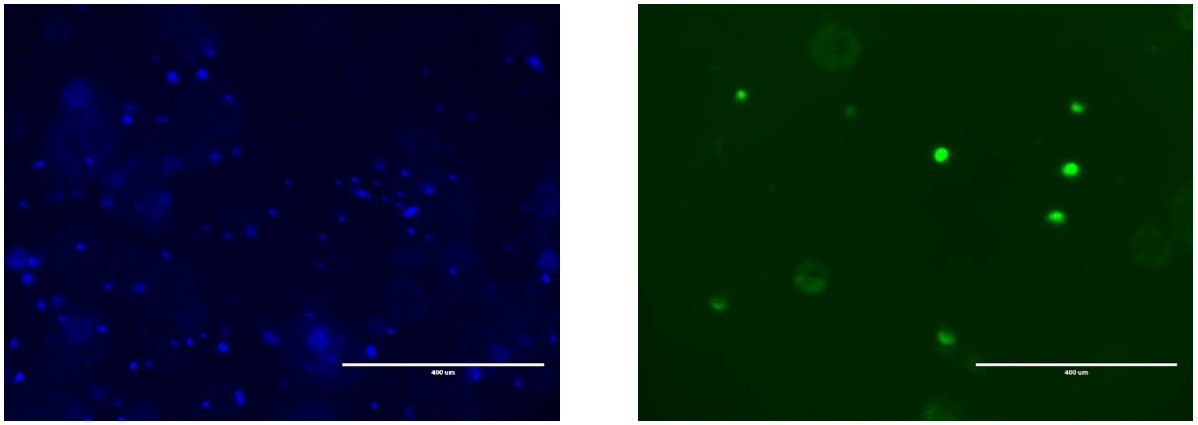

(a) (b)

Figure 3.21. *Results of fluorescence analysis of one structure of the second cellular test with SK-N-AS cells, immediately after printing: 400*10^3 cells per ml of hydrogel. Cells nuclei marked in blue by Hoechst 33258 (a) and live cells marked in green by Calcein AM (b), in one area of the structure; 10X magnification.*

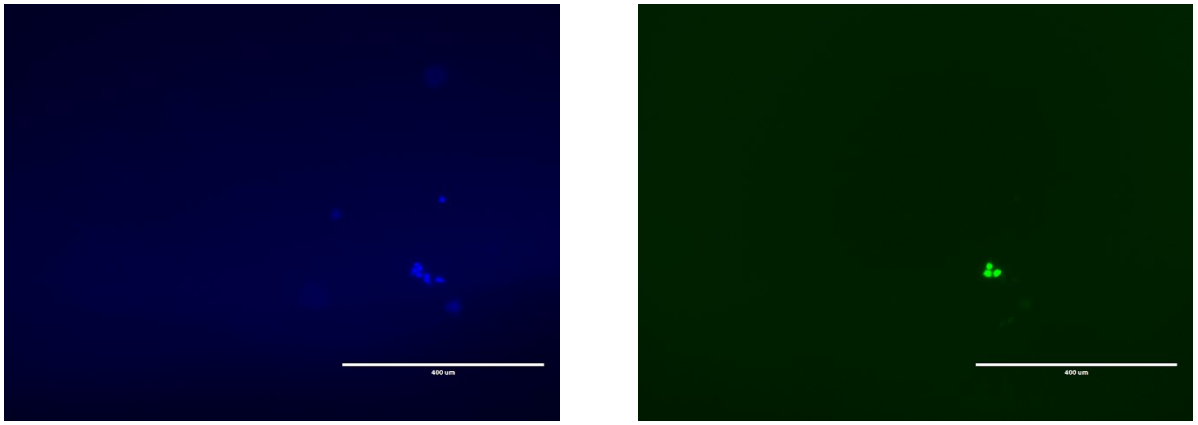

(a) (b)

Figure 3.22. *Results of fluorescence analysis of one structure of the second cellular test with SK-N-AS cells, immediately after printing: 40*10^3 cells per ml of hydrogel. Cells nuclei marked in blue by Hoechst 33258 (a) and live cells marked in green by Calcein AM (b), in one area of the structure; 10X magnification.*

3.3.2 Bioprinting with MSC cells: results

Tests with MSC cells were performed by printing the 8 channels ladder-like structure. Two cellular tests were carried out and in the first and second case, three and two structures were bioprinted, respectively. Structures were always efficiently bioprinted with high definition (Figure 3.23), as already verified in previous applications with SK-N-AS cells[2].

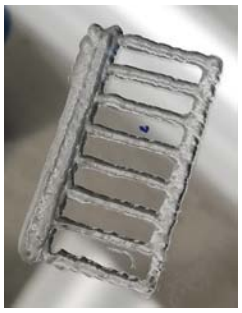

Figure 3.23. *Ladder-like structure designed for cellular tests with MSC cells, bioprinted with high definition in a petri dish.*

About the first cellular test, the bioprinted structures were analyzed after 3, 7 and 14 days of incubation, with fluorescent marker analysis using Hoechst 33258and Calcein AM. In Figure 3.24, 3.25 and 3.26, images of structures analyzed on each scheduled day are shown: cells nuclei are marked in blue (Hoechst 33258), while live cells are marked in green (Calcein AM).
As evident, there were staining problems of cells nuclei with Hoechst 33258 and high material autofluorescence prevented results interpretation in terms of viability. Most importantly, encapsulated cells were still alive after 3, 7 and even 14 days of incubation in GelMA hydrogels, indicative of the complete evaporation of ethanol during the preparation of the hydrogel.
The second cellular test confirmed these results: staining problems of cells nuclei were still encountered and the autofluorescence of the hydrogels made it difficult to interpret results in terms of cells viability. Cells were viable even after 14 days of incubation although always showing a rounded shape.

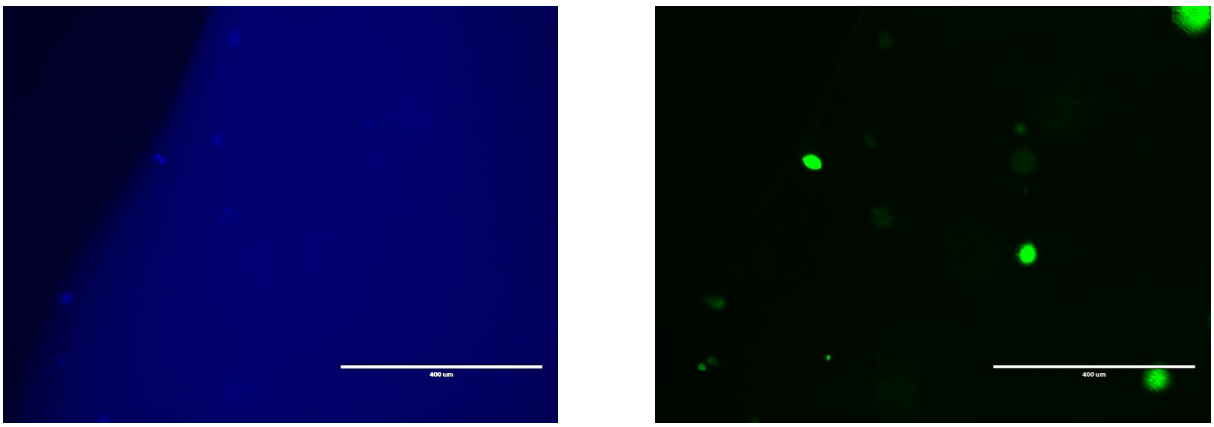

(a) (b)

Figure 3.24. *Results of fluorescence analysis of one structure of the first cellular test with MSC cells, after 3 days of incubation. Cells nuclei marked in blue by Hoechst 33258 (a) and live cells marked in green by Calcein AM (b), in the same area of the structure; 10X magnification.*

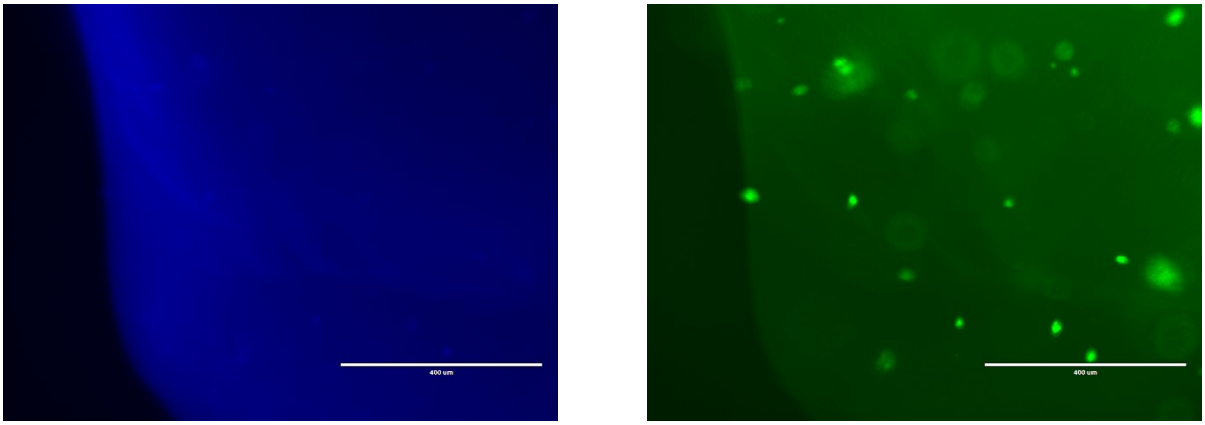

(a) (b)

Figure 3.25. *Results of fluorescence analysis of one structure of the first cellular test with MSC cells, after 7 days of incubation. Cells nuclei marked in blue by Hoechst 33258 (a) and live cells marked in green by Calcein AM (b), in the same area of the structure; 10X magnification.*

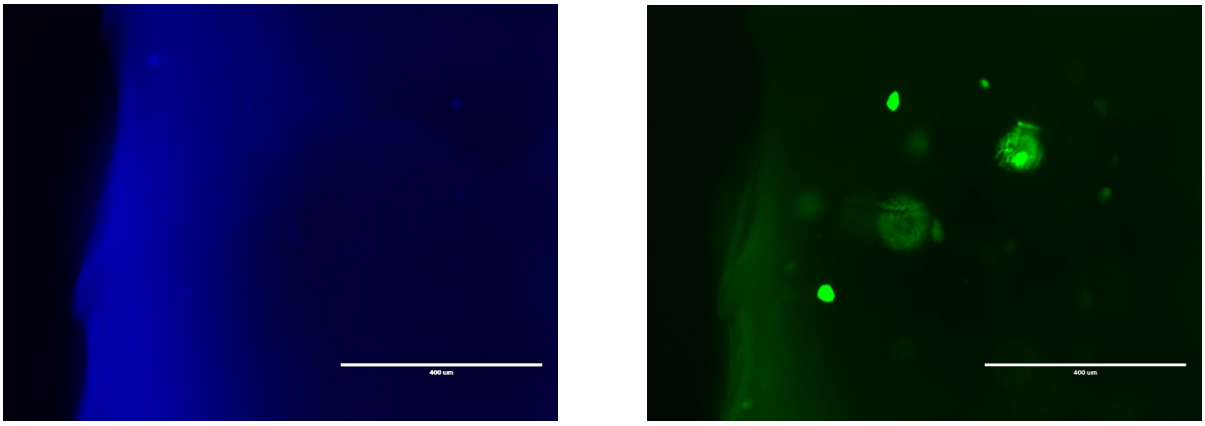

(a) (b)

Figure 3.26. *Results of fluorescence analysis of one structure of the first cellular test with MSC cells, after 14 days of incubation. Cells nuclei marked in blue by Hoecst 33258 (a) and live cells marked in green by Calcein AM (b), in the same area of the structure; 10X magnification.*

3.3.3 3D cylindrical scaffolds for cell cultures: results

Cellular tests performed by using cylindrical hydrogel scaffolds prepared with GelMA purified with ethanol, described in §2.4.5.1 (summarized in Table 2.2-4) and §2.4.5.2, led to similar results compared to the ones of bioprinting tests, already discussed. Especially, the same issues previously verified in bioprinted structures with encapsulated cells were identified also in the case of cylindrical hydrogels scaffolds.

First of all, independently of GelMA concentration in hydrogels and independently of cellular concentration tested, after 24 hours of incubation, encapsulated cells always showed pre-apoptotic and apoptotic shapes. Cells were clearly characterized by the presence of vesicular apoptotic bodies, resulting from cells disassembly (Figure 3.27). The presence of ethanol in hydrogels, common factor to all samples, was evaluated as the only reason for cells death, since no bacteriological contaminations were verified.

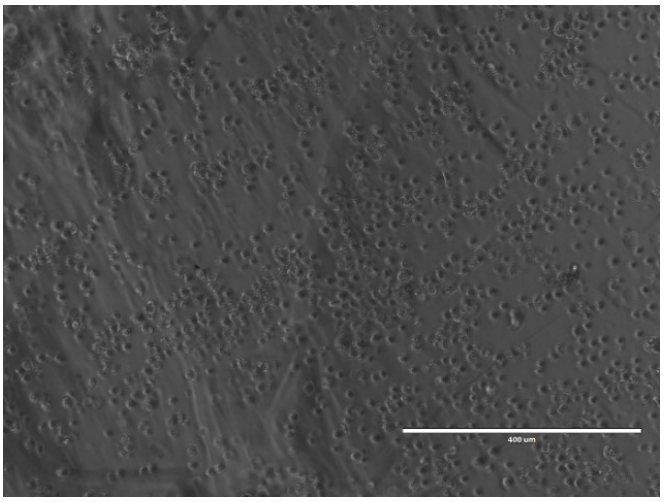

Figure 3.27. *First cellular test with HEK cells, cylindrical scaffold at 5% GelMA concentration, 1.5*10^6 cells per ml of hydrogel, after 1 days of incubation, seen on optical microscopy; 10X magnification. Cells are characterized by pre-apoptotic shapes.*

Secondly, in most samples staining problems were verified, with the staining solution seemingly not reaching the inner core of samples. High material autofluorescence was again verified and limited correct evaluation of cells viability. Significant results in terms of cells viability were found with the analysis of hydrogels cylindrical scaffolds prepared with GelMA purified through dialysis, used for HEK cells encapsulation, to perform the fourth viability test described in §2.4.5.1 and summarized in Table 2.5.

For every tested condition, fluorescence analysis results of day 1 and 3 of incubation, are shown in Figure 3.28 and 3.29: cells nuclei marked in blue using Hoechst 33258, and cells' cytoplasm stained green with Calcein AM. Hydrogels autofluorescence was not verified, even on samples examined after 3 days of incubation, and staining problems were not encountered since all cells were marked, even if placed in the inner part of samples.

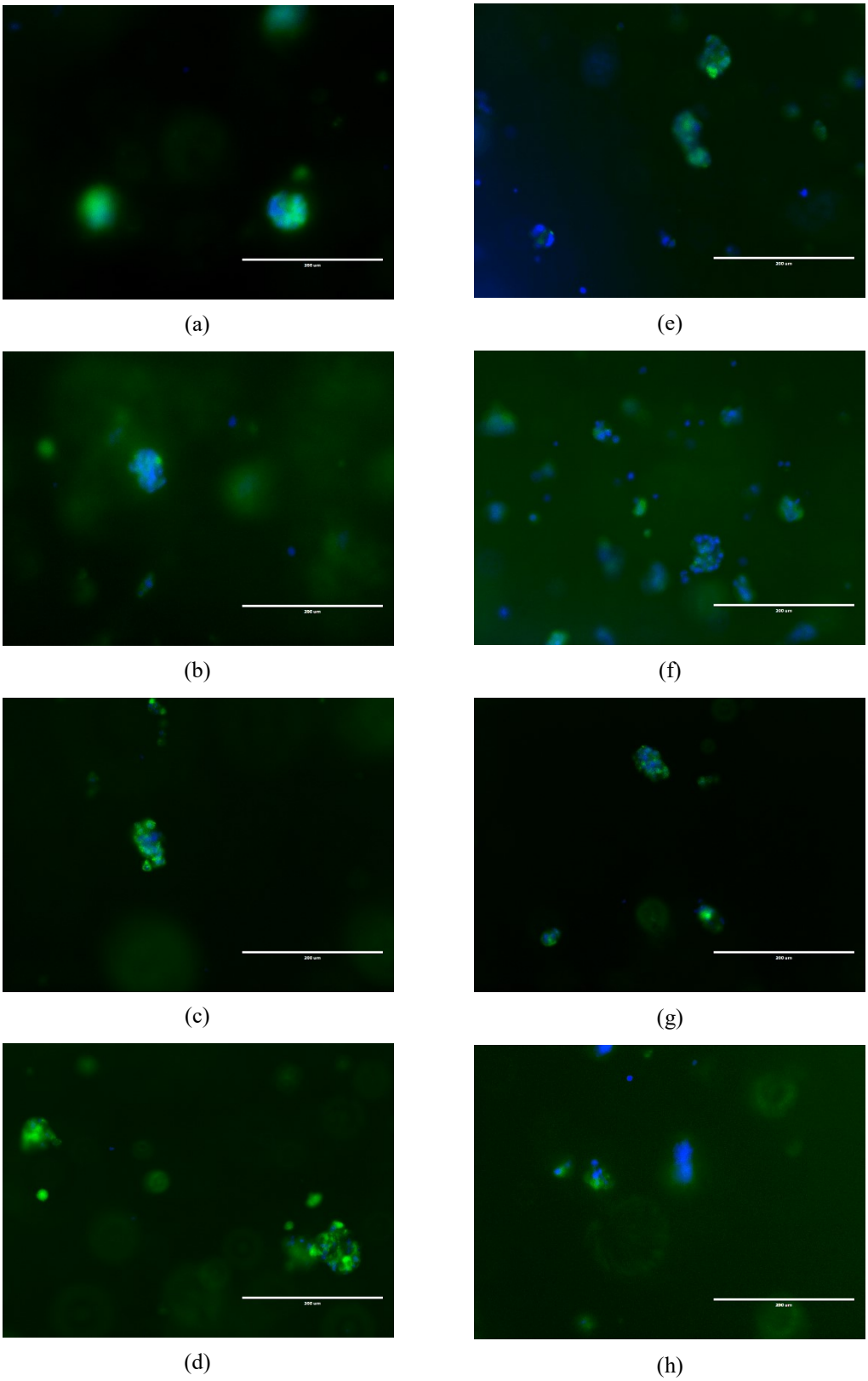

Figure 3.28. *Results of fluorescence analysis performed on 8% GelMA hydrogel samples after 1 (a-d) and 3 (e-h) days of incubation; cellular concentration of $1.5*10^6$ (a,e,c,g) and $3*10^6$ (b,d,f,h) of cells per ml of hydrogels; GelMA functionalized at 80% (a,e,b,f) and at 71% (c,g,d,h); 20X magnification.*

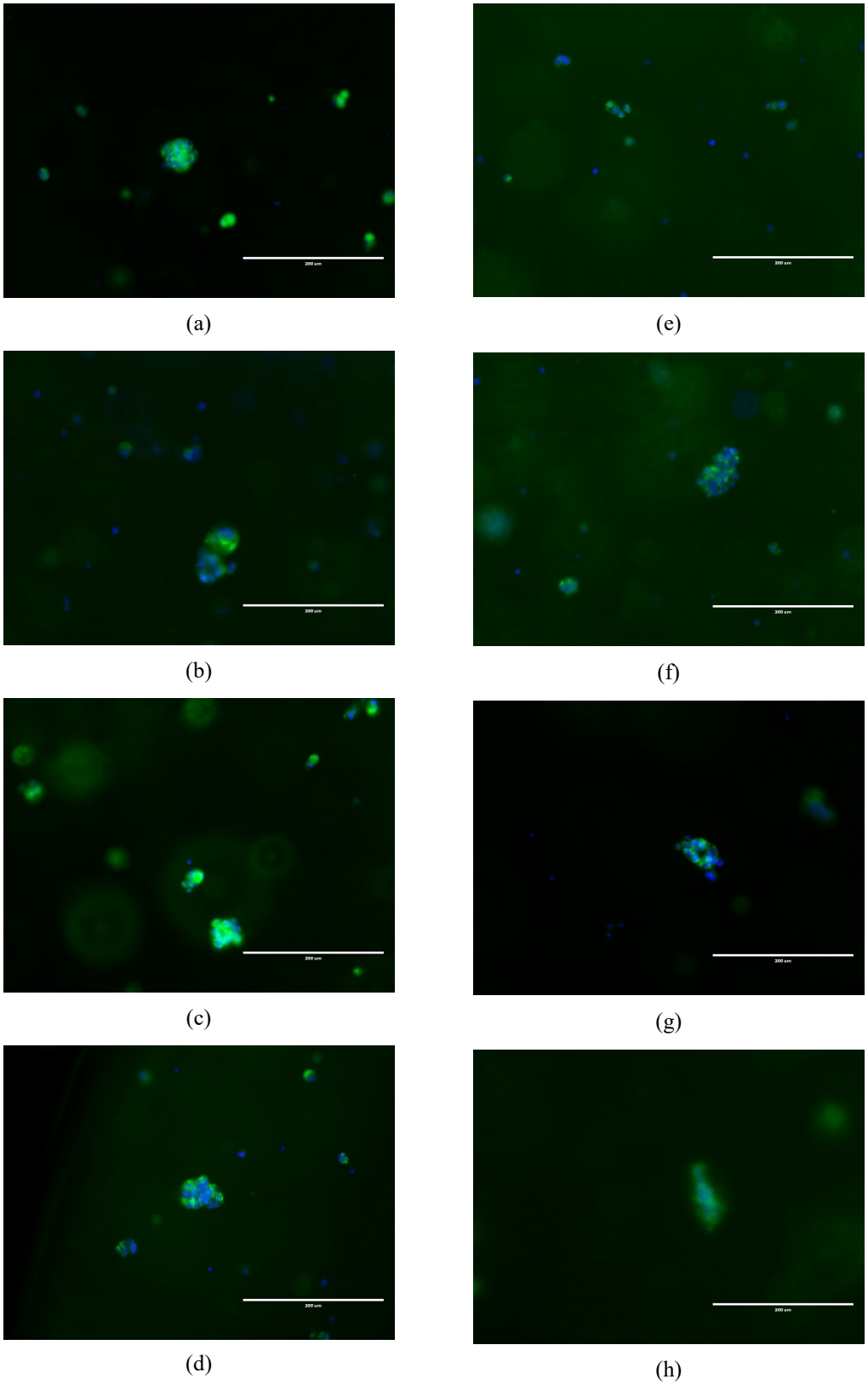

Figure 3.29. *Results of fluorescence analysis performed on 10% GelMA hydrogel samples after 1 (a-d) and 3 (e-h) days of incubation; cellular concentration of 1.5*10^6 (a,e,c,g) and 3*10^6 (b,d,f,h) of cells per ml of hydrogels; GelMA functionalized at 80% (a,e,b,f) and at 71% (c,g,d,h); 20X magnification.*

From a biological standpoint, independently of GelMA DoF and concentration in the hydrogel, and regardless of the tested cellular concentration, high cells viability was verified even after 3 days of incubation in every sample; especially, vesicular apoptotic bodies, resulting from cells disassembly, were not identified. Cells were mainly identified in clusters, probably a consequence of a non-uniform cell distribution in the hydrogels during hydrogel preparation.

In fluorescence analysis images, cells nuclei and cytoplasm were clearly distinguished, suggesting that cells were encapsulated in a favorable microenvironment to their survival. Cells showed rounded shapes even after 3 days of incubation, probably indicative of too high GelMA functionalization or concentration in the hydrogel. In order to draw definite conclusions, tests should be repeated increasing incubation time and by using hydrogels prepared at lower and higher GelMA concentration at parity of GelMA functionalization, and also using GelMA with higher and lower DoF at parity of GelMA concentration in hydrogels.

Conclusion

The aim of this thesis project was the development of three-dimensional polymeric structures for studies on neuroblastoma cancer cells, through the production of printable gelatin methacrylate hydrogels and using micro extrusion bioprinting technologies.
Three dimensional polymeric systems allow to overcome the limitations of two-dimensional ones, better mimicking the complexity of *in vivo* environments, while avoiding animal experimentation: in a three dimensional micro-environment, cells do not flatten but maintain a normal 3D structure, can experience a normal life cycle interacting with both the environment and other surrounding cells, can migrate without restriction in a plane, and their polarization is normal. The main advantage in the use of 3D polymeric constructs is the microscopic control over their structures through the manipulation of original macromolecules, to obtain suitable environment for cells encapsulation.
GelMA-based hydrogels are widely used in biological applications of tissue engineering and cell culture studies in general. GelMA-based hydrogels were thus selected as suitable materials to study in a 3D system a possible correlation between neuroblastoma cancer cells migration and cluster formation, and the presence of exosomes, cell-derived nanovescicles, that appear to be involved in metastasis formation.
On the basis of the main aim of this work, starting from the results of an earlier project[2], several sub targets were set and pursued.

First, two different methods of synthesis to obtain gelatin methacrylate molecules characterized by degree of functionalization in a specific range, compatible with planned biological applications, were tested in order to identify the most reproducible and efficient one.
Method A was already in use[2], while Method B was introduced as an improved version of the original synthesis method[38]. A comparison between Method A and Method B, in terms of reproducibility, was not possible because of problems related to the purification of GelMA obtained with Method A; however, it was anyway possible to verify the high reproducibility of Method B. Especially, Method B was applied six times and, in all cases, the DoF of GelMA molecules fell within the expected range of interest, and exactly between 50 and 70%. To draw conclusions about the reproducibility of Method A, GelMA synthesis should be repeated and followed by the application of the purification method evaluated as efficient.
Method B was then also identified as the most efficient one, since reaction conditions allow for the minimization of the molar excess of methacrylic anhydride, with consequent costs reduction, and because of the lower dependence of functionalization results on the operator intervention.

Second, two methods for GelMA purification were applied to have the separation of un-reacted anhydride, salts and methacrylic acid from the solution after gelatin methacrylation, in order to identify the most efficient one among them. The first purification method was already in use[2], in combination with Method A, and required the use of ethanol and vacuum drying. The second purification method was based on dialysis against deionized water, followed by freeze-drying. The first purification method proved to be inefficient since the complete removal of ethanol from the dried material was not possible. Specifically, the presence of ethanol in GelMA was firstly verified in the non-homogeneity of the final material and was then confirmed by H NMR analysis results. The second purification method, used both in combination with Method A and Method B, resulted in the complete removal of unreacted methacrylic anhydride, salts and methacrylic acid from GelMA molecules was possible.

Characterization analysis were performed on GelMA obtained with Method B and purified through dialysis: the degree of functionalization of gelatin molecules was verified with Nuclear Magnetic Resonance analysis; Fourier Transform Infrared Spectroscopy analysis were performed to identify and compare characteristic groups of pure gelatin and GelMA; thermogravimetric analysis were performed in order to verify the efficiency of freeze-drying applied to dry GelMA after dialysis; Differential Scanning Calorimetry analysis were then used to study the semi-crystalline nature of GelMA.

From the comparison of FTIR spectra of pure gelatin powder and GelMA samples, it was clear that the methacrylation of gelatin could not be verified with this analysis, because of the limited functionalization of free amino groups of lysine of gelatin molecules. In both gelatin and GelMA spectra, peaks associated with the stretching vibration of amine, CH groups, secondary amide and carbonyl groups were identified.

Thermogravimetric analysis of GelMA samples firstly demonstrated the efficiency of freeze-drying process, since the residue water weight percentage in analyzed samples was lower than 7%. It was then possible to evaluate the thermal stability temperature range of GelMA both in inert and oxygen conditions. In the temperature range from ambient temperature and up to approximately 220°C, GelMA samples showed thermal stability both in inert and oxygen conditions, while above this upper limit value, and up to 300°C, thermal degradation (in inert atmosphere) and thermal oxidative degradation phenomena (in oxygen atmosphere) determined significant percentage weight loss, that were anyway dependent on the degree of crystallization of the material.

Differential scanning calorimetry analysis on GelMA samples confirmed the semi crystalline nature of the material: a second order glass transition was identified at approximately 47.5°C, while two endothermic transitions, one at 84.6°C and the other more relevant one at 154.5°C, demonstrated the presence of crystals characterized by different sizes. No significant information was obtained about the behavior of the material below 0°C, in the storage

temperature range. Since this analysis was performed only on samples from a single synthesis batch, to get further confirmation about the glass transition and melting temperature values of GelMA, analysis should be repeated on more samples, from other synthesis batches.

GelMA obtained with Method B, purified through dialysis, and with DoF in the specific range of interest, was used to prepare hydrogels at different polymer concentrations, compatible with biological applications. Hydrogel samples were analyzed to evaluate how GelMA concentration affects the morphology of the polymeric network, hydrogels swelling, porosity and viscoelastic properties, and therefore to verify the suitability of these materials for cells encapsulation.
It was first verified that the fractional increase of hydrogel weight due to the absorption of fluids and water retention, increase at most linearly with the decrease of GelMA concentration; it was therefore clear that hydrogels prepared at lower GelMA concentration are best suited to ensure the exchange of fluids, providing a better microenvironment for cells encapsulation.
The porous structure of freeze-dried hydrogels, prepared at different GelMA concentration, was then studied with scanning electron microscopy analysis. Images revealed that hydrogels are characterized by a honeycomb-like super-porous structure, with interconnected pores with diameters ranging between 6 and 80 μm, mainly distributed in the range from 10 to 20 μm, independently of GelMA concentration. It was therefore verified that hydrogels prepared at GelMA concentration in the range from 5 to 13% (w/v) are characterized by suitable porous structure for cells encapsulation. Such diameters suggest that cells can easily accommodate into the hydrogels microstructure, assume 3D shapes and experience a normal life cycle, growing and interacting with the surrounding microenvironment.
The viscoelastic properties of hydrogels prepared at the same GelMA concentrations, already characterized in terms of swelling properties and porosity, were then also studied with dynamic oscillatory shear tests, performed in strain mode. It was verified that, independently of GelMA concentration in the analyzed frequency range, hydrogels were characterized by a predominantly elastic response to the applied deformations. No significant differences in the ratio between G' and G'' were highlighted in hydrogels prepared at different GelMA concentrations. Dynamic oscillatory shear tests should be repeated using hydrogels samples prepared at 8% (w/v) GelMA concentration, since problems related to their preparation caused the failure of the tests.
Swelling tests, porosity determination and viscoelastic properties evaluation, should be repeated on hydrogels prepared by varying not only GelMA concentration, but also other factors such as the DoF of gelatin molecules, the photo initiator concentration, and UV exposure time. These tests should be repeated to understand the microscopic control over hydrogels structures through the manipulation of original macromolecules, and other factors involved in their preparation, to study how to obtain environment even more suited to cells encapsulation.

Gelatin methacrylate hydrogels were used to perform cellular tests with SK-N-AS neuroblastoma cells, MSC cells, and HEK 293 cells. The main aims were to study the viability of different cells line within the synthesized hydrogels in view of planned co-culture tests, and to verify migration and cluster formation of neuroblastoma cells in the presence of neuroblastoma derived exosomes.

Initially, gelatin methacrylate hydrogels were prepared and used as bioinks for three dimensional bioprinting tests both with cancerous and non-cancerous cells, following protocols already in use[2]. Especially, hydrogels for cells encapsulation were prepared using GelMA obtained with Method A, purified with ethanol, at 13% (w/v) GelMA concentration, optimized for bioprinting applications[2]. Three dimensional structures were designed in order to study the aforementioned phenomena. Due to the failure of all the cellular tests performed, simple viability tests were performed by decreasing GelMA concentration in hydrogels down to the 5% (w/v), and realizing 3D cylindrical scaffolds, simply using PDMS molds. Tests failure was finally traced to the inefficiency of the application of the first method applied for GelMA purification, and therefore to the presence of ethanol in the dried material used for hydrogels preparation. The residual presence of ethanol, did not only determine the death of all encapsulated cells, but it was probably also the cause of the high material autofluorescence when analyzed with cells staining solutions.

These problems were solved with the introduction of the second purification method of GelMA molecules, certainly much more complicated and time consuming than the first one, but efficient. First significant results were actually found by performing simple viability tests with HEK cells, using hydrogels prepared with GelMA synthetized with Method A and Method B, purified through dialysis. Hydrogels were prepared using GelMA characterized by DoF compatible with cells encapsulation (70% and 80%), and at too low GelMA concentration to use bioprinting technologies (8% and 10% w/v) and two cellular conditions were tested ($1.5*10^6$ and $3*10^6$ cells per ml of hydrogel); simple cylindrical scaffolds were therefore realized by using PDMS molds. Different conditions were tested in order to identify differences in cells behavior, and high cells viability was verified, even after three days of incubation, independently of the tested conditions. In fluorescence analysis images, cells nuclei and cytoplasm were clearly distinguished, suggesting that cells were encapsulated in a favorable microenvironment to their survival; cells anyway maintained rounded shapes. No staining problems were verified and, no significant hydrogels autofluorescence was detected. These tests results cannot however be used to draw up definite conclusions on the optimal conditions for cells encapsulation: tests should be repeated increasing incubation time and by using hydrogels prepared at lower and higher GelMA concentration at parity of GelMA functionalization, and also using GelMA with higher and lower DoF at parity of GelMA concentration in hydrogels.

3D cylindrical hydrogels scaffolds with encapsulated cells were used in this context, as a temporary solution to obtain biological results even at low GelMA concentration, verified to be compatible with cells encapsulation[45], but not printable. If biological results are verified repeating tests using cylindrical scaffolds, printability tests with hydrogels prepared using GelMA obtained with both Method A and Method B and purified through dialysis should be performed, in order to optimize hydrogels for three dimensional bioprinting tests. If necessary, natural-based additives could be used to increase the viscosity of hydrogels, keeping GelMA concentration at the desired value, obtaining printable bioinks.

Appendix

A.1 H NMR graphs

The H NMR graphs, result of the analysis of GelMA samples from three synthesis batch, obtained with Method B, purified through dialysis and freeze-dried, are shown in Figure A.1.1 – A.1.3. The H NMR graph result of the analysis of one GelMA sample, obtained with Method A, purified and freeze-dried, is instead shown in Figure A.1.4. These graphs were compared to the H NMR graph of pure Type A gelatin (gel strength 300) in order to evaluate the degree of functionalization of gelatin molecules.

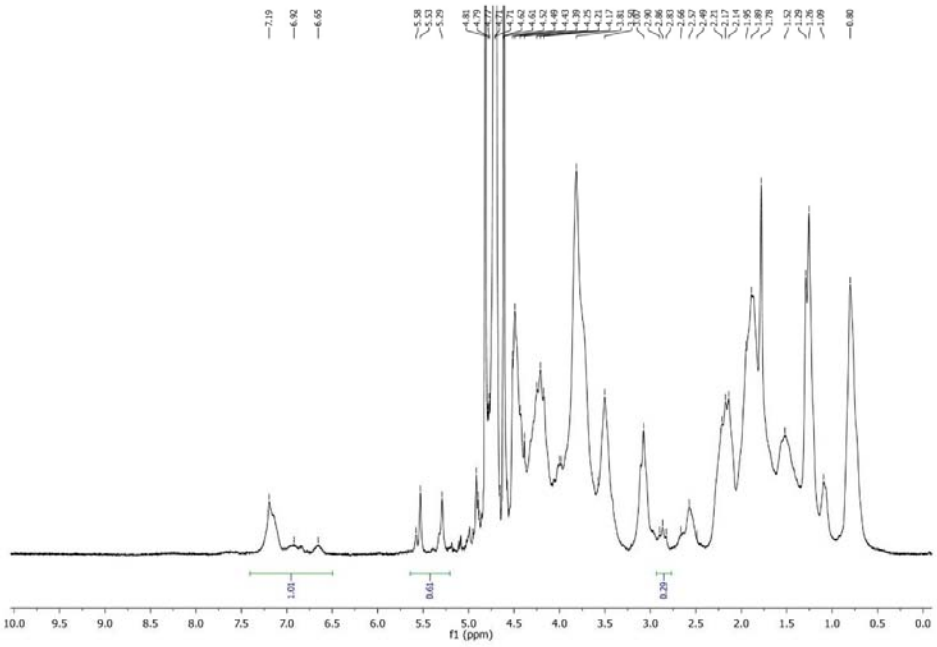

Figure A.1.1. *H NMR graph of GelMA obtained with Method B, purified through dialysis and freeze-dried. The estimated degree of functionalization of gelatin molecules is 60* ± 10*%.*

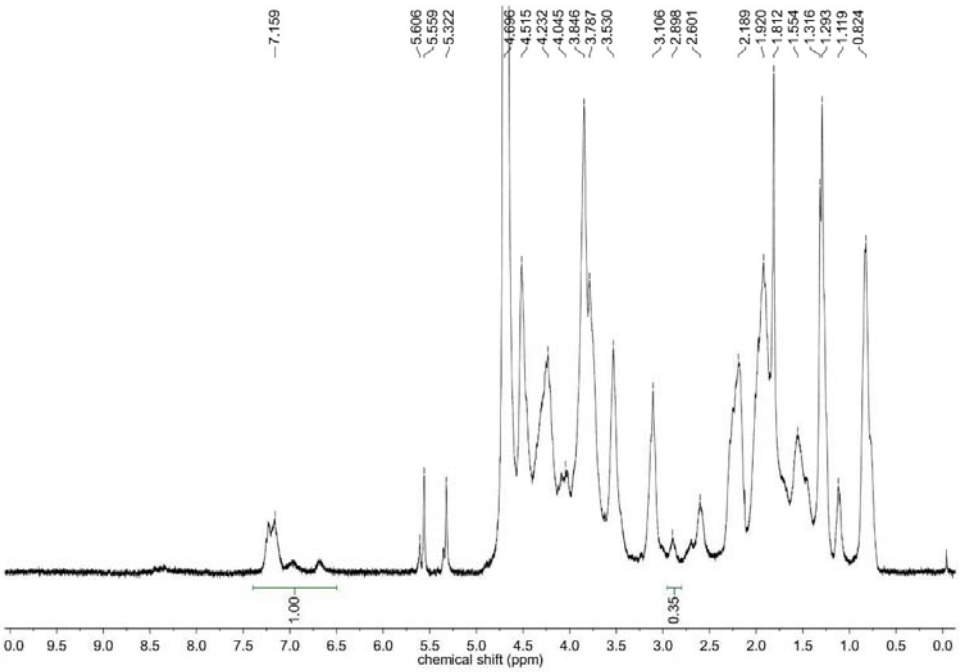

Figure A.1.2. *H NMR graph of GelMA obtained with Method B, purified through dialysis and freeze-dried. The estimated degree of functionalization of gelatin molecules is 55* ± 10*%.*

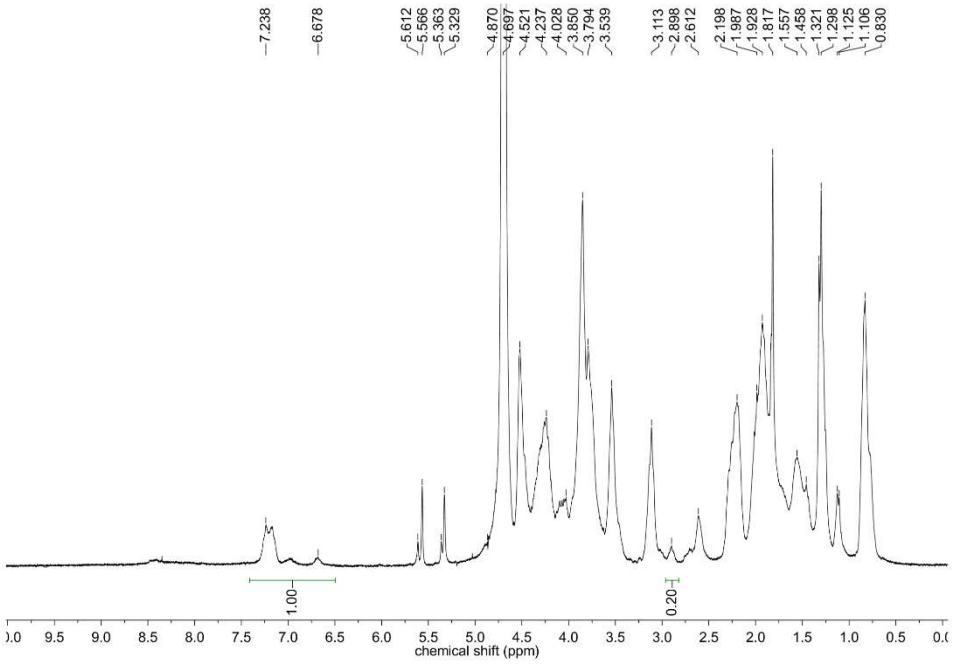

Figure A.1.3. *H NMR graph of GelMA obtained with Method B, purified through dialysis and freeze-dried. The estimated degree of functionalization of gelatin molecules is 71* ± 10*%.*

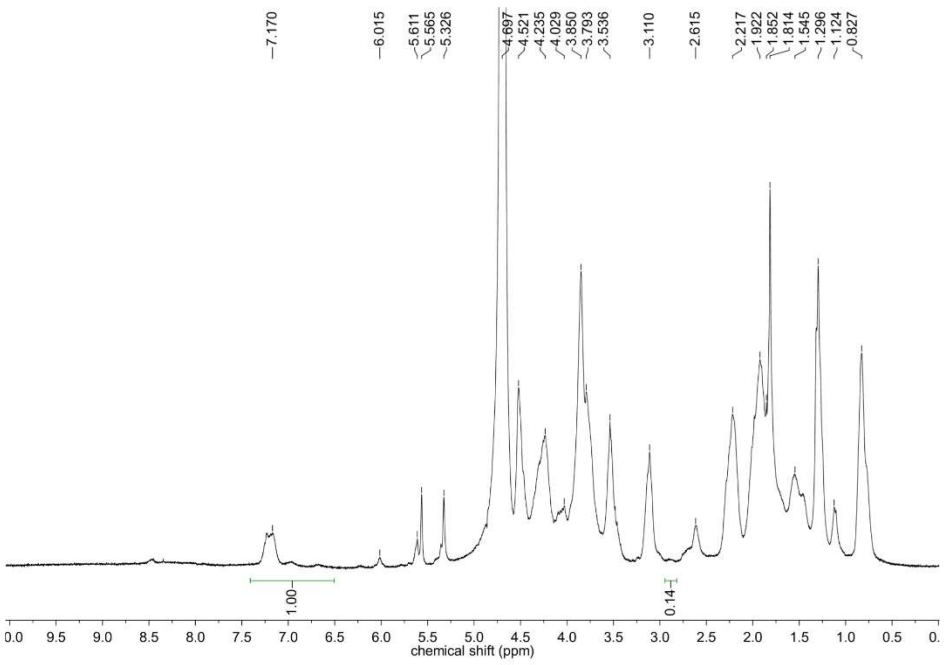

Figure A.1.4. *H NMR graph of GelMA obtained with Method A, purified through dialysis and freeze-dried. The estimated degree of functionalization of gelatin molecules is 80* ± 10*%.*

A.2 Swelling tests results

Due to the inefficiency of the first purification method, swelling tests performed on hydrogels prepared with GelMA purified with ethanol gave unreliable results. In Table A.1, results of swelling tests performed on hydrogels samples at 5, 8, 10 and 13% (w/v) of GelMA are shown.

Table A.1. *Results of swelling tests performed on hydrogels samples prepared at different GelMA concentrations, using GelMA obtained with the first synthesis method and purified through ethanol.*

GelMA [%]	*UV exposure time [s]*	*Swelling Ratio [%]*	*Water content [%]*
5	120	1227 ± 54	92.5 ± 0.3
8	60	1028 ± 24	91.0 ± 0.2
10	60	1090 ± 71	92.0 ± 0.9
13	60	801 ± 40	88.2 ± 0.3

Bibliography

1. Donglai L. V., Zongtao H. U., Lin L. U., Husheng L. U. and Xiuli X. U. (2017). Three-dimensional cell culture: A powerful tool in tumor research and drug discovery (Review). *ONCOLOGY LETTERS*, **14**, 6999-7010.
2. Mantovani M. (2019). Synthesis, optimization and 3D bioprinting of gelatin methacrylate hydrogels for cell culture studies. *Master Thesis*, University of Padova.
3. Mouw J. K., Ou G. and Weaver V. M. (2014). Extracellular Matrix Assembly: A Multiscale Deconstruction. *Nature Reviews Molecular Cell Biology*, **15**, 771-785.
4. Baker B. M. and Chen C.S. (2012). Deconstructing the third dimension - how 3D culture microenvironments alter cellular cues. *Journal of Cell Science*, **125**, 3015-3024.
5. Martino F., Peresterlo A. R., Vinarsky V., Pagliari S. and Forte G. (2018). Cellular Mechanotransduction: From Tension to Function. *Frontiers in Physiology*, **9**.
6. Chen Y., Ju L., Rushdi M., Ge C. and Zhu C. (2017). Receptor-mediated cell mechanosensing. *Molecular Biology of the Cell*, **28**(23), 3134-3155.
7. Guilak F., Cohen D. M., Estes B. T., Gimble J. M., Liedtke W. and Chen C. S. (2009). Control of stem cell fate by physiscal interactions with the extracellular matrix. *Cell Stem Cell*, **5**, 17-26.
8. Hanahan D. and Weinberg R. A. (2011). Hallmarks of Cancer: The Next Generation. *Cell*, **144**, 646-674.
9. Wullkopf L., West A. K. V., Leijnse N., Cox T. R., Madsen C. D., Oddershede L. B. and Erler J. T. (2018). Cancer cells' ability to mechanically adjust to extracellular matrix stiffness correlates with their invasive potential. *Molecular Biology of the Cell*, **29**, 2359-2369.
10. Cox T. R. and Erler J. T. (2011). Remodeling and homeostasis of the extracellular matrix: implications for fibrotic diseases and cancer. *Disease Models & Mechanisms*, **4**, 165-178.
11. Walker C., Mojares E. and del Rìo Hernàndez A. (2018). Role of Extracellular Matrix in Development and Cancer Progression. *International Journal of Molecular Sciences*, **19**, 3028.
12. Zheng Y., Nan H., Liu Y., Fan Q., Wang X., Liu R., Liu L., Ye F., Sun B. and Jiao Y. (2019). Modeling cell migration regulated by cell extracellular-matrix micromechanical coupling. *Physical Review E*, **100**.
13. Thomas M. A., Klesit A. B. and Volkman B. F. (2018). Decoding the Chemotactic Signal. *J Leukoc Biol,* **104**, 359-374.
14. Brunk A., Kolbe N. and Sfakianakis N. (2016). Chemotaxis and Haptotaxis on Cellular Level. *Theory, Numerics and Applications of Hyperbolic Problems I*, p. 249-261.
15. Mantellan C. and del Rìo Hernàndez A. (2019). Engineering the cellular mechanical microenvironment – from bulk mechanics to the nanoscale. *Jouranl of Cell Science*, **132**.

16. Zheng Y., Nan H., Fan Q., Wang X., Liu L., Liu R., Ye F., Sun B. and Jiao Y. (2019). Modeling cell migration regulated by cell-ECM micromechanical coupling. *Physical Review Journals*, **100**, p. 11.
17. Yamada K. M. and Cukieraman E. (2007). Modeling Tissue Morphogenesis and Cancer in 3D. *Cell Press Selections, Stem Cells: Toward Precision Medicine*, **130**, 601-610.
18. Caliari S. R. and Burdick J. A. (2016). A practical guide to hydrogels for cell culture. *Nature Methods*, **13**, 405-414.
19. Pereira R. F. and Bártolo P. J. (2015). 3D bioprinting of photocrosslinkable hydrogel constructs. *Journal of Applied Polymer Science*, **132** (48).
20. Murphy S. V. and Atala A. (2014). 3D bioprinting of tissues and organs. *Nature Biotechnology*, **32** (8), 773-785.
21. Selcan G. O. P., Inci I., Zhang Y. S., Khademhosseini A. and Dokmeci M. R. (2018). Bioiks for 3D bioprinting: an overview. *Biomaterials Science*.
22. Cidonio G., Glinka M., Dawson J. I. and Oreffo R. O. C. (2019). The cell in the ink: Improving biofabrication by printing stem cells for skeletal regenerative medicine. *Biomaterials*, **209**, 10-24.
23. Enas M. A. (2013). Hydrogel: Preparation, characterization, and applications: A review. *Journal of Advanced Research*, **6**, 105-121.
24. Tibbitt M. W. and Anseth K. S. (2009). Hydrogels as Extracelluar Matrix Mimics for 3D Cell Culture. *Biotechnology & Bioengineering,* **103** (104), 655-663.
25. Catoira M. C., Fusaro L., Di Francesco D., Ramella M. and Boccafoschi F. (2019). Overview of natural hydrogels for regenerative medicine applications. *Journal of Materials Science: Materials in Medicine*, **30**, 115.
26. Williams G. C., Malik A. N., Kim K. T., Manson P. N. and Elisseeff J. H. (2005). Variable Cytocompatibility of Six Cell Lines With Photoinitiators Used for Polymerizing Hydrogels and Cell Encapsulation. *Biomaterials*, **26**, 1211-8.
27. Chai Q., Jiao Y. and Yu X. (2017). Hydrogels for Biomedical Applications: Their Characteristics and the Mechanisms behind Them. *Gels*, **3**, p.6.
28. Klotz B. J., Gawlitta D., Rosenberg A. J., Malda J. and Melchels F. P. (2016). Gelatin-Methacryloyl Hydrogels: Towards Biofabrication-Based Tissue Repair. *Trends in Biotecnology*, **34** (5), 394-407.
29. Lee B. H., Shirahama H., Cho N. J. and Tan L. P. (2015). Efficient and controllable synthesis of highly substituted gelatin methacrylamide for mechanically stiff hydrogels. *RSC Advances*, **5**, 106094-106097.
30. Yue K., Trujillo-de Santiago G., Alvarez M. M., Tamayol A., Annabi N. and Khademhosseini A. (2015). Synthesis, properties, and biomedical applications of gelatin methacryloyl (GelMA) hydrogels. *Biomaterials*, **73**, 254-271.

31. Seager R. J., Hajal C., Spill F., Kamm R. D. and Zaman M. H. (2017). Dynamic interplay between tumour, stroma and immune system can drive or prevent tumour progression. *Convergent Science Physical Oncology*, **3**.
32. Xiong G. and Xu R. (2016). Function of cancer cell-derived extracellular matrix in tumor progression. *Journal of Surveillance, Security and Safety*, **2**, 357-364.
33. Wang M., Zhao J., Zhang L., Wei F., Lian Y., Wu Y., Gong Z., Zhang S., Zhou J., Cao K., Li X., Xiong W., Li G., Zeng Z. and Guo C. (2017). Role of tumor microenvironment in tumorigenesis. *Journal of Cancer*, **8** (5), 761-773.
34. Deaaboul G. (2019). For Clinical Utility, Exosomes Require New Isolation and Analysis Tools. *Genetic Engineering & Biotechnology News*, **39**.
35. Maia J., Caja S., Moraes M. C. S., Couto N. and Costa-Silva B. (2018). Exosome-Based Cell-Cell Communication in the Tumor Microenvironment. *Frontiers in Cell and Developmental Biology*, **6**.
36. Ayob A. Z. and Ramasamy T. S. (2018). Cancer Stem Cells as Key Drivers of Tumour Progression. *Journal of Biomedical Science*, **25**.
37. Loessner D., Meinert C., Kaemmerer E., Martine L. C., Yue K., Levett P. A., Klein T. J., Melchels F. P. W., Khademhosseini A. and Hutmacher D. W. (2016). Functionalization, preparation and use of cell-laden gelatin methacryloyl–based hydrogels as modular tissue culture platforms. *Nature Protocols,* **11** (4), 727-746.
38. Van Den Bulcke A. I., Bogdanov B., Rooze N. D., Schacht E. H., Cornelissen M. and Berghmans H. (2000). Structural and Rheological Properties of Methacrylamide Modified Gelatin Hydrogels. *Biomacromolecules*, **1** (1), 31-38.
39. Modaresifar K., Hadjizadeh A. and Niknejad H. (2018). Design and fabrication of GelMA/chitosan nanoparticles composite hydrogel for angiogenic growth factor delivery. *Artificial Cells, Nanomedicine, and Biotechnology*, **8**, 1799-1808.
40. Shirahama H., Lee B. H., Tan L. P. and Cho N. J. (2016). Precise Tuning of Facile One-Pot Gelatin Methacryloyl (GelMA) Synthesis. *Scientific Reports*, **6**.
41. Brigo L., Urciuolo A., Giulitti S., Della Giustina G., Tromayer M., Liska R., Elvassore N. and Brusatin G. (2017). 3D high-resolution two-photon crosslinked hydrogel structures for biological studies. *Acta Biomaterialia*, **55**, 373-384.
42. Raju P. M. S. (2012). Infiltration growth processig of YBCO nanocomposites: shape forming, microstructural and magnetic studies. *Doctoral Thesis*, University of Hyderabad.
43. Sabere A. S. B. M. (2016). Formulation and charcaterization of conventional and 3-D printed mini-tablets and inserts for ocular use. *Doctoral Thesis*, University College London.
44. Bae H., Ahari A. F., Shin H., Nichol J. W., Hutson C. B., Masaeli M., Kim S. H., Aubin H., Yamanlarab S. and Khademhosseini A. (2011). Cell-laden microengineered pullulan methacrylate hydrogels promote cell proliferation and 3D cluster formation. *The Royal Society of Chemistry*, **7** (5), 1903-1911.

45. Pepelanova I., Kuppa K., Scheper T. and Lavrentieva A. (2018). Gelatin-Methacryloyl (GelMA) Hydrogels with Defined Degree of Functionalization as a Versatile Toolkit for 3D Cell Culture and Exstrusion Bioprinting. *Bioengineering*, **5** (3), 55.
46. Aldana A. A., Malatto L., Atiq Ur Rehman M., Boccaccini A. R., Agraham G. A. (2018). Fabrication of Gelatin Methacrylate (GelMA) Scaffolds with Nano- and Micro-Topographical and Morphological Featrures. *Nanomaterials*, **9**, 120.

Web Sites

http://www.startoncology.net/public-area/neuroblastoma-en/?lang=en (Last Access 08/02/2020)
http://www.bio.unipd.it/piccolo/mechanotransduction.html. (Last Access: 12/12/2019)
https://www.nature.com/scitable/topicpage/cell-division-and-cancer-14046590/ (Last Access: 28/12/2019)
https://www.airc.it/cancro/informazioni-tumori/guida-ai-tumori-pediatrici/neuroblastoma-pediatrico. (Last Access: 20/12/2019)
https://www.childrenwithcancer.org.uk/childhood-cancer-info/cancer-types/neuroblastoma/ (Last Access: 13/12/2019)
https://www.medicalnewstoday.com/articles/285666.php#what_is_bone_marrow. (Last Access: 22/12/2019)

Ringraziamenti

Desidero ringraziare la professoressa Cimetta, per avermi dato l'opportunità di lavorare nel suo laboratorio, e soprattutto la ringrazio per la fiducia, la disponibilità e la pazienza.

Ringrazio di cuore i compagni di laboratorio e i dottorandi. In particolare voglio ringraziare Marco e Sara, per la spensieratezza di questi mesi, per le risate, e per avermi aiutato in quello che per me rappresentava l'ostacolo più grande, tornare alla normalità nel migliore dei modi.

Ringrazio tutti gli amici dell'università, in particolare Riccardo, Rossana, Serena e Marco, per i cinque anni trascorsi insieme a ridere e scherzare tra una lezione e l'altra e per il grande lavoro di squadra.

Ringrazio le amiche del collegio, per avermi sempre fatto sentire a casa, e in particolare ringrazio chi mi ha aiutato nei momenti più difficili, quando anche solo respirare sembrava impossibile.

Ringrazio Camilla, Federica, Alessandro e Giorgio, per essermi stati accanto in questi anni, in particolare nell'ultimo.

Ringrazio Rosa, Elisabetta e Luca, per il grande sostegno e per l'affetto.

Ringrazio infine la mia famiglia, papà, mamma, Francesco ed Elisa, che mi hanno sempre sostenuto in questi anni, e mi hanno rialzato da terra nell'ultimo; vi ringrazio per la speranza e per tutto l'amore che mi avete dato e mi date ogni giorno. Vi voglio tanto bene.

Gaia